UDK 66:54(05) CODEN HMIDA 8 ISSN 0367–598X

4

Hemijska industrija

Vol. 77

Časopis Saveza hemijskih inženjera Srbije

Chemical Industry

Specijalna sveska: Primena i tehologija materijala

Special Issue: Materials application and technology

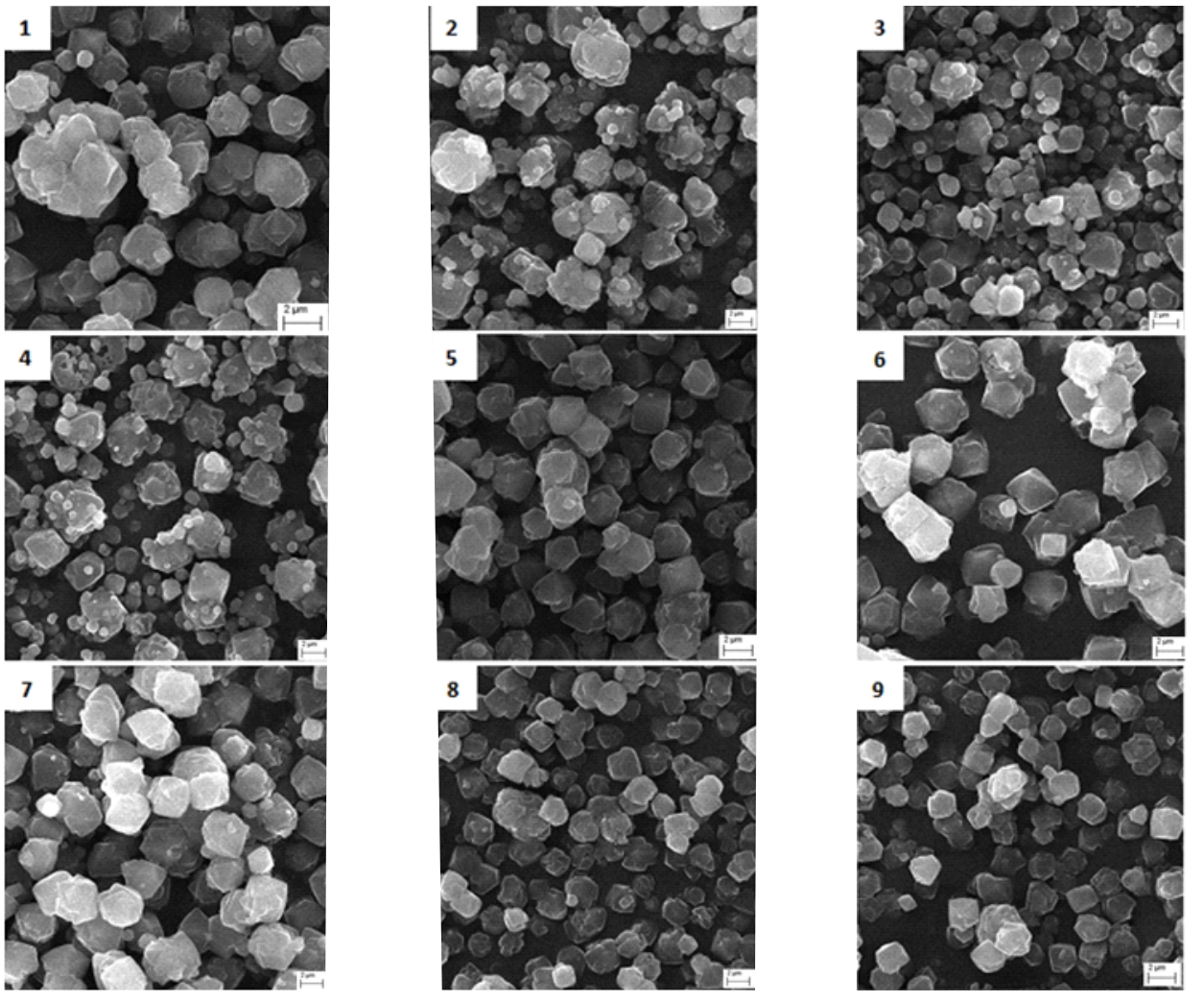

BEOGRAD, OKTOBAR - DECEMBAR 2023. HMIDA 8, 77(4) 231-304 (2023)

Aktivnosti Saveza hemijskih inženjera Srbije pomažu:

**MINISTARSTVO NAUKE,
TEHNOLOŠKOG RAZVOJA
I INOVACIJA
REPUBLIKE SRBIJE**

Tehnološko-metalurški fakultet
Univerziteta u Beogradu

Prirodno-matematički fakultet
Univerziteta u Novom Sadu

Institut za tehnologiju nuklearnih i
drugih mineralnih sirovina, Beograd

Tehnološki fakultet
Univerziteta u Novom Sadu

Institut za hemiju, tehnologiju i metalurgiju
Univerziteta u Beogradu

Fakultet tehničkih nauka
Univerziteta u Novom Sadu

Tehnološki fakultet
Univerziteta u Nišu, Leskovac

Fakultet tehničkih nauka
Univerziteta u Prištini
Kosovska Mitrovica

Institut IMS, Beograd

DCP HEMIGAL
Leskovac

Barič

Elixir Prahovo

Chemical Industry
Химическая промышленность

Hemijska industrija

Časopis Saveza hemijskih inženjera Srbije
Journal of the Association of Chemical Engineers of Serbia
Журнал Союза химических инженеров Сербии

VOL. 77 **Beograd, oktobar-decembar 2023.** **Broj 4**

Redakcija
11000 Beograd, Kneza Miloša 9/I
Tel/fax: 011/3240-018
E-pošta: shi@ache.org.rs
www.ache.org.rs

Izlazi kvartalno, rukopisi se ne vraćaju

Za izdavača: Ivana T. Drvenica

Sekretar redakcije: Slavica Desnica

Izdavanje časopisa pomaže
Republika Srbija, Ministarstvo nauke, tehnološkog razvoja i inovacija

Uplata pretplate i oglasnog prostora vrši se na tekući račun Saveza hemijskih inženjera Srbije, Beograd, broj 205-2172-71, Komercijalna banka a.d., Beograd

Menadžer časopisa i kompjuterska priprema
Aleksandar Dekanski

Štampa
Razvojno-istraživački centar grafičkog inženjerstva, Tehnološko-metalurški fakultet, Univerzitet u Beogradu, Karnegijeva 4, 11000 Beograd

Indeksiranje
Radovi koji se publikuju u časopisu *Hemijska Industrija* ideksiraju se preko *Thompson Reuters Scietific®* servisa *Science Citation Index - Expanded™* i *Journal Citation Report (JCR)*

Specijalna sveska:
Primena i tehologija materijala

Special Issue:
Materials application and technology

Gostujuće urednice / Guest Editors
Željka Antić and Milica Sekulić
VINČA Institute of Nuclear Sciences, University of Belgrade, Belgrade, Serbia

SADRŽAJ/CONTENTS

Advanced materials application in biotechnologies and biomedicine

Željka Antić and Milica Marčić

Center of Excellence for Photoconversion, Vinča Institute of Nuclear Sciences – National Institute of the Republic of Serbia, University of Belgrade, Belgrade, Serbia

Abstract

Materials matter: any breakthrough that changes society owes its success to the molecular building blocks used to create it. Advanced materials are essential to economic security and human well-being, with applications in industries aimed at addressing challenges in clean energy, national security, and human welfare. Therefore, speeding up the pace of development and implementation of advanced material systems is critical for achieving global competetiveness in the 21st century. In recent decades, significant progress has been evident in the processing and properties of materials intended for use in various biotechnologies, biomedicine, and dentistry. This volume specifically introduces new materials based on natural and synthetic substances with improved properties relevant to applications in biomedicine and biotechnologies.

Keywords: Antimicrobial applications; natural products; orthopedic and dental implants.

Available on-line at the Journal web address: http://www.ache.org.rs/HI/

EDITORIAL

UDC: 66.017:355.687

Hem. Ind. **77(4)** 231-233 (2023)

1. MATERIALS FOR ANTIMICROBIAL APPLICATIONS

The spread of infection by pathogenic microorganisms is a real, widespread issue and an actual and global problem. Furthermore, due to the uncontrolled use of antibiotics, microorganisms have developed a growing resistance to the numerous antimicrobial agents currently available. As a result, it is critical to limit the spread of infection, particularly in healthcare settings. The demand for efficient, long-lasting, easily available, non-toxic, and reasonably priced antimicrobial agents for medical, healthcare, hygiene, and protective textile materials is rapidly increasing as their production continues to rise [1]. In this respect, microbial survival on textile materials must be reduced because germs can degrade both the fabric and the wearer's comfort. In other words, the microbial presence may have many negative impacts, including the production of offensive odor, stains, material decolorization, and a reduction in the mechanical strength of the fabric [2]. Silver and its compounds, which were previously known to be effective biocides for over 650 different microbes, have gained new interest due to the growing problem of multi-antibiotic-resistant microorganisms [3]. Without significantly influencing the color of the fabric, silver can be added to textile materials to provide the appropriate amount of antibacterial activity [4]. Additionally, a concentration of silver below the level of toxicity of 1 mg dm^{-3} is sufficient to obtain adequate antimicrobial effects [5].

2. MATERIALS FOR CONTROLLED DRUG DELIVERY

Hydrogels are highly valuable materials endowed with unique properties for the controlled delivery of various active substances. pH-responsive hydrogels, constructed from poly(methacrylic acid) (PMAA) crosslinked by poly(ethylene glycol) diacrylate (PEGDA), have emerged as compelling materials for drug delivery applications. PMAA, serving as a hydrophilic polymer, proves to be a judicious choice for the synthesis of pH-sensitive hydrogels with adjustable swelling/deswelling behavior. PEGDA, recognized for its biocompatibility and non-toxic nature and commonly employed in pharmacy and biomedicine, effectively crosslinks PMAA-based hydrogels, imparting robust mechanical properties and the possibility for loading and controlled release of ciprofloxacin and oxaprozin. The swelling behavior and

Corresponding authors: Željka Antić, Center of Excellence for Photoconversion, Vinča Institute of Nuclear Sciences – National Institute of the Republic of Serbia, University of Belgrade, Belgrade, Serbia

Paper received: 21 May 2023; Paper accepted: 23 October 2023; Paper published: 16 November 2023.

E-mail: zeljkaa@gmail.com

https://doi.org/10.2298/HEMIND231211030A

mechanical properties exhibited by processed hydrogels based on PMAA substantiate the potential for their application in biomedicine as carriers for controlled drug delivery within the gastrointestinal tract.

3. MATERIALS BASED ON NATURAL PRODUCTS

Natural phenolics are broadly distributed in plants and are the most abundant secondary metabolites of plants. Plant polyphenols have drawn increasing attention as potential preventative measures against cancer and heart disorders [6]. It is widely acknowledged that the reactivity of the phenolic moiety causes phenolic compounds to serve as antioxidants. Biological activities of phenolic compounds include anti-inflammatory, anti-ulcer, antispasmodic, antiviral, antidiarrheal, and antitumor effects [7].

By scavenging free radicals and lowering oxidative stress, antioxidants can postpone, limit, or completely halt the oxidation of an oxidizable substrate. Antioxidants from outside sources are necessary in these circumstances to counteract the harmful effects of oxidative stress. Phenolics have been considered powerful antioxidants *in vitro* and proved to be more potent antioxidants than Vitamin C and E and carotenoids. A variety of putative pathways have been indicated as routes in which polyphenols might function as antioxidants. The most significant mechanism of their antioxidant activity is free radical scavenging, in which polyphenols can stop a free radical chain reaction, as well as suppress free radical formation by controlling the enzyme activity or chelating metal ions involved in free radical production.

4. MATERIALS FOR MEDICAL APPLICATIONS

An orthopaedic implant is a medical device used to replace a damaged or deformed bone, joint, or cartilage. The selection of materials, shape and geometry of the implants, dimensional accuracy, and adequate mechanical properties are the primary features required for the success of an orthopaedic implant. Chemical stability and toxicity, unlike other manufactured products, are of increased importance due to the need for biocompatibility over an implant's life, which could span several years while remaining sufficiently safe for use [8]. Thus, the clinical usefulness of biomaterials in orthopaedic and musculoskeletal trauma surgery is determined by the combination of mechanical and biological properties. Stainless steel, cobalt-based alloys, polymer materials (such as polyethylene), and titanium are used in the implants because they are strong and long-lasting [9]. Titanium is a common metal used in orthopaedic surgery as well as the 'gold standard' for dental implant fabrication. While titanium is a metallic element, the majority of "titanium implants" are actually alloys that are a good choice for such implants due to their appropriate mechanical properties, corrosion resistance, and biocompatibility.

We believe that the studies presented in this special issue will contribute to a better understanding of the importance of advanced materials development, inspiring future research toward different applications, not just in biotechnologies. We would like to thank all the authors for their efforts in preparing the articles or revising them in response to the reviewers' comments. We would also like to thank the reviewers for their valuable contributions. Special thanks to Prof. Dr. Bojana Obradović, Editor-in-Chief, for her guidance and support, and to the editorial staff for their assistance in producing this issue.

REFERENCES

[1] Wong YWH, Yuen CWM, Leung MYS, Ku SKA, Lam LI. Selected applications of nanotechnology in textiles. *Autex Res J.* 2006; 6: 1-8 https://doi.org/10.1515/aut-2006-060101

[2] Gao Y, Cranston R. Recent advances in antimicrobial treatments of textiles. *Text Res J* 2008; 78: 60–72 https://doi.org/10.1177/0040517507082

[3] Ilić V, Šaponjić Z, Vodnik V, Potkonjak B, Jovančić P, Nedeljković J, Radetić M. The influence of Silver Content on Antimicrobial Activity and Color of Cotton Fabrics Functionalized with Ag Nanoparticles. *Carbohyd Polym.* 2009; 78: 564-569 https://doi.org/10.1016/j.carbpol.2009.05.015.

[4] El-Rafie MH, Ahmed HB, Zahran MK. Characterization of nanosilver coated cotton fabrics and evaluation of its antibacterial efficacy. *Carbohyd Polym.* 2014; 107: 174-181. https://doi.org/10.1016/j.carbpol.2014.02.024.

[5] Lazić V, Mihajlovski K, Mraković A, Illés E, Stoiljković M, Ahrenkiel SP, Nedeljković J. Antimicrobial activity of silver nanoparticles supported by magnetite. *ChemistrySelect.* 2019; 4: 4018-4024 https://doi.org/10.1002/slct.201900628.

[6] Ćetković GS, Mandić AI, Čanadanović-Brunet JM, Djilas SM and Tumbas VT. HPLC screening of phenolic compounds in winter savory (Satureja montana L.) extracts. *J Liq Chromatogr Relat Technol.* 2007; 30: 293-306. https://doi.org/10.1080/10826070601063559.

[7] Gomes, F, Dias, MI, Lima, Â, Barros, L, Rodrigues, ME, Ferreira, IC, and Henriques, M. Satureja montana L. and Origanum majorana L. decoctions: Antimicrobial activity, mode of action and phenolic characterization. *Antibiotics.* 2020; 9(6): 294. https://doi.org/10.3390/antibiotics9060294

[8] Szczęsny G., Kopec M., Politis DJ., Kowalewski ZL, Łazarski A, and Szolc T. A Review on Biomaterials for Orthopaedic Surgery and Traumatology: From Past to Present, *Materials* 2022; 15(10): 3622, https://doi.org/10.3390/ma15103622

[9] Ong K, Yun M, White J. New biomaterials for orthopedic implants. *Orthop Res Rev.* 2015; 7: 107-130, https://doi.org/10.2147/ORR.S63437

Primena naprednih materijala u biotehnologijama

Željka Antić i Milica Maričić

Centar izuzetnih vrednostu za konverziju svetlosne energije, Institut za nuklearne nauke Vinča – Nacionalni institut Republike Srbije, Univerzitet u Beogradu, Beograd, Srbija

(Reč uredika)

Izvod

Materijali su važni: svaki napredak koji menja društvo duguje svoj uspeh molekularnim gradivnim blokovima koji se koriste za njegovo stvaranje. Napredni materijali su od suštinskog značaja za ekonomsku bezbednost i ljudsko blagostanje, sa primenom u industrijama usmerenim na rešavanje izazova u pogledu čiste energije, nacionalne bezbednosti i ljudskog blagostanja. Stoga je ubrzanje tempa razvoja i implementacije naprednih materijalnih sistema kritično za postizanje globalne konkurentnosti u 21. veku. Poslednjih decenija evidentan je značajan napredak u obradi i svojstvima materijala namenjenih upotrebi u različitim biotehnologijama, biomedicini i stomatologiji. Ova tematska sveska posebno predstavlja nove materijale zasnovane na prirodnim i sintetičkim supstancama sa poboljšanim svojstvima relevantnim za primenu u biomedicini i biotehnologiji.

Ključne reči: antimikrobne primene; prirodni proizvodi; ortopedski i zubni implantati

Poly(methacrylic acid) hydrogels crosslinked by poly(ethylene glycol) diacrylate as pH-responsive systems for drug delivery applications

Vukašin Ugrinović[1], Maja Marković[1], Bojan Božić[2], Vesna Panić[1] and Đorđe Veljović[3]

[1]*Innovation Center of Faculty of Technology and Metallurgy, Belgrade, Serbia*
[2]*University of Belgrade, Institute of Physiology and Biochemistry „Ivan Đaja", Belgrade, Serbia*
[3]*University of Belgrade, Faculty of Technology and Metallurgy, Belgrade, Serbia*

Abstract

Hydrogels are attractive materials for drug delivery applications due to biocompatible, porous structure with the possibility to load and deliver drugs in a controllable manner. In this paper, poly(methacrylic acid) (PMAA) hydrogels are described, which are synthesized by free-radical polymerization, using poly(ethylene glycol) diacrylate (PEGDA) as a crosslinker. Influence of the PEGDA content on hydrogel properties was investigated and compared to commonly used crosslinker - *N,N*'-methylenebisacrylamide (MBA). The increasing concentration of crosslinkers led to a higher degree of crosslinking, which was demonstrated by a higher degree of conversion, lower swelling capacity, and improved thermal stability and mechanical properties. Also, the PEGDA-crosslinked hydrogels demonstrated a higher degree of crosslinking than the corresponding MBA-crosslinked hydrogels. Potential application of the synthesized hydrogels for controlled drug delivery was investigated by using two model drugs - oxaprozin and ciprofloxacin. In vitro drug release tests indicated that the interactions between drug, polymer and medium have a key influence on the drug release behavior, rather than the swelling rate. Drug release tests in simulated gastrointestinal conditions indicated that PEGDA-crosslinked PMAA hydrogels are suitable for colon-targeted delivery of oxaprozin.

Keywords: smart materials; colon-specific delivery; ciprofloxacin; oxaprozin.

Available on-line at the Journal web address: http://www.ache.org.rs/HI/

ORIGINAL SCIENTIFIC PAPER

UDC: 544.773.432+77.018.62:615.012

Hem. Ind. **77(4)** 235-249 (2023)

1. INTRODUCTION

Hydrogels are three-dimensional crosslinked networks based on hydrophilic polymers, which have been extensively applied in a wide range of different fields. Due to their unique properties such as high porosity, permeability and ability to absorb high amounts of water without being dissolved, hydrogels have found practical application in cosmetics and personal care [1], drug delivery [2,3], enzyme immobilization [4,5], but also in the food industry [6], agriculture [7,8], water treatment [9,10], sensors and actuators [11], *etc.* Due to the structure resembling living tissues, biocompatibility and the possibility to incorporate cells and drugs, hydrogels have been largely explored for biomedical applications [12-15]. Development of stimuli-responsive hydrogels has opened the door to new approaches and strategies in controlled drug delivery. Stimuli-responsive hydrogels can be designed to react in response to different external stimuli which include, but are not limited to changes in pH [16-18], temperature [19,20], and ionic strength [21], as well as exposure to light [22], magnetic and electric fields [23]. Among the family of stimuli-responsive hydrogels, pH-sensitive ones have been particularly interesting for applications as self-regulatory drug delivery systems (DDS) [24]. Due to the presence of ionizable side groups, properties of pH-sensitive hydrogels can be rapidly changed in response to changes in the pH of the environment.

Poly(methacrylic acid) (PMAA) is an ionizable, hydrophilic polymer that is frequently used for fabrication of pH-sensitive materials as it imparts remarkable swelling/deswelling properties due to the protonation/deprotonation effect of carboxylic groups present in the polymer structure [25]. This effect causes low swelling of PMAA hydrogels in acidic environments and remarkably higher swelling in neutral/basic conditions, which can be effectively used for gastro-

Corresponding authors: Vukašin Đ. Ugrinović, Innovation Center of Faculty of Technology and Metallurgy, Belgrade, Karnegijeva 4, 11000 Belgrade, Serbia
E-mail: vugrinovic@tmf.bg.ac.rs
Paper received: 28 December 2022; Paper accepted: 18 July 2023; Paper published: 18 September 2023.
https://doi.org/10.2298/HEMIND221228018U

intestinal drugs to reduce the effect of the harsh gastric conditions and increase the bioavailability of the drug [26]. However, due to the soft nature and rapid degradation of physically crosslinked hydrogels in the physiological environment, hydrogels have been frequently crosslinked by using chemical crosslinkers, which may compromise biocompatibility of the hydrogels. Specifically, PMAA hydrogels, as well as different vinyl-based polymers applied in biomedicine, such as poly(acrylic acid) and poly(acrylamide) have been typically crosslinked by using *N*,*N*'-methylenebisacrylamide (MBA), ethylene glycol diacrylate and ethylene glycol dimethacrylate, which are known to be toxic [27-31]. MBA has been proven to be an effective crosslinker for PMAA hydrogels, however, unreacted molecules of MBA may cause toxicity when applied *in vivo*. Subsequent rinsing of the hydrogels to remove the unreacted molecules prevents the possibility of pre-polymerization drug loading, as the drug will leak out of the hydrogel during the rinsing. Therefore, one of the simplest solutions for this problem is to use crosslinkers which are non-toxic and safe for *in vivo* applications.

Poly(ethylene glycol) diacrylate (PEGDA) is a derivative of poly(ethylene glycol) which is one of the most applied materials in pharmacy and biomedicine due to its biocompatibility, non-toxicity, hydrophilicity and relatively good mechanical properties [32]. Terminal acrylate groups of PEGDA provide creation of bifunctional radicals during the free radical polymerization process, used to crosslink vinyl-based hydrogels [33-35]. Nevertheless, PEGDA-crosslinked vinyl-based hydrogels have been scarcely reported in literature. For example, there has been only one study reporting the PEGDA-crosslinked PMAA hydrogels [36]. In this study, PEGDA-crosslinked PMAA nanoparticles were synthesized and investigated for controlled release of 5-fluorouracil. Even though the obtained PMAA nano-gels demonstrated a pH-sensitive drug release, a stable, three-dimensional structure could not be formed, which may narrow the possible range of biomedical applications. Therefore, synthesis of three-dimensional PMAA hydrogels crosslinked by PEGDA, and investigation of the PEGDA influence on the properties of such hydrogels would be highly beneficial for these applications.

Ciprofloxacin (1-cyclopropyl-6-fluoro-1, 4-dihydro-4-oxo-7-(1-piperazinyl)-3-quinoline carboxylic acid) is a synthetic fluoroquinolone-based antibiotic, which has a good antibacterial activity against gram-positive and gram-negative bacteria. It has been widely used to treat various infections such as skin and bone infections, gastrointestinal tract (GIT) infections caused by multiresistant pathogens, sexually transmitted diseases, complicated urinary infections, lower respiratory tract diseases, pneumonia, *etc.* [37] However, the use of ciprofloxacin has been associated with serious adverse effects, while traditional administration methods are characterized by low bioavailability, and do not provide prolonged drug release. In addition, most of the ciprofloxacin is degraded by lysosomes before killing bacteria, which usually results in low intracellular drug concentration [38]. Therefore, development of a DDS that can provide sustained and controlled delivery of ciprofloxacin is of great practical significance.

On the other hand, oxaprozin is a propanoic acid non-steroidal anti-inflammatory drug (NSAID) that has intrinsic advantages over similar NSAIDs widely applied for the treatment of musculoskeletal inflammatory diseases [39]. It is as effective as aspirin but applied at significantly lower doses [40]. However, oral administration of NSAIDs could impose serious adverse effects on the gastrointestinal system. Most of the complications are related to the gastroduodenal area and include gastroduodenal subepithelial hemorrhages, erosions and ulcerations. These pathological conditions may lead to death, and impose substantial health risks and economic burden [41]. DDS which can provide controlled drug delivery to a lower GIT may reduce the risks related to NSAIDs oral administration.

The aim of this work was to synthesize PEGDA-crosslinked PMAA hydrogels (PMAA-P) and to investigate their potential application for controlled release of ciprofloxacin and oxaprozin. Hydrogels were synthesized by thermally induced free-radical polymerization and crosslinked by different amounts of PEGDA. In parallel, hydrogels with the same amounts of commonly applied MBA were also synthesized (PMAA-M), for comparison with the novel PMAA-P. The final aim was to investigate the selected optimal PMAA-P hydrogel for controlled ciprofloxacin and oxaprozin release.

2. MATERIALS AND METHODS

2. 1. Materials

Methacrylic acid (MAA) (99.5 %) was supplied from Merck KgaA (Germany). PEGDA (M_n = 700), MBA and ciprofloxacin were obtained from Sigma Aldrich (USA). The initiator, 2,2'-azobis[2-(2-imidazoline-2-yl)propane]

dihydrochloride (VA-044) (99.8 %) was supplied by Wako Pure Chemical Industries (Japan). All chemicals were used as received.

2. 2. Synthesis of hydrogels, oxaprozin and drug-loaded composite hydrogels

PMAA hydrogels were synthesized *via* thermally induced free radical polymerization. 0.4 cm^3 of methacrylic acid (MAA), and desired amount of crosslinker were dissolved in 1 cm^3 of distilled water, and the solution was stirred for 5 min. In the last step, 2 mg of initiator (VA-044) was added, and the solution was stirred for additional 3 min before it was poured into a Teflon mold and placed in an oven at 65 °C for 5 h to complete the reaction. The amount of crosslinker (PEGDA or MBA) added corresponded to the crosslinker/polymer molar ratio of 0.1, 0.2, 0.5 and 1.0 mol.% and were denoted as PMAA-XY, where X = M for MBA or P for PEGDA, and Y = 0.1, 0.2, 0.5 or 1.0 corresponding to the mol.% of the crosslinker added.

Oxaprozin was synthesized by the previously described procedure [42,43].

Drug-loaded hydrogels were synthesized by the same procedure with the addition of 4 mg of the drug (ciprofloxacin or oxaprozin). The obtained hydrogels were cut into equal cylinder-shaped samples and further prepared according to the testing method requirements.

2. 3. Characterization

2. 3. 1. Degree of conversion

The degree of monomer conversion (DC) into the gel phase was determined by using the equation:

$$\mathrm{DC} = \frac{m_0}{m_\mathrm{p}} \tag{1}$$

where m_0 is the mass of the xerogel obtained by drying hydrogels to constant mass after 24 h of swelling in phosphate buffered saline (PBS) at pH 7.4 and t = 37 °C, and m_p is the mass of the xerogel obtained by drying hydrogels to constant mass right after the polymerization process.

2. 3. 2. Determination of the swelling degree and water content

Dynamic swelling measurements were carried out in alternating acidic (pH 1.2) and basic conditions (pH 7.4), as well as in simulated GIT conditions. Acidic conditions were simulated by HCl/KCl buffer, while phosphate buffer solution (PBS) (pH 7.4) was used for basic conditions. During the swelling in GIT, hydrogels were initially swollen in HCl/KCl buffer which simulated stomach conditions (pH 1.2), and after 2 h were transferred to PBS (pH 6.8), which simulated the small intestine conditions where they were kept for 2 h. Subsequently, they were transferred to PBS (pH 7.4), which mimicked colon- conditions for 6 h [44]. The experiments were performed by immersing three samples from different batches of the same type of hydrogel (approximately 3×0.1 g of dry hydrogel in 10 cm^3 of the appropriate liquid) to obtain an average value for at least three batches of the same hydrogel. At regular time intervals, samples were removed from the swelling medium and weighed, after which the samples were returned to the medium again The swelling ratio (SR) of hydrogels was calculated using the equation [28]:

$$\mathrm{SR} = \frac{m}{m_0} \tag{2}$$

where m was the mass of the swollen hydrogel at a specific time. The equilibrium swelling ratio (ESR) was calculated using the same equation except that m_{eq} (mass of the hydrogel swollen at equilibrium *i.e.* after not changing significantly during three consecutive measurements) was used instead of m. ESR measurements were carried out in HCl/KCl buffer (pH 1.2), acetate buffer (pH 4.0) and PBS (pH 7.4). The point of ESR was established.

2. 3. 3. Differential scanning calorimetry measurements

Thermal analysis of the PMAA-M0.1, PMAA-M1.0, PMAA-P0.1 and PMAA-P1.0 xerogels was performed by using a differential scanning calorimeter - DSC (DSC-60Plus differential scanning calorimeter, Shimadzu, Japan). Before the DSC

analysis, the xerogels were ground into powder. The weight of the samples was limited to 3±0.2 mg and all DSC measurements were carried out using hermetic aluminum pans. All the samples were first heated from -50 to 0 °C at 10 °C min^{-1} under a nitrogen purge gas flow of 30 cm^3 min^{-1}. After this treatment, the thermal analysis of the samples was conducted by heating samples from 25 to 300 °C at 10 °C min^{-1} under the same nitrogen purge gas flow rate. The DSC analysis of the M1, M4, P1 and P4 xerogels was conducted according to the procedure reported in the literature [45]. This procedure was adopted for the analysis of the effect of the change in the crosslinker amount on the thermal stability of the hydrogels based on PMAA.

2. 3. 4. Mechanical properties

Mechanical properties of the obtained hydrogels were evaluated by using the Universal Testing Machine AG-Xplus (Shimadzu, Japan), equipped with a 1000 N force load cell (force range from 0.01 to 1000 N). Before testing, cylinder-shaped samples (8.0±1.0 mm in diameter and 8.0±1.0 mm in height) were swollen to equilibrium in PBS at 37 °C. Compression was performed until the sample failure, at a compression rate of 10 mm min^{-1}. Automatic detection of the contact between the plate and hydrogel was performed by setting a contact force of 0.05 N. The values of compressive strength were determined at the point of failure, while the compressive modulus was calculated by measuring the slope of the stress-strain curve within 0-10 % of deformation. At least three specimens were tested for each hydrogel type and the mean values are presented.

2. 3. 5. Drug release

Drug release behavior was examined in HCl/KCl buffer (pH 1.2) and PBS (pH 7.4) at 37 °C, as well as in simulated GIT conditions as described in 2.3.2. The obtained drug-loaded hydrogel samples were cut into four cyllinder-shaped samples (R = 1 cm, H = 2 cm, $m \approx 1$ g) and immersed in 20 cm^3 of buffer. The aliquots of 2 cm^3 were taken out at specific time intervals and analyzed for drug using Shimadzu UV-1800 UV/Vis spectrophotometer (Shimadzu, Japan), after which they were returned to the medium. The obtained drug concentrations at certain intervals were converted into masses, and curves of cumulative drug release *vs* time were ploted.

3. RESULTS AND DISCUSSION

3. 1. Synthesis and chemical structure of PMAA hydrogels

PMAA hydrogels were synthesized *via* thermally induced free-radical polymerization using MAA as a functional monomer, VA-044 as the initiator and MBA or PEGDA as crosslinking agents. Both MBA and PEGDA are bifunctional crosslinkers with terminal acrylate groups on both sides of their molecules. During free-radical polymerization, when the acrylate group of MBA or PEGDA is attacked by a growing macromer radical, it is incorporated into the macromolecular chain and covalently bonds to monomer units. When both ends of crosslinker groups are incorporated in two independent macromolecular chains, they become crosslink points and the obtained hydrogel is covalently crosslinked. As the number of crosslinking points increases, the network becomes more rigid and mechanically stronger. On the other hand, the unreacted crosslinker molecules may not only affect mechanical properties, but they can also reduce the biocompatibility of the hydrogels. However, PEGDA is a non-toxic compound and its potential leaking from a hydrogel would not cause harmful effects on human health [46]. Structures of MBA and PEGDA, as well as the schematic of the free-radical polymerization reaction are presented in Figure 1.

3. 2. Degree of conversion

The degree of conversion (DC) of monomers into a polymer network directly affects the physical and mechanical properties of the synthesized hydrogels, as it shows how much MAA monomer was incorporated into the structure of the polymer. To determine the DC, masses of xerogels obtained after the synthesis were measured and compared with the xerogel masses obtained after 24 h of rinsing of the hydrogels in PBS at 37 °C.

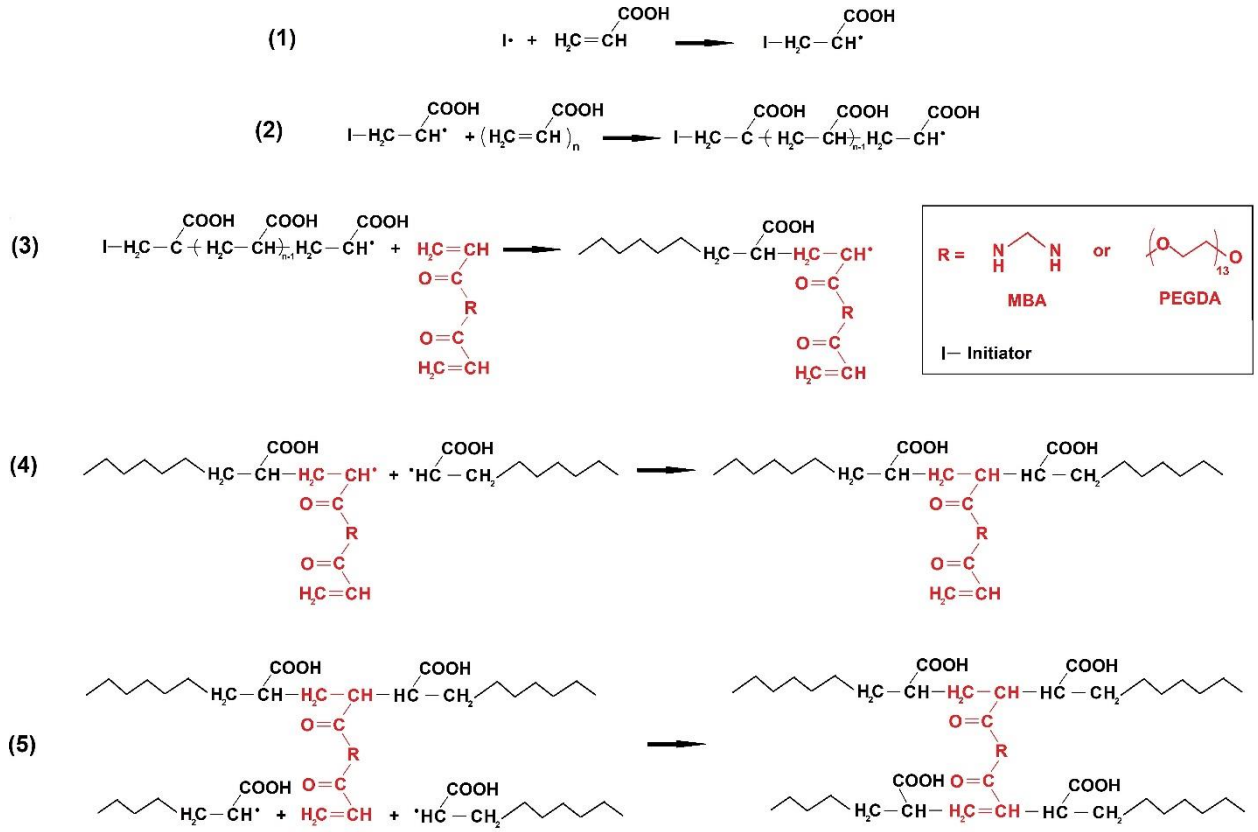

Figure 1. *Simplified schematic of free-radical polymerization of MAA and creation of three-dimensional crosslinked hydrogels: (**1**) initiation -creation of MAA radicals; (**2**) propagation -addition of MAA monomers to a growing chain; (**3**) incorporation of a vinyl group of the crosslinker to the growing chain; (**4**) termination - the reaction of the growing chain with another growing chain; (**5**) reaction of the second vinyl group of the crosslinker with another growing chain -creation of crosslinking points*

The obtained results indicated high polymerization degrees of all hydrogels, as the masses of xerogels after synthesis were similar to the theoretical ones (the total mass of monomer, crosslinker and initiator). On the other hand, the masses of xerogels after rinsing were lower and were highly dependent on the crosslinker type and content. Figure 2 demonstrates the dependence of DC on MBA and PEGDA content.

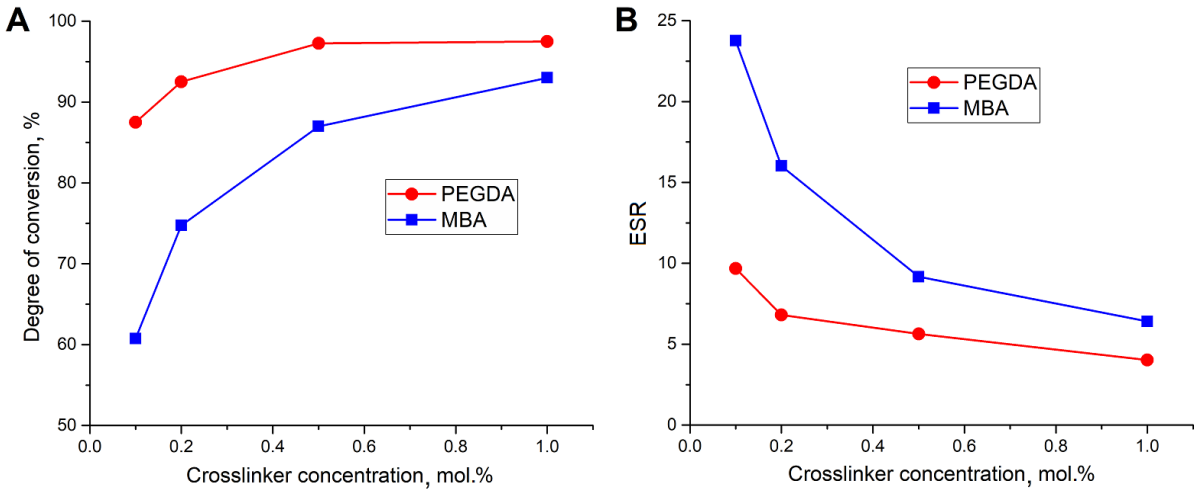

Figure 2. *Influence of the crosslinker content on DC (A) and ESR (B)*

It can be observed that the increase in crosslinker content yielded hydrogels with higher DC. Moreover, the influence of PEGDA on DC was significantly higher compared to that of MBA, at the same molar concentrations. Knowing the fact that all hydrogels had a high degree of polymerization, *i.e*. that practically negligible amounts of unreacted monomer molecules were left after the polymerization reaction, the mass loss after rinsing could be the consequence of smaller and less crosslinked polymer chains, which could easily diffuse out of the structure. Therefore, the increase in crosslinker content resulted in a more interconnected network and a lower amount of soluble phase (unreacted monomer and crosslinker, non-crosslinked oligomeric and polymeric chains) [47]. As higher DC of PMAA-P hydrogels were obtained compared to those of PMAA-M, we assume that PEGDA molecules had a higher tendency to react with free radicals and eventually get incorporated in the growing chains as explained in Section 3. 1., which resulted in efficiently crosslinked hydrogel networks. This can be explained by the lower reactivity of acrylamides compared to methacrylates [48].

3. 3. Swelling studies

Swelling ability is one of the most important characteristics of hydrogels aimed for controlled DD since this property could affect the delivery profiles of active compounds. It is also an indication of the crosslinking density and can be used for evaluation of crosslinking degree of hydrogels. Swelling ability of hydrogels was determined after 24 h of swelling in PBS at 37 °C. In the case of both crosslinkers, the increase in crosslinker content led to decreased ESR of the hydrogels, indicating a higher degree of crosslinking (Fig. 2B) [25]. The ESR of PMAA-P hydrogels was lower than those of PMAA-M opposite to our initial hypothesis that using PEGDA as a crosslinker would yield hydrogels with higher ESR due to longer, flexible crosslinking molecules. However, these results were in agreement with DC results, and the reason for this behavior could be that not all molecules of MBA were incorporated into the hydrogel network, which led to a lower crosslinking degree than it would be initially assumed [47]. To confirm the efficacy of the PEGDA as a crosslinking agent, PMAA hydrogel without any crosslinker added was also synthesized, which completely dissolved under the applied conditions, as it was only physically crosslinked through hydrogen bonds. This confirmed that PEGDA can be effectively applied to crosslink the PMAA network.

3. 4. DSC analysis

DSC thermograms of the synthesized hydrogels, demonstrated in Figure 3, exhibited two endothermic peaks, the sharp one in the range from 193 to 207 °C (T_1) and the wide one, around 240°C.

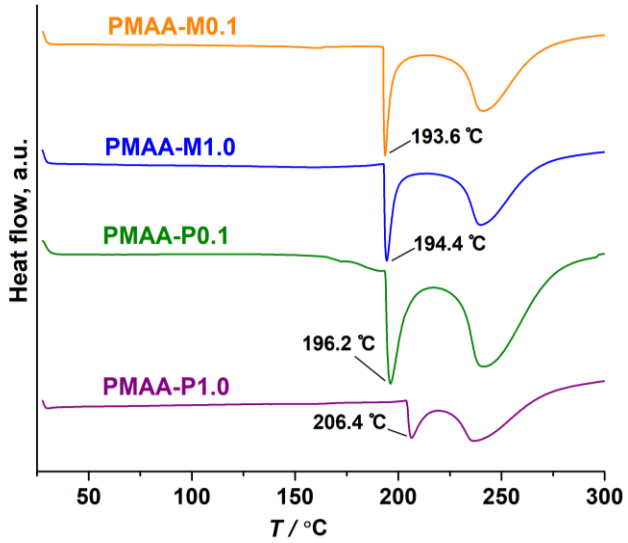

Figure 3. *DSC curves for PMAA hydrogels crosslinked with different amounts of MBA and PEGDA*

Both peaks were ascribed to different degradation phases of the hydrogel networks. As it is well-known from the thermogravimetric analysis (TGA) of PMAA, the first peak refers to dehydration of carboxyl groups and formation of cyclic polyanhydride [49], while the second is related to further degradation of the main PMAA chains, including

decarboxylation, depolymerization, and "decrosslinking" processes [45,46]. The increase in crosslinker content shifted the first degradation stage towards higher temperatures indicating the increase in thermal stability of more crosslinked hydrogels. Additionally, if the effects of the crosslinker type are compared, the samples crosslinked with PEGDA exhibited higher thermal stability than the corresponding analogs crosslinked with MBA. For example, when the MBA content increased 10-fold, the T_1 increased for 0.8 °C, while the 10-fold increase in the PEGDA content led to the T_1 increase of more than 10.4 °C. The increase in the thermal stability of hydrogels was another evidence of successful and efficient crosslinking.

3. 5. Mechanical properties

Compressive mechanical properties of the hydrogels were investigated by using the unconfined compression test. Stress-strain curves of hydrogels are plotted in Figures 4A and B, while the trends of compressive modulus (E_c) and compressive strength (σ_c) *vs*. PEGDA and MBA concentrations are presented in Figures 4C and D.

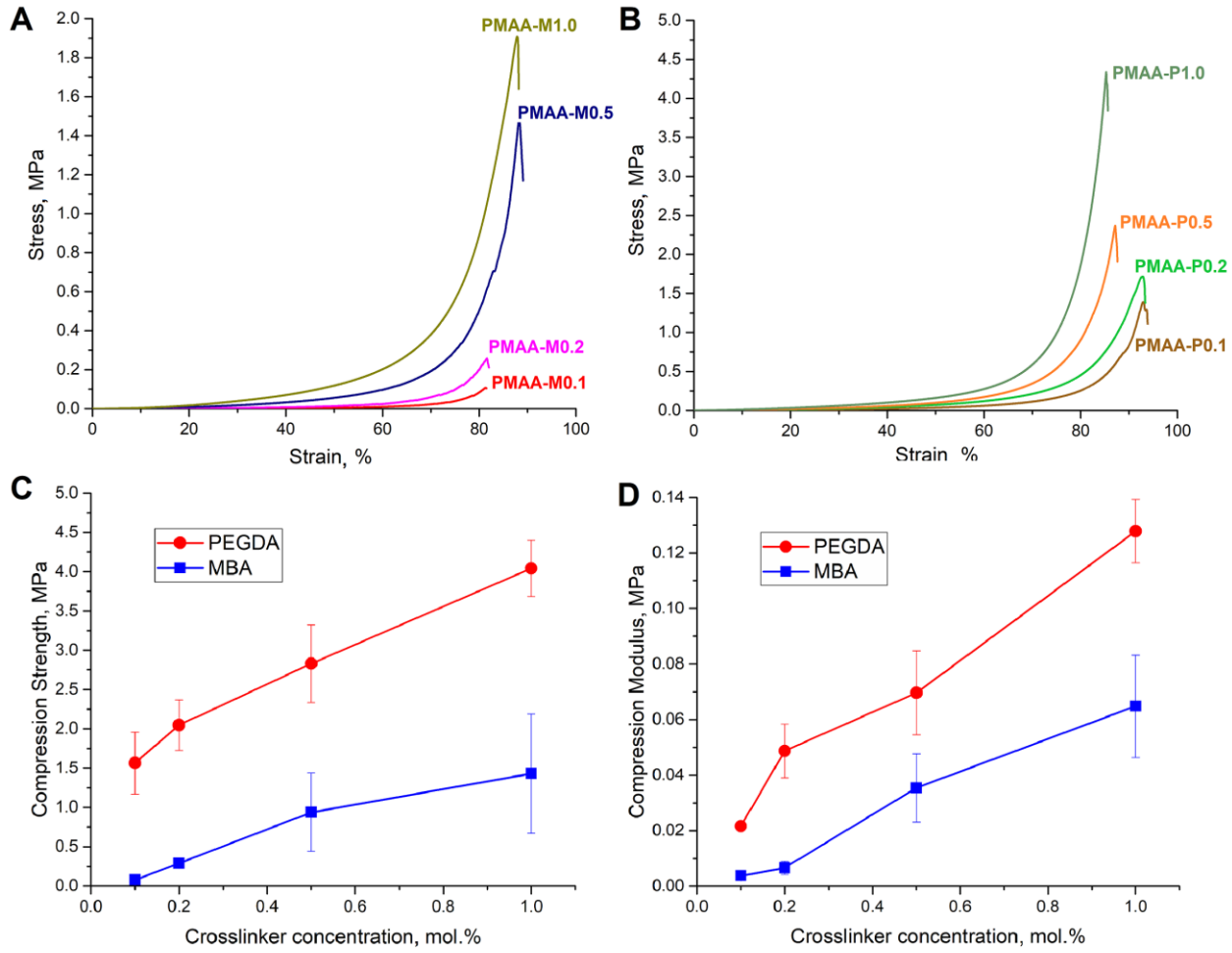

Figure 4. *Stress-strain curves of hydrogels with different contents of MBA (A) and PEGDA (B). The influence of crosslinkers content on the compression strength (C) and compression modulus (D) of the hydrogels*

Compressive strength and compressive modulus significantly increased as the crosslinker concentration increased in both cases. For example, the values of σ_c and E_c of PMAA-M1.0 were 20-fold greater than the corresponding values of PMAA-M0.1, while the σ_c and E_c of PMAA-P1.0 were 2.5- and 6-fold greater than the corresponding values of PMAA-P0.1. In both cases, compression strength and modulus values had almost linear dependences on the crosslinker content. If the influence of different crosslinkers is compared, it could be noticed that using PEGDA yielded hydrogels with significantly higher compression strengths and moduli, which agrees with the DC and swelling results. A hydrogel

crosslinked to a lower degree with higher water content is characterized by lower mechanical properties as compared to the same type of hydrogel crosslinked at a higher degree of croslinking with less water in the structure. Compression strength values for the obtained PMAA-P hydrogels were of the same order of magnitude as the value of the peak stress exerted on a human knee (a human weighing 90 kg exerts 2.5 MPa pressure on the knee during walking [51]), which confirmed the mechanical competence of these materials for biomedical applications.

3. 6. pH sensitivity

In this study, pH-sensitive swelling behavior of hydrogels was investigated in the physiologically relevant pH range of 1.2 to 7.4, at 37 °C, as well as in simulated GIT conditions. The hydrogels were also subjected to an oscillatory swelling-deswelling study to investigate the reversibility and response rate of the swelling process in acidic and basic conditions. The ESR as a function of the pH, for hydrogels with different types and concentrations of crosslinker, is presented in Figures 5A and 5B.

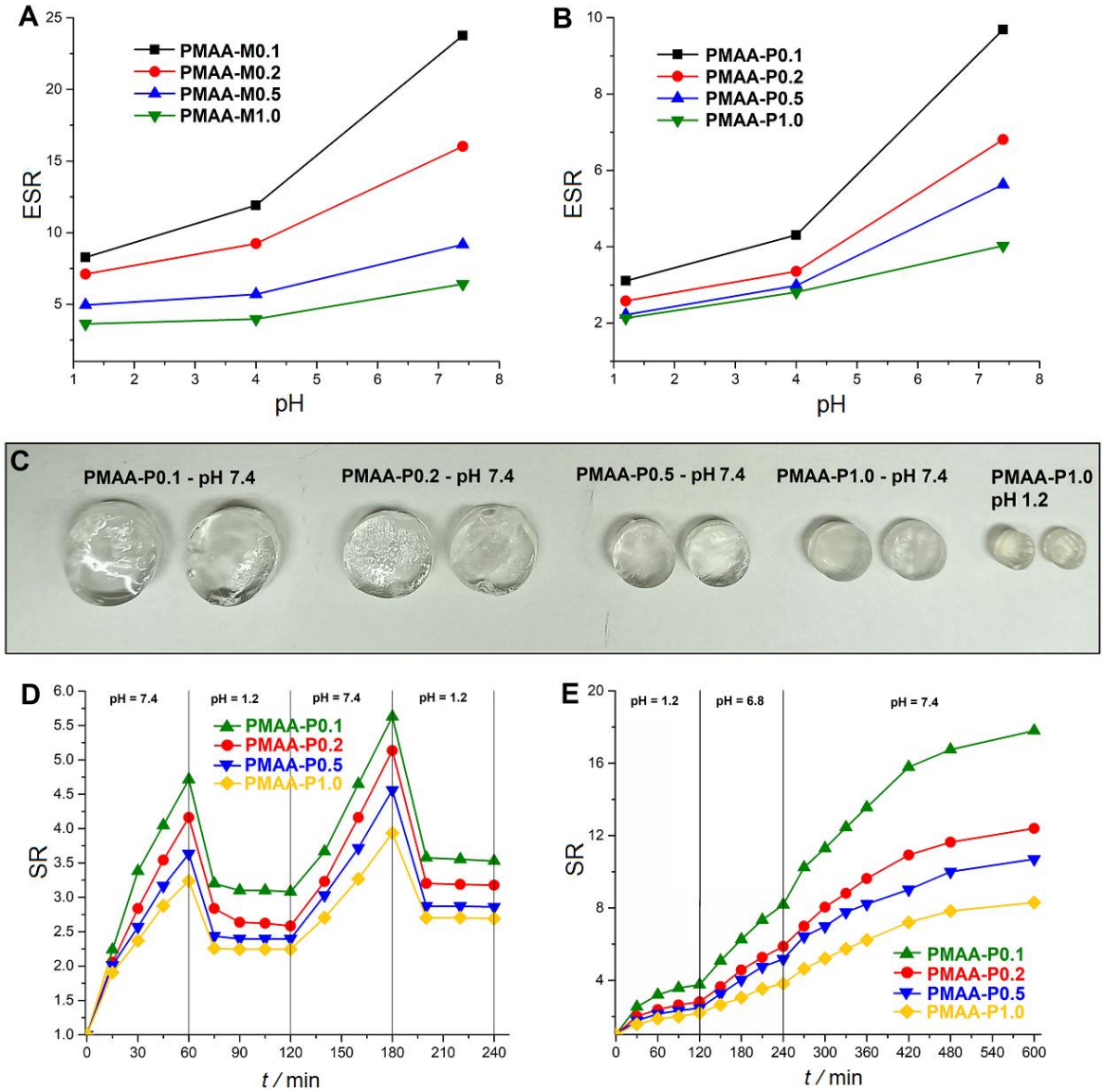

Figure 5. *Dependence of ESR on pH for hydrogels crosslinked by different amounts of MBA (**A**) and PEGDA (**B**). Photographs of PMAA-P hydrogels after swelling in pH 7.4 and pH 1.2 (**C**). Swelling of PMAA-P hydrogels under alternating basic-acidic conditions (**D**) and simulated GIT conditions (**E**)*

All hydrogels demonstrated pH-sensitive behavior during swelling. At pH 1.2, which is below the pK_a value of PMAA (≈4.8), the ESR was low for all hydrogels. As the pH value of the environment exceeded the pK_a value of PMAA, carboxylic

groups became ionized. This caused repulsive forces between negatively charged carboxylate ions and contributed to a higher ionic density, which led to higher ESR. The effect was more pronounced as the concentration of crosslinker decreased. In general, the MBA-crosslinked hydrogels demonstrated markedly higher ESR compared to PEGDA, due to a structure crosslinked to a lower extent. Nevertheless, using PEGDA as a crosslinker did not affect the pH-sensitive nature of the PMAA hydrogels. Figure 5C presents photographs of PMAA-P hydrogels after attaining the swelling equilibrium at pH 7.4, as well as PMAA-P1.0 hydrogel after swelling at pH 1.2.

The oscillatory swelling-deswelling study on PMAA-P hydrogels demonstrated rapid swelling in basic conditions, followed by rapid deswelling in acidic conditions (Fig. 5D). The reversibility of hydrogel swelling slightly decreased with a decrease in the crosslinker content. This was due to higher stretching of macromolecules and formation of new physical bonds in the hydrogel structure under basic conditions, preventing full relaxation under the applied acidic conditions. This effect was more pronounced when the molecular stretching was higher as was the case with less crosslinked hydrogels.

Swelling results obtained in simulated GIT conditions are presented in Figure 5E. The values of SR were relatively low at pH 1.2, but they significantly increased when the samples were transferred to buffers with higher pH values. Lower swelling capacity of PMAA-P hydrogels in acidic pH, and higher swelling capacity in slightly alkaline pH are very advantageous for design of colon-specific drug delivery systems. Such systems could thus protect the drug from the harsh gastric environment and enable controlled delivery in the small intestine and colon. These drug release profiles are also very beneficial for delivery of drugs which can impose serious negative effects on the upper GIT.

3. 7. Drug release studies

Applicability of the obtained PMAA-P hydrogels as DDS for controlled delivery of ciprofloxacin and oxaprozin was investigated *in vitro* under different pH conditions, and the results are presented in Figure 6. The *in vitro* ciprofloxacin release from the hydrogels at pH 7.4 indicated that the crosslinker content had a major influence on the ciprofloxacin release kinetics (Fig. 6A). Increase in the crosslinker content led to a slower ciprofloxacin release, due to the limited diffusion through the more crosslinked network. On the other hand, the crosslinker content and correspondingly the crosslinking degree, did not have a significant influence on the oxaprozin release (Fig. 6B). Hydrogels crosslinked to a lesser degree (*i.e.* PMAA-P0.1 and PMAA-P0.2) had a more pronounced burst effect, however, after 30 h they released a slightly higher amount of drug than the PMAA-P0.5 and PMAA-P1.0 hydrogels. The pH value influenced the ciprofloxacin release rate, so that the total released amount of this drug was almost 5-fold higher at pH 1.2 compared to pH 7.4 (Fig. 6C), even though the swelling tests demonstrated almost 2-fold lower ESR at pH 1.2 compared to pH 7.4. Obviously, the swelling capacity did not have a major influence on the ciprofloxacin release in this case, and diffusion was not the rate-determining step.

It can be assumed that the drug solubility had the main influence on the drug release based on the acid/base equilibrium, as well as the interactions between the drug, medium and the polymer. Ciprofloxacin has two main pK_a values corresponding to two main proton binding sites - the carboxyl group (pK_1 = 5.89) and the nitrogen atom in the piperazine ring (pK_2 = 8.61). Thus according to the pH of the environment, ciprofloxacin can be in the form of cation, anion, or zwitterion [52]. On the other hand, the pK_a of methacrylic acid is 4.65. As shown in Figure 7, when the pH value of the environment was 1.2, which is lower than the pK_a of carboxyl groups on the polymer chains, these carboxyl groups were protonated and in a neutral state, while the molecules of ciprofloxacin were in cationic form, which prevented electrostatic interactions between molecules. At the same time, due to the high solubility of ciprofloxacin in the acidic environment, weak physical bonds between the molecules of ciprofloxacin and hydrogel matrix were relatively easily broken, and ciprofloxacin passed into the medium. In this case diffusion was the only limiting step for the drug to reach the outer solvent, and diffusion rate was dependent on the swelling rate. On the other hand, when the pH of the medium was 7.4, most of the polymer carboxyl groups were ionized and in the anionic form, while ciprofloxacin was in a zwitterionic state, which allowed electrostatic interactions between positively charged groups of ciprofloxacin and negatively charged groups of the hydrogel polymer. Taken into account also the low solubility of ciprofloxacin in basic conditions, this resulted in a low drug release rate, as the drug molecules preferred interactions with the hydrogel, instead of the medium [36].

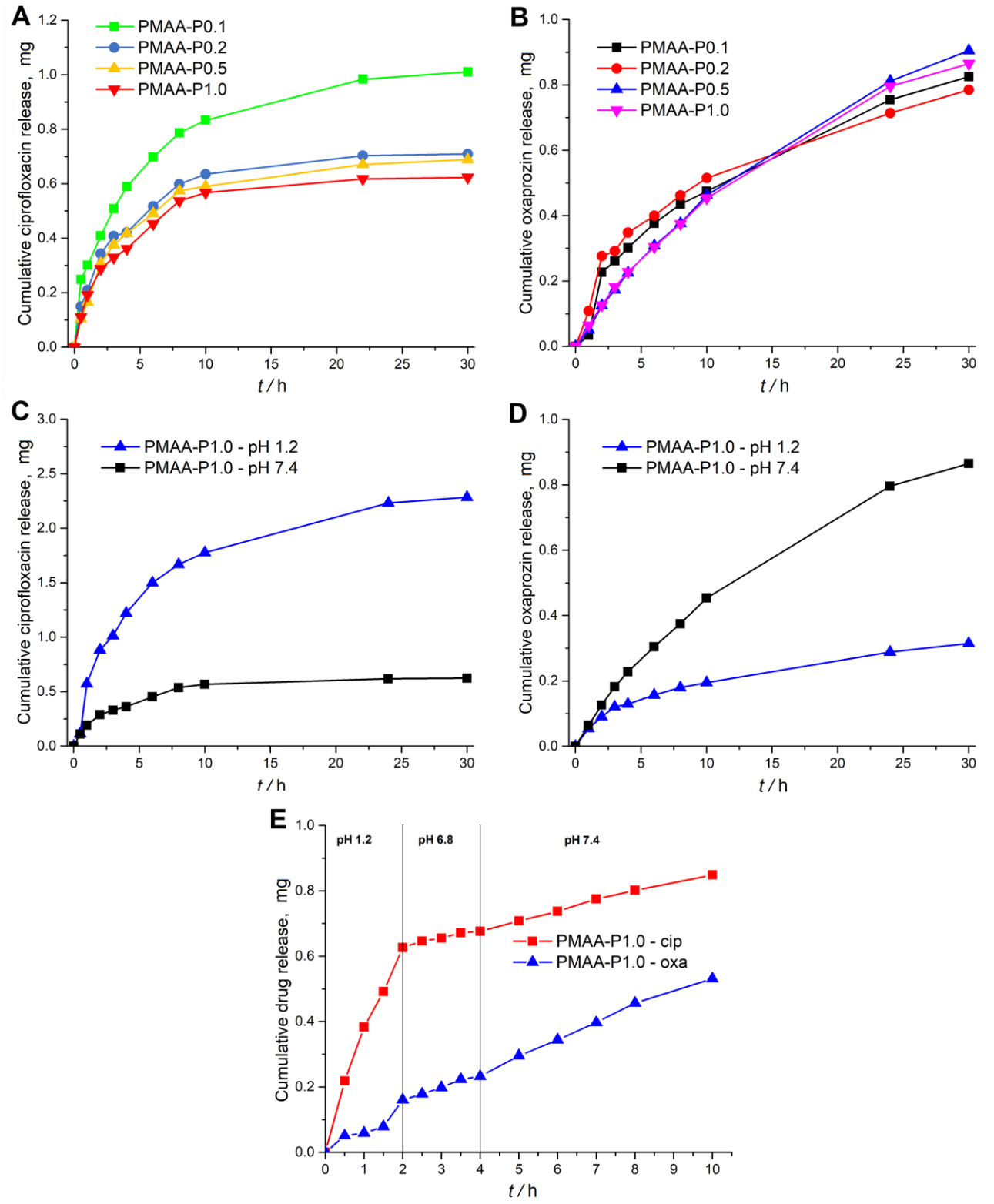

Figure 6. *Cumulative in vitro ciprofloxacin (**A**), and oxaprozin (**B**) release from hydrogels with different contents of PEGDA at* pH *7.4. Cumulative in vitro ciprofloxacin (**C**) and oxaprozin (**D**) release from the PMAA-P1.0 hydrogel at different pH conditions. The in vitro ciprofloxacin and oxaprozin release from the PMAA-P1.0 hydrogel in simulated GIT conditions (**E**)*

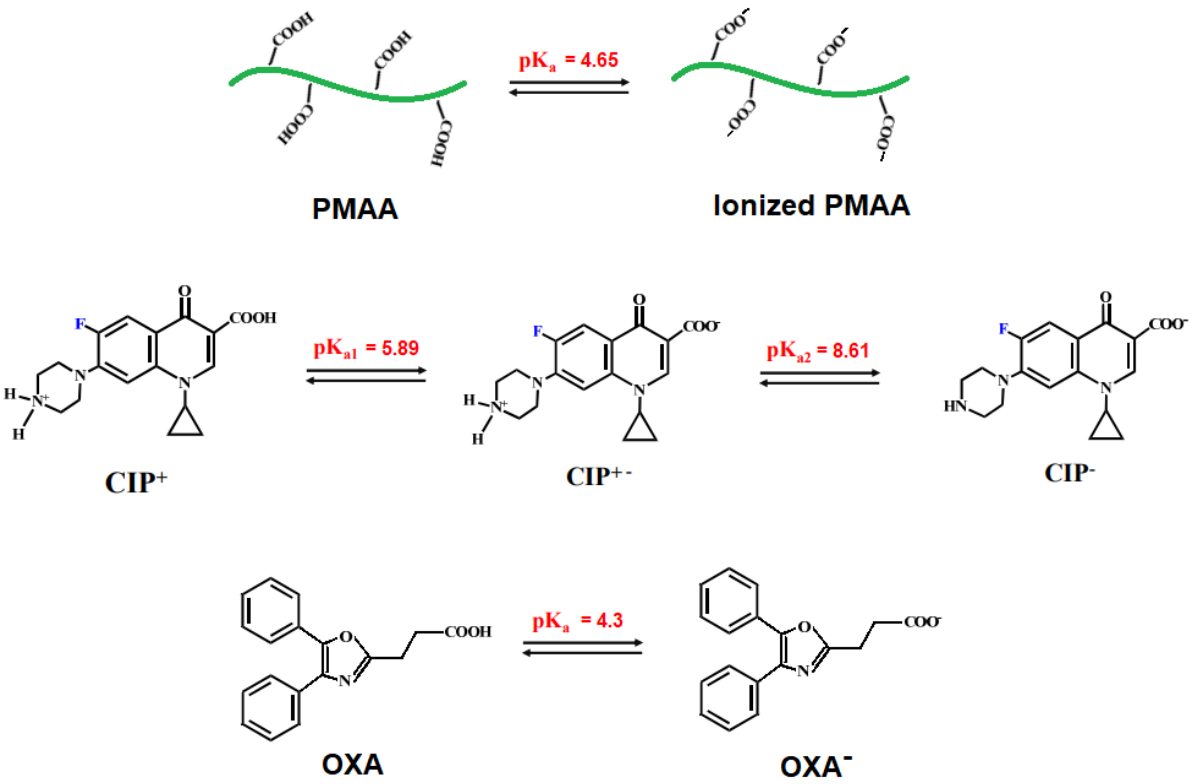

Figure 7. *Structures of the molecules of PMAA, ciprofloxacin (CIP) and oxaprozin (OXA), and their respective ionization states*

However, the situation was reversed in the case of oxaprozin release. The oxaprozin release rate and the total amount of the released drug were significantly higher at pH 7.4 as compared to pH 1.2 (Fig. 6D). In acidic conditions both, the hydrogel and oxaprozin were in the protonated state (the pK_a of oxaprozin is 4.3) and could establish interactions by hydrogen bonds. Moreover, oxaprozin is insoluble in aqueous solutions at pH 1.2, thus its release was additionally hindered. In contrary, when the pH of the medium was 7.4, carboxylic groups in the hydrogel and oxaprozin were in the form of negatively charged carboxylate anions (Fig. 7) that repelled each other, which in combination with the high solubility of oxaprozin in basic conditions led to a significantly higher drug release rate.

Comparison of oxaprozin and ciprofloxacin release curves under different pH conditions demonstrates higher release rates in the case of ciprofloxacin, which indicates higher release tendency of this drug under the applied *in vitro* conditions. This result can be assigned to the ability of this molecule to be in different ionic states.

The *in vitro* oxaprozin and ciprofloxacin release in simulated GIT conditions followed similar trends as in corresponding pH conditions (Fig. 6E). For example, during the first two hours of release in simulated gastric conditions (at pH 1.2), the PMAA-P1.0 hydrogel released more than 0.6 mg of ciprofloxacin, which was more than 70 % of the released amount during 10 h of the experiment at this pH. This means that most of ciprofloxacin would be released in the stomach. On the other hand, during the first 2 h of release in simulated gastric conditions, the same hydrogel released only 30 % of the total amount of oxaprozin released during the experiment at pH 1.2. Most of this drug (≈ 60 %) was released when the hydrogel was transferred to simulated colonic conditions (pH 7.4). The obtained results indicated that PEGDA-crosslinked PMAA hydrogels were more suitable for colon-targeted delivery of oxaprozin in comparison with ciprofloxacin.

4. CONCLUSION

Novel PEGDA-crosslinked PMAA hydrogels were successfully synthesized and investigated for drug delivery applications. Increase in the PEGDA content significantly improved the degree of conversion, compressive mechanical properties and thermal stability of the PMAA hydrogels, while reducing the swelling capacity. The experiments

confirmed an effective crosslinking of PMAA hydrogels by this crosslinker, which is nontoxic and relatively biocompatible. The hydrogels retained the pH-sensitive behavior, which was confirmed by oscillating swelling-deswelling experiments, and swelling studies in simulated GIT conditions. Drug release profiles from the hydrogels demonstrated dependence on the physicochemical properties of the released drug, as a consequence of different physical interactions between the functional groups of the matrix and drug, as well as between the drug and medium. Overall, the presented work demonstrated the possibility to apply PEGDA as a crosslinker for vinyl-based hydrogels, which would be greatly beneficial especially in biomedical applications. Furthermore, such hydrogels can be effectively applied as a vehicle for controlled drug delivery in the gastrointestinal tract.

Acknowledgements: The authors would like to acknowledge the financial support of the Ministry of Education, Science and Technological Development of the Republic of Serbia (Contracts No. 451-03-68/2022-14/200287, 451-03-68/2022-14/200135, 451-03-9/2021-14/200026 and 451-03-68/2022-14/200178).

REFERENCES

[1] Bashari A, Rouhani Shirvan A, Shakeri M. Cellulose-based hydrogels for personal care products. *Polym Adv Technol.* 2018; 29(12): 2853-2867 https://doi.org/10.1002/pat.4290.

[2] Valuev LI, Valuev IL, Vanchugova L V, Obydennova I V. Glucose-Sensitive Hydrogels for the Controlled Release of Insulin. *Polym Sci Ser A.* 2018; 60(4): 495-498 https://doi.org/10.1134/S0965545X18040132.

[3] Popova E V, Morozova P V, Uspenskaya M V, Radilov AS. Sodium alginate and carbopol microcapsules: preparation, polyphenol encapsulation and release efficiency. *Russ Chem Bull.* 2021; 70(7): 1335-1340 https://doi.org/10.1007/s11172-021-3220-5.

[4] Bogdanova LR, Rogov AM, Zueva OS, Zuev YF. Lipase enzymatic microreactor in polysaccharide hydrogel: structure and properties. *Russ Chem Bull.* 2019; 68(2): 400-404 https://doi.org/10.1007/s11172-019-2399-1.

[5] Kadimaliev DA, Devyataeva AA, Grunyushkin IP, Malafeev AN, Revin V V. Influence of Bacterial Cellulose Gel Film Modification on Its Mechanical Properties and Ability to Covalently Bind Enzymes. *Polym Sci Ser B.* 2021; 63(3): 232-238 https://doi.org/10.1134/S1560090421030088.

[6] Shewan HM, Stokes JR. Review of techniques to manufacture micro-hydrogel particles for the food industry and their applications. *J Food Eng.* 2013; 119(4): 781-792 https://doi.org/10.1016/j.jfoodeng.2013.06.046.

[7] Ilyasov LO, Panova IG, Khrabrov NA, Kushchev PO, Loiko NG, Nikolaev YA, Yaroslavov AA. Loosely Crosslinked Hydrogel with Combined Water-Retaining and Anti-Erosion Effect. *Polym Sci Ser B.* 2021; 63(6): 866-873 https://doi.org/10.1134/S1560090421060105.

[8] Panova IG, Ilyasov LO, Khaidapova DD, Ogawa K, Adachi Y, Yaroslavov AA. Polyelectrolytic Gels for Stabilizing Sand Soil against Wind Erosion. *Polym Sci Ser B.* 2020; 62(5): 491-498 https://doi.org/10.1134/S1560090420050103.

[9] Temel S, Yaman E, Ozbay N, Gokmen FO. Synthesis, characterization and adsorption studies of nano-composite hydrogels and the effect of SiO_2 on the capacity for the removal of Methylene Blue dye. *J Serb Chem Soc.* 2020; 85(7): 939-952 https://doi.org/10.2298/JSC190517114T.

[10] Bogdanova LR, Makarova AO, Zueva OS, Zakharova LY, Zuev YF. Encapsulation of diagnostic dyes in the polysaccharide matrix modified by carbon nanotubes. *Russ Chem Bull.* 2020; 69(3): 590-595 https://doi.org/10.1007/s11172-020-2803-x.

[11] Huang X, Wang C, Ao X, Li C, Yang L. Preparation and Properties of Cellulose Nanofiber-Reinforced Ionic Conductive Hydrogels Sensor. *Polym Sci Ser A.* 2022; 64(6): 765-774 https://doi.org/10.1134/S0965545X22700420.

[12] Radonjić M, Petrović J, Milivojević M, Stevanović M, Stojkovska J, Obradović B. Chemical engineering methods in analyses of 3d cancer cell cultures: hydrodynamic and mass transport considerations: Scientific paper. *Chem Ind Chem Eng Q.* 2022; 28(3): 211-223 https://doi.org/10.2298/CICEQ210607033R.

[13] Sultanova EM, Oripova MZ, Oshchepkova YI, Salikhov SI. Chitosan-Based Hydrogel Composition with Megosine. *Pharm Chem J.* 2020; 54(5): 514-517 https://doi.org/10.1007/s11094-020-02230-x.

[14] Gorshkova MY, Vanchugova L V, Volkova IF, Obydennova I V, Valuev IL, Valuev LI. Novel mucoadhesive carriers based on alginate-acrylamide hydrogels for drug delivery. *Mendeleev Commun.* 2022; 32(2): 189-191 https://doi.org/10.1016/j.mencom.2022.03.012.

[15] Len'shina NA, Konev AN, Baten'kin AA, *et al.* Alginate Functionalization for the Microencapsulation of Insulin Producing Cells. *Polym Sci Ser B.* 2021; 63(6): 640-656 https://doi.org/10.1134/S1560090421060129.

[16] Dubashynskaya N V, Petrova VA, Romanov DP, Skorik YA. pH-Sensitive Drug Delivery System Based on Chitin Nanowhiskers-Sodium Alginate Polyelectrolyte Complex. *Materials.* 2022; 15(17): 5860 https://doi.org/10.3390/ma15175860.

[17] Gorshkova MY, Volkova IF, Grigoryan ES, Valuev LI. Sodium Alginate Interpolymer Complexes as a Platform for pH-Tunable Drug Carriers. *Polym Sci Ser B.* 2020; 62(6): 678-684 https://doi.org/10.1134/S1560090420060044.

[18] Odinokov A V, Dzhons DY, Budruev A V, Mochalova AE, Smirnova LA. Chitosan modified with terephthaloyl diazide as a drug delivery system. *Russ Chem Bull.* 2016; 65(4): 1122-1130 https://doi.org/10.1007/s11172-016-1423-y.

[19] Mirković I, Nikolić MS, Ostojić S, Maletaškić J, Petrović Z, Djonlagić J. Thermo-responsive hydrogels based on poly(N-isopropyl-acrylamide) and hyaluronic acid cross-linked with nanoclays. *J Serb Chem Soc.* 2020; 85(9): 1197-1221 https://doi.org/10.2298/JSC200109023M.

[20] Urošević MZ, Nikolić LB, Ilić-Stojanović S, Zdravković A, Nikolić V. Synthesis and characterization of poly(N-isopropylmethacrylamide-co-N-isopropylacrylamide) copolymers. *Hem Ind.* 2020; 74(2): 103-117 https://doi.org/10.2298/HEMIND190717007U.

[21] Xiang T, Lu T, Zhao W-F, Zhao C-S. Ionic-Strength Responsive Zwitterionic Copolymer Hydrogels with Tunable Swelling and Adsorption Behaviors. *Langmuir.* 2019; 35(5): 1146-1155 https://doi.org/10.1021/acs.langmuir.8b01719.

[22] Zhao Y-L, Stoddart JF. Azobenzene-Based Light-Responsive Hydrogel System. *Langmuir.* 2009; 25(15): 8442-8446 https://doi.org/10.1021/la804316u.

[23] Markovic MD, Seslija SI, Ugrinovic VD, Kunaver M, Panic VV, Pjanovic RV, Spasojevic PM. Green pH- and magnetic-responsive hybrid hydrogels based on poly(methacrylic acid) and Eucalyptus wood nanocellulose for controlled release of ibuprofen. *Cellulose.* 2021; 28(17): 11109-11132 https://doi.org/10.1007/s10570-021-04222-w.

[24] Qi X, Wei W, Li J, Liu Y, Hu X, Zhang J, Bi L, Dong W. Fabrication and Characterization of a Novel Anticancer Drug Delivery System: Salecan/Poly(methacrylic acid) Semi-interpenetrating Polymer Network Hydrogel. *ACS Biomater Sci Eng.* 2015; 1(12): 1287-1299 https://doi.org/10.1021/acsbiomaterials.5b00346.

[25] Panic V, Adnadjevic B, Velickovic S, Jovanovic J. The effects of the synthesis parameters on the xerogels structures and on the swelling parameters of the poly(methacrylic acid) hydrogels. *Chem Eng J.* 2010; 156(1): 206-214 https://doi.org/10.1016/J.CEJ.2009.10.040.

[26] Prusty K, Biswal A, Biswal SB, Swain SK. Synthesis of soy protein/polyacrylamide nanocomposite hydrogels for delivery of ciprofloxacin drug. *Mater Chem Phys.* 2019; 234: 378-389 https://doi.org/10.1016/j.matchemphys.2019.05.038.

[27] Markovic MD, Panic VV, Seslija SI, Spasojevic PM, Ugrinovic VD, Boskovic-Vragolovic NM, Pjanovic RV. Modification of hydrophilic polymer network to design a carrier for a poorly water-soluble substance. *Polym Eng Sci.* 2020; 60(10): 2496-2510 https://doi.org/10.1002/pen.25487.

[28] Ugrinovic V, Panic V, Spasojevic P, Seslija S, Bozic B, Petrovic R, Janackovic D, Veljovic D. Strong and tough, pH sensible, interpenetrating network hydrogels based on gelatin and poly(methacrylic acid). *Polym Eng Sci.* 2022; 62(3): 622-636 https://doi.org/10.1002/pen.25870.

[29] Das D, Ghosh P, Dhara S, Panda AB, Pal S. Dextrin and Poly(acrylic acid)-Based Biodegradable, Non-Cytotoxic, Chemically Cross-Linked Hydrogel for Sustained Release of Ornidazole and Ciprofloxacin. *ACS Appl Mater Interfaces.* 2015; 7(8): 4791-4803 https://doi.org/10.1021/am508712e.

[30] Fan W, Zhang Z, Liu Y, Wang J, Li Z, Wang M. Shape memory polyacrylamide/gelatin hydrogel with controllable mechanical and drug release properties potential for wound dressing application. *Polymer.* 2021; 226: 123786 https://doi.org/10.1016/j.polymer.2021.123786.

[31] Tu C-W, Tsai F-C, Chen J-K, *et al.* Preparations of Tough and Conductive PAMPS/PAA Double Network Hydrogels Containing Cellulose Nanofibers and Polypyrroles. *Polymers.* 2020; 12(12): 2835 https://doi.org/10.3390/polym12122835.

[32] D'souza AA, Shegokar R. Polyethylene glycol (PEG): a versatile polymer for pharmaceutical applications. *Expert Opin Drug Deliv.* 2016; 13(9): 1257-1275 https://doi.org/10.1080/17425247.2016.1182485.

[33] Koga T, Tomimori K, Higashi N. Transparent, High-Strength, and Shape Memory Hydrogels from Thermo-Responsive Amino Acid-Derived Vinyl Polymer Networks. *Macromol Rapid Commun.* 2020; 41(7): 1900650 https://doi.org/10.1002/marc.201900650.

[34] Nalampang K, Panjakha R, Molloy R, Tighe BJ. Structural effects in photopolymerized sodium AMPS hydrogels crosslinked with poly(ethylene glycol) diacrylate for use as burn dressings. *J Biomater Sci Polym Ed.* 2013; 24(11): 1291-1304 https://doi.org/10.1080/09205063.2012.755601.

[35] Zhong C, Wu J, Reinhart-King CA, Chu CC. Synthesis, characterization and cytotoxicity of photo-crosslinked maleic chitosan-polyethylene glycol diacrylate hybrid hydrogels. *Acta Biomater* 2010; 6(10): 3908-3918 https://doi.org/10.1016/j.actbio.2010.04.011.

[36] Cao H, Wang Q, Li M, Chen Z. Synthesis of stimuli-responsive poly(ethylene glycol) diacrylate/methacrylic acid-based nanogels and their application as drug delivery vehicle. *Colloid Polym Sci.* 2015; 293(2): 441-451 https://doi.org/10.1007/s00396-014-3422-6.

[37] Das D, Pal S. Dextrin/poly (HEMA): pH responsive porous hydrogel for controlled release of ciprofloxacin. *Int J Biol Macromol.* 2015; 72: 171-178 https://doi.org/10.1016/j.ijbiomac.2014.08.007.

[38] Hanna DH, Saad GR. Encapsulation of ciprofloxacin within modified xanthan gum- chitosan based hydrogel for drug delivery. *Bioorg Chem.* 2019; 84: 115-124 https://doi.org/10.1016/j.bioorg.2018.11.036.

[39] Lazou M, Hatzidimitriou AG, Papadopoulos AN, Psomas G. Zinc-oxaprozin compounds: Synthesis, structure and biological activity. *J Inorg Biochem.* 2019; 195: 101-110 https://doi.org/10.1016/j.jinorgbio.2019.03.016.

[40] Jamar R, Dequeker J. Oxaprozin versus aspirin in rheumatoid arthritis: a double-blind trial. *Curr Med Res Opin.* 1978; 5(6): 433-438 https://doi.org/10.1185/03007997809111911.

[41] Peng S, Duggan A. Gastrointestinal adverse effects of non-steroidal anti-inflammatory drugs. *Expert Opin Drug Saf.* 2005; 4(2): 157-169 https://doi.org/10.1517/14740338.4.2.157.

[42] Brown K. Oxazoles. U.S. Patent No. 3,578,671, 1971
[43] Božić B, Rogan J, Poleti D, Trišović N, Božić B, Uščumlić G. Synthesis, characterization and antiproliferative activity of transition metal complexes with 3-(4, 5-diphenyl-1, 3-oxazol-2-yl) propanoic acid (oxaprozin). *Chem Pharm Bull.* 2012; 60(7): 865-869 https://doi.org/10.1248/cpb.c12-00185.
[44] Ribeiro LNM, Alcântara ACS, Darder M, Aranda P, Araújo-Moreira FM, Ruiz-Hitzky E. Pectin-coated chitosan-LDH bionanocomposite beads as potential systems for colon-targeted drug delivery. *Int J Pharm.* 2014; 463(1): 1-9 https://doi.org/10.1016/j.ijpharm.2013.12.035.
[45] Hervás Pérez JP, López-Ruiz B, López-Cabarcos E. Synthesis and characterization of microparticles based on poly-methacrylic acid with glucose oxidase for biosensor applications. *Talanta.* 2016; 149: 310-318 https://doi.org/10.1016/j.talanta.2015.11.053.
[46] McAvoy K, Jones D, Thakur RRS. Synthesis and Characterisation of Photocrosslinked poly(ethylene glycol) diacrylate Implants for Sustained Ocular Drug Delivery. *Pharm Res.* 2018; 35(2): 36 https://doi.org/10.1007/s11095-017-2298-9.
[47] Lei J, Mayer C, Freger V, Ulbricht M. Synthesis and Characterization of Poly(ethylene glycol) Methacrylate Based Hydrogel Networks for Anti-Biofouling Applications. *Macromol Mater Eng.* 2013; 298(9): 967-980 https://doi.org/10.1002/mame.201200297.
[48] Kucharski M, Lubczak R. Copolymerization of hydroxyalkyl methacrylates with acrylamide and methacrylamide I. Determination of reactivity ratios. *J Appl Polym Sci.* 1997; 64(7): 1259-1265 https://doi.org/10.1002/(SICI)1097-4628(19970516)64:7<1259::AID-APP3>3.0.CO;2-I.
[49] Fyfe CA, McKinnon MS. Investigation of the thermal degradation of poly(acrylic acid) and poly(methacrylic acid) by high-resolution carbon-13 CP/MAS NMR spectroscopy. *Macromolecules.* 1986; 19(7): 1909-1912 https://doi.org/10.1021/ma00161a021.
[50] Schild HG. Thermal degradation of poly(methacrylic acid): Further studies applying TGA/FTIR. *J Polym Sci Part A Polym Chem.* 1993; 31(9): 2403-2405 https://doi.org/10.1002/pola.1993.080310925.
[51] Yang F, Zhao J, Koshut WJ, Watt J, Riboh JC, Gall K, Wiley BJ. A Synthetic Hydrogel Composite with the Mechanical Behavior and Durability of Cartilage. *Adv Funct Mater.* 2020; 30(36): 2003451 https://doi.org/10.1002/adfm.202003451.
[52] Czyrski A. The spectrophotometric determination of lipophilicity and dissociation constants of ciprofloxacin and levofloxacin. *Spectrochim Acta Part A Mol Biomol Spectrosc.* 2022; 265: 120343 https://doi.org/10.1016/j.saa.2021.120343.

Хидрогелови на бази поли(метакрилне киселине) умрежени коришћењем поли(етилен-гликол) диакрилата, као pH-осетљиви носачи за контролисано отпуштање лекова

Вукашин Ђ. Угриновић[1], Маја Д. Марковић[1], Бојан Ђ. Божић[2], Весна В. Панић[1] и Ђорђе Н. Вељовић[3]

[1]Иновациони центар Технолошко-металуршког факултета, Београд, Србија
[2]Универзитет у Београду, Институт за биологију и биохемију „Иван Ђаја“,Београд, Србија
[3]Универзитет у Београду, Технолошко-металуршки факултет, Београд, Србија

(Научни рад)

Извод

Због своје биокомпатибилне, високо-порозне структуре и могућности да носе и контролисано отпуштају лекове, хидрогелови су нашли широку примену у биомедицини. У овом раду, хидрогелови на бази поли(метакрилне киселине) (ПМК), умрежени помоћу поли(етилен-гликол) диакрилата (ПЕГДА), синтетисани су методом топлотно-индуковане слободно-радикалске полимеризације. Испитан је утицај садржаја ПЕГДА на својства хидрогелова и упоређен са утицајем најчешће коришћеног умреживача – *N,N'* – метиленбисакриламида (МБА). Повећање количине оба умреживача довело је до већег степена умрежења, што је било манифестовано повећањем степена конверзије мономера, смањењем равнотежног степена бубрења и побољшаним топлотним и механичким својствима. Такође, хидрогелови умрежени помоћу ПЕГДА показали су већи степен умрежења у односу на одговарајуће хидрогелове умрежене помоћу МБА. Могућност примене добијених хидрогелова за контролисано отпуштање лекова, испитивано је коришћењем два лека – оксапрозина и ципрофлоксацина. In vitro тестови отпуштања показали су да пресудан утицај на кинетику отпуштања имају међусобне интеракције између лека, хидрогела и медијума, а не степен и брзина бубрења хидрогела. Према томе, отпуштање ципрофлоксацина је било интензивније у киселој средини, а оксапрозина у базној. Отпуштање у симулираним гастроинтестиналним условима показало је да су ПЕГДА-умрежени хидрогелови погодни за контролисано отпуштање оксапрозина у дебело црево..

Кључне речи: Паметни материјали; колон-циљано отпуштање лекова; ципрофлоксацин; оксапрозин

Optimization of the extraction process from *Satureja montana* L.: physicochemical characterization of the extracts

Natalija Čutović[1], Petar Batinić[1], Tatjana Marković[1], Dragoja Radanović[1], Aleksandar Marinković[2], Branko Bugarski[2] and Aleksandra A. Jovanović[3]

[1]*Institute for Medicinal Plants Research "Dr Josif Pančić", Belgrade, Serbia*
[2]*University of Belgrade, Faculty of Technology and Metallurgy, Belgrade, Serbia*
[3]*University of Belgrade, Institute for the Application of Nuclear Energy INEP, Belgrade, Serbia*

Abstract

The presented study aimed to optimize polyphenol extraction from *Satureja montana* L. obtained from the experimental field of the Institute for Medicinal Plants Research "Dr Josif Pančić", Serbia, by varying the most important parameters for maceration, solid-to-solvent ratio, and extraction time. The obtained extracts were characterized regarding the total polyphenol content (TPC), total flavonoid content (TFC), antioxidant potential, extraction yield, conductivity, density, surface tension, and viscosity. The TPC and TFC were ~7 to 92 mg GAE (gallic acid equivalent)/g and 3.7 to 10.9 mg CE (catechin equivalent)/g, respectively. The highest extraction yield (86 %) as well as the highest antioxidant activities were obtained for the extracts prepared using a solid-to-solvent ratio of 1 g :50 cm^3. On the other hand, the extraction time did not have a significant influence. The highest conductivity was measured in the extract prepared at a 1 g :10 cm^3 ratio, while the highest density and surface tension were in the extract prepared at a 1 g :40 cm^3 ratio (941 kg m^{-3} and 29.0 mN m^{-1}, respectively). The highest viscosity was measured in the extract prepared at a 1 g : 20 cm^3 ratio (2.89 mPa·s). Our study shows the possibilities for the production of polyphenol-rich extract of *S. montana* which might be used in pharmaceutical, food, or cosmetic products.

Keywords: antioxidant activity; flavonoids; isolation; polyphenols; winter savory.

Available on-line at the Journal web address: http://www.ache.org.rs/HI/

ORIGINAL SCIENTIFIC PAPER

UDC: 615.451.1:544.344.016

Hem. Ind. **77(4)** 251-263 (2023)

1. INTRODUCTION

The *Satureja* genus comprises about 30 species [1], but due to the ease of cross-pollination, the same genus comprises also a great number of subspecies and varieties. However, only nine species from this genus may be found in the central and western Balkans, including Serbia [2]. One of the species is *Satureja montana* L., also known by its common name, winter savory. It is a perennial, semi-evergreen medicinal and aromatic species, which spontaneously grows in the sub-Mediterranean area [2], preferably in arid, sunny, stony, and rocky settings [3].

Ever since ancient times, *S. montana* has been used for medicinal purposes, as it exhibits good antioxidant, stimulant, mutagenic, anti-inflammatory, and many other beneficial biological activities [4]. In addition to its long-standing use in folk medicine, numerous scientific studies have already demonstrated its significant pharmacological efficacy, including antimicrobial activity against a variety of multidrug-resistant pathogens [5-9], as well as diuretic [10], antidiarrheal, and antispasmodic [11], anti-HIV-1 [12], antioxidant [6,13], anticholinesterase [8], and cytotoxic activities [14].

The chemical composition of *S. montana* extracts is characterized by the presence of polyphenolic compounds. Simple polyphenols, phenolic acids (derivatives of benzoic and cinnamic acids), lignans, lignins, coumarins, styrylpyrones, flavonoids, stilbenes, flavonolignans, and tannins are only a few of the many phytochemicals classified as plant phenolics [15]. The identification and measurement of polyphenolic compounds can provide important information on the role of polyphenols as antioxidants, their influence on the quality of food, and potential health benefits.

Corresponding authors: Natalija Čutović, Institute for Medicinal Plants Research "Dr Josif Pančić", Belgrade, Serbia
E-mail: ncutovic@mocbilja.rs
Paper received: 13 December 2022; Paper accepted: 21 August 2023; Paper published: 24 August 2023.
https://doi.org/10.2298/HEMIND221213020C

Due to their robust antioxidant properties and prevalence in a wide variety of regularly consumed fruits, vegetables, and spices, phenolic compounds have recently attracted significant attention as potential preventative measures against cancer and heart disorders [16]. It is widely acknowledged that the reactivity of the phenolic moiety causes phenolic compounds to serve as antioxidants. Biological activities of phenolic compounds have been the subject of several investigations [17-20] including anti-inflammatory, anti-ulcer, antispasmodic, antiviral, antidiarrheal, and antitumor effects [21].

By scavenging free radicals and lowering oxidative stress, antioxidants can postpone, limit, or completely halt oxidation of an oxidizable substrate. Antioxidants from outside sources are necessary in these circumstances to counteract the harmful effects of oxidative stress. A variety of putative pathways have been indicated as routes in which polyphenols might function as antioxidants. The most significant mechanism of their antioxidant activity is free radical scavenging, in which polyphenols can stop a free radical chain reaction, as well as suppress free radical formation by controlling the enzyme activity or chelating metal ions involved in free radical production.

Extraction is a method used in separation processes of target substances from a mixture. The mixture, specifically plant material, is brought into contact with a solvent, in which target substances are soluble. A widely known type of extraction of plant material is maceration. It entails immersing the plant material in a liquid (such as water, oil, alcohol, *etc*.) within an airtight container during different extraction times, depending on the plant material and liquid employed. The only disadvantage of this method in comparison to others is the extended period for obtaining the products [22,23]. As polyphenols from various plant materials have different structures, optimization of the extraction process is essential. Therefore, extraction of target compounds from particular plant material should be examined by varying extraction parameters, such as time, extraction medium, temperature, pH, solid-to-solvent ratio, *etc*. [23].

In the present study, the obtained extracts of *S. montana* were characterized *via* analyzing total polyphenol content (TPC), total flavonoid content (TFC), antioxidant potential (2,2'-azino-bis(3-ethylbenzothiazoline-6-sulfonic acid (ABTS), 2,2-Diphenyl-1-picrylhydrazyl (DPPH), ferric ion reducing antioxidant power (FRAP), and cupric ion reducing antioxidant capacity (CUPRAC) assays), conductivity, density, surface tension, and viscosity (Figure 1), with the aim to optimize the extraction time and solid-to-solvent ratio for achieving the highest extraction efficiency.

Figure 1. Flow diagram of the extraction process and the physico-chemical characterization of the extracts

2. EXPERIMENTAL

2. 1. Plant material and reagents

Plant material used in this study derives from a six year old plant cultivated during a trial with *S. montana* of a very rare chemotype of its essential oil, ct. thymol (≈70 wt.%). Cultivation was conducted at the experimental field of the Institute for Medicinal Plants Research "Dr Josif Pančić", Pančevo, Serbia. The following reagents were used: Folin-Ciocalteu reagent, 2,2-diphenyl-1-picrylhydrazyl (DPPH), potassium ferricyanide, gallic acid, catechin, (±)-6-Hydroxy-2,5,7,8-tetramethylchromane-2-carboxylic acid-Trolox, iron(II)sulfate, and iron(III)chloride bought from Sigma Aldrich (USA), sodium-carbonate from Zdravlje (Serbia), sodium nitrite from Alkaloid Skopje (Macedonia), aluminum chloride, and trichloroacetic acid from Kemika (Croatia), sodium hydroxide from NRK Inženjering (Serbia), 2,2'-azino-bis(3-ethyl-benzothiazoline-6-sulfonic acid)-ABTS$^{\bullet+}$ from Roche Diagnostics GmbH (Germany), neocuproine from Acros Organics (Belgium), monosodium phosphate and disodium phosphate from Merck (USA), cuprum chloride from Fluka (Germany), ammonium acetate and ethanol from Zorka Pharma (Serbia).

2. 2. Preparation of the extracts

S. montana extracts were obtained in maceration (25 °C), using different extraction times (15, 30, 45, 60, 90, and 120 min) and solid-to-solvent ratios: 1 g :10 cm^3, 1 g :20 cm^3, 1 g :30 cm^3, 1 g :40 cm^3 and 1 g :50 cm^3 . Namely, grinded and sieved dried herb (the particle size of 0.5 mm) and extraction medium (50 % ethanol) are mixed and filtered after the extraction. The extracts were stored at 4 °C until further analyses.

2. 3. Determination of the total polyphenol content

The total polyphenol content (TPC) of the obtained *S. montana* extracts was determined by using a slightly modified Folin-Ciocalteu method, previously described in literature [24]. An appropriately diluted sample (0.02 cm^{-3}) was added to 1.5 cm^3 of distilled water and mixed with 0.1 cm^3 of the previously diluted Folin-Ciocalteu reagent (volume ratio of water : reagent is 2:1) [25]. Following this, 0.300 cm^3 of 20 wt.% Na_2CO_3 solution was added, and the mixture was filled up to the volume of 2 cm^3 using distilled water. After 2 h of the incubation in a dark place at room temperature, the absorbances were measured at a wavelength of 765 nm (1800 UV/Vis spectrophotometer, Shimadzu, Japan). The blank was obtained by mixing distilled water, extraction solvent (50 % ethanol), Folin-Ciocalteu reagent, and Na_2CO_3 solution, without adding the extract. Every sample was prepared in three parallels. Gallic acid solution was used to make the calibration curve. Results are expressed as mg of gallic acid equivalent (GAE) per g of the plant material.

2. 4. Determination of the total flavonoid content

The total flavonoid content (TFC) determination for the plant extracts was performed by using a modified version of the Smolinski-Savi method [26]. Appropriately diluted sample (0.25 cm^3) was mixed with 0.075 cm^3 of 5 wt.% solution of $NaNO_2$ and 1.250 cm^3 of distilled water. After the incubation time of 5 min, 0.15 cm^3 of 10 wt.% $AlCl_3$ solution was added, followed by the addition of 0.5 cm^3 of 1M NaOH solution [25]. The mixture was then diluted to a volume of 3 cm^3. The absorbance was measured relative to the blank sample at a wavelength of 510 nm. Catechin monohydrate was used to obtain the calibration curve. TFC was determined three times for every sample. Results are expressed as mg of catechin equivalent (CE) per g of the plant material.

2. 5. Determination of antioxidant capacity

2. 5. 1. ABTS assay

The analytical procedure published in literature [27] served as the foundation for the ABTS scavenging test with slight adjustments. The ABTS$^{\bullet+}$ solution was diluted in 96 vol.% ethanol to the absorbance value of 0.70±0.02 at a wavelength of 734 nm [19,20]. Extract sample (20 µl, diluted with 50 % ethanol in a volume ratio 1:9) was mixed with 2 cm^3 of ABTS$^{\bullet+}$ solution and incubated for 6 min in the dark at room temperature. The assay was performed in three

parallel tries. The scavenging capacity was calculated as $\Delta A = A_c - A_x$, where A_c refers to the absorbance of 2 cm^3 ABTS$^{\bullet+}$ solution and 20 µL of the solvent; A_x is the absorbance of the sample. A calibration curve was calculated by using Trolox (concentrations of 0.2-1 mM, $y = 0.374x$, where y was ΔA and x was concentration), and the antioxidant activity was expressed as µmol Trolox equivalents (TE) per g of the plant material.

2. 5. 2. DPPH assay

The DPPH assay was performed according to the procedure previously published [28] with some modifications. The DPPH$^{\bullet}$ solution was prepared by dissolving 0.252 mg of DPPH$^{\bullet}$ in 9 cm^3 of ethanol. After that, 2 cm^3 of this solution was mixed with 20 µl of the extract (diluted with 50 % ethanol in a ratio 1:9), and incubated for 20 min at room temperature, without the presence of light [25]. The absorbance was measured at 517 nm, after which the scavenging activity ($SC_{DPPH}{}^{\bullet}$) was determined according to $SC_{DPPH}=/(A_c-A_s) / A_c) 100$, where A_c is the absorbance of 2 cm^3 DPPH$^{\bullet}$ solution and 20 µL of solvent; A_s is the absorbance of the sample, and the results are presented as IC_{50} (mg cm^{-3}), *i.e*. the concentration of the extract required to neutralize 50 % of DPPH$^{\bullet}$ radicals. Values of IC_{50} were calculated from the calibration curve prepared from five different concentrations of *S. montana* extract (0.2-2 mg cm^{-3}) and inhibition of DPPH radicals, %. The analyses were performed in triplicates.

2. 5. 3. Ferric reducing antioxidant power (FRAP) assay

The ferric reducing antioxidant power (FRAP) assay is based on the capacity of the sample to reduce Fe^{2+} contained in the potassium-hexacyanoferrate complex to Fe^{3+}. Namely, 10 mL of the extract is mixed with 1 cm^{3}of phosphate buffer and 1 cm^3 of the $K_3Fe(CN)_6$ solution [29]. The mixture is incubated at 50 °C for 4 h. After the incubation, 0.5 cm^3 of the prepared sample is mixed with 0.25 cm^{-3} of 10 vol.% trichloroacetic acid solution, and following that, 0.75 cm^3 of H_2O and 0.17 cm^3 of $FeCl_3$ (0.1 % m/v) were added. The negative control contained all reagents, except the extract. The assay was determined in three parallel tries, while the absorbance was measured at 750 nm. The calibration curve was obtained using ferrous sulphate, and the results are expressed as µmol Fe^{2+}/g of the plant material.

2. 5. 4. Cupric ion reducing antioxidant capacity assay

For the cupric ion reducing antioxidant capacity (CUPRAC) assay, a mixture was prepared by adding 1 cm^3 of $CuCl_2{\times}2H_2O$, 1 cm^3 of neocuproine, and 1.2 cm^3 of ammonium acetate buffer (pH ~7) to 0.8 cm^3 of extract [30]. The sample was then incubated at room temperature, in the dark for 30 min, after which the absorbance was measured at 450 nm. The assay determination was repeated three times for every extract. The calibration curve for this method was obtained using Trolox. The acquired results are expressed as mol of Trolox equivalent (TE) per g of the plant material.

2. 6. Determination of the extraction yield

The extraction yield (*EY*) was calculated as *EY* / % =((weight of the dried sample)/(weight of the initial sample)) 100 [31].

2. 7. Conductivity measurement

Conductivity of the extracts was determined by photon correlation spectroscopy (PCS) using the instrument Zetasizer Nano Series, Nano ZS (Malvern Instruments Ltd., UK). Each sample was measured three times at room temperature.

2. 8. Density, surface tension, and viscosity measurements

Density and surface tension of *S. montana* extracts were measured by using silicon crystal (as the immersion body) and Wilhelmy plate, respectively, in the Force Tensiometer K20 (Kruss, Germany). Each sample was examined three times at room temperature.

Viscosity was determined by using the Rotavisc *lo-vi* device equipment with a VOL-C-RTD chamber, VOLS-1 adapter, and spindle (IKA, Germany). Each sample was examined three times at room temperature.

2. 9. Statistical analysis

In the present study, the statistical analysis was performed by the analysis of variance (one-way ANOVA) followed by the Duncan's *post hoc* test using the statistical software, STATISTICA 7.0 (TIBCO Software Inc., CA, USA) [23]. The differences were considered statistically significant at p <0.05, n = 3.

3. RESULTS AND DISCUSSION

Different *S. montana* extracts, obtained by using 50 vol.% ethanol at different extraction times and solid-to-solvent ratios in maceration, were examined in terms of chemical (TPC, TFC, and antioxidant potential) and physical characteristics (extraction yield, conductivity, density, surface tension, and viscosity).

3. 1. Total polyphenol and flavonoid contents in the extracts

Polyphenols, and particularly flavonoids, are the chemical components that most significantly contribute to antioxidant capabilities of extracts obtained from plant materials. As can be seen in Table 1, the extraction time had a statically significant influence on polyphenol contents in *S. montana* ethanol extracts, but not at all levels. Namely, in the first 45 min of the maceration, TPC did not differ significantly (~32 mg GAE/g), whereas the polyphenol concentration significantly rose at 60 min (34.0±0.3 mg GAE/g) and reached a plateau (results were not statistically different after 90 and 120 min, 34.6±0.7 and 34.4±0.8 mg GAE/g, respectively). The obtained results are comparable to the previous findings [25] where the highest TPC in *Thymus serpyllum* extracts was achieved at 60 min in maceration. According to the literature, concentrations of the extracted bioactive compounds are increased with the prolonged extraction time. Namely, in polyphenol extraction, there are two levels: (1) an initial increment of TPC during 15 min and (2) slow extraction after 60 min [23,32]. However, further lengthening of the extraction time can reduce the TPC, due to enzymatic degradation and oxidation of polyphenols in the aqueous phase (the extraction medium in the case of *S. montana* extracts contains 50 vol.% of water), as well as polymerization of insoluble molecules [33].

The extraction time had a statistically significant impact on total flavonoids as well (Table 1). The highest flavonoid yield was achieved after 30 min of maceration (8.0±0.1 mg CE/g) and it stayed constant up to 90 min (8.1±0.9 mg CE/g).

Table 1. *Total polyphenol content (TPC), total flavonoid content (TFC), and antioxidant capacity (ABTS, DPPH, FRAP and CUPRAC assays) of Satureja montana L. extracts obtained using different extraction times and solid-to-solvent ratios; 50 vol.% ethanol and maceration*

Extraction time, min (solid-to-solvent ratio of 1:20)	TPC, mg GAE/g	TFC, mg CE/g	ABTS, μmol TE/g	DPPH IC_{50}, mg cm^{-3}	FRAP, μmol Fe^{2+}/g	CUPRAC, mol TE/g
15	32.6±0.8^{b*}	6.7±0.2^{b}	229.5±29.2^{c}	4.01±0.24^{b}	14.2±0.5^{ab}	61.1±1.9^{a}
30	31.7±1.8^{b}	8.0±0.2^{a}	294.1±5.1^{a}	3.71±0.26^{ab}	14.0±0.4^{ab}	56.3±2.1^{b}
45	32.4±0.5^{b}	7.9±1.0^{a}	287.7±5.5^{a}	3.26±0.21^{a}	14.3±0.2^{a}	51.5±1.5^{c}
60	34.0±0.3^{a}	8.1±0.9^{a}	285.7±8.4^{a}	3.32±0.23^{a}	14.3±0.0^{a}	43.3±1.2^{d}
90	34.6±0.7^{a}	7.6±0.3^{a}	290.4±6.2^{a}	3.53±0.21^{a}	13.5±0.5^{b}	33.9±2.2^{e}
120	34.4±0.8^{a}	5.4±0.4^{c}	270.1±4.1^{b}	3.47±0.26^{a}	13.8±0.1^{b}	33.7±2.5^{f}
Solid-to-solvent ratio, g cm^{-3} ** (extraction time 30 min)						
1 : 10	7.1±0.2^{d}	3.7±0.1^{d}	147.3±1.4^{d}	6.63±0.02^{d}	7.0±0.4^{e}	15.0±0.3^{e}
1 : 20	34.0±0.3^{c}	8.1±0.9^{b}	285.5±8.1^{c}	3.32±0.03^{c}	14.3±0.0^{d}	43.3±1.2^{c}
1 : 30	50.1±1.1^{b}	10.4±0.3^{a}	426.7±5.4^{a}	2.71±0.07^{a}	20.3±0.3^{c}	37.3±1.4^{d}
1 : 40	63.6±2.4^{a}	10.9±0.3^{a}	378.2±5.1^{b}	3.04±0.15^{b}	26.7±0.2^{b}	50.4±1.1^{b}
1 : 50	52.2±2.5^{b}	5.9±0.1^{c}	441.2±17.3^{a}	3.06±0.13^{b}	34.2±0.1^{a}	78.9±1.2^{a}

*Values with different letters (a-f) in variable group showed statistically significant differences (p <0.05; n = 3; analysis of variance, Duncan's *post-hoc* test); GAE, gallic acid equivalent; CE, catechin equivalent; TE, Trolox equivalent; IC_{50} (mg/mL), the concentration of the extract required to neutralize 50 % of DPPH• radicals; **the solid-to-solvent ratio represents the mass of plant material per volume of the extraction solvent

However, a significant drop in the TFC can be noticed after 120 min (5.4±0.4 mg CE/g), probably due to the previously mentioned degradation, oxidation, and polymerization reactions that occur during extended extraction time [33]. These findings are in accordance with the literature, where the extraction times were varied in a range from 30 to 105 min,

resulting in the maximum values for both TPC and TFC obtained after a 60 min maceration process. Further extension of the extraction time over 60 min was shown to induce a decrease in both TPC and TFC values [34-36].

As was expected, the solid-to-solvent ratio had a statistically significant influence on the TP yield in all examined levels (Table 1). The lowest TPC was measured in the extract obtained using a 1 g : 10 cm^3 ratio (7.1±0.2 mg GAE/g), because of the high plant material content and thus higher viscosity of the extraction surrounding. Therefore, diffusion of polyphenolic compounds through the extraction solvent was very slow, which resulted in a lower TP yield. Further, polyphenol concentration was increased continuously with the decrease in the solid-to-solvent ratio and reached the maximum at the 1 g : 40 cm^3 ratio (63.6±2.4 mg GAE/g). This phenomenon can be explained by high solubility of polyphenolic compounds in the ethanol/water mixture, particularly glycoside forms (glucoside, fructoside, glucuronide, *etc*.). Namely, a higher quantity of the extraction medium provides faster polyphenol diffusion and recovery [23,37]. However, in the case of a 1 g : 50 cm^3 ratio, the sample added to the reaction mixture in the Folin-Ciocalteu test is quite diluted, and thus showed significantly lower TPC (52.2±2.5 mg GAE/g), which implies that the Folin-Ciocalteu reagent is not sensitive enough for the testing of samples with lower concentrations of polyphenols. Additionally, the TF yield was also increasing continuously with the decrease in the solid-to-solvent ratio up to 1 g : 30 cm^3 and 1 g : 40 cm^3 ratios (10.4±0.3 and 10.9±0.3 mg GAE/g, respectively), while there was a significant drop in the flavonoid amount at the 1 g : 50 cm^3 ratio (5.9±0.1 mg GAE/g), as in the case of polyphenol content. Despite the fact that the extracted amount of the target compounds, calculated per g of the plant material, should reach a plateau approaching the value reached in the infinite amount of the liquid solvent, in the Folin-Ciocalteu method, 20 µl of the liquid sample (the same volume for every employed solid-to-solvent ratio) was added to the reaction mixture. The added extract sample was already diluted due to the higher amount of the extraction medium, therefore, the determined flavonoid concentration was lower. Namely, in the case of *S. montana* extracts, a higher quantity of the extraction medium did not provide higher polyphenol and flavonoid concentrations in the liquid extract. Since the aim was the preparation of the liquid extract with the highest polyphenol and flavonoid contents using the lowest amount of plant material, the comparison of different solid-to-solvent ratios was carried out after the calculation of the amount of polyphenol and flavonoid contents per g of the plant material.

The gradual increase in the TP yield with the decrease in the solid-to-solvent ratio from 1 g : 10 cm^3 to 1 g : 40 cm^3 is also in accordance with the literature, where it is stated that the highest polyphenol yield values were acquired at a ratio of 1 g : 30 cm^3 [18,23]. This is also in agreement with the findings of G. D'Alessandro *et al.* [38], in regards to the increase in TPC and TFC values, with the change in the solid-to-solvent ratio, which was in this paper up to the 1 g : 40 cm^3 ratio.

3. 2. Antioxidant capacity of the extracts

The antioxidant potential of various *S. montana* extracts was determined by using four antioxidant assays (ABTS, DPPH, FRAP, and CUPRAC tests) and the results are presented in Table 1.

$ABTS^{\bullet+}$ and $DPPH^{\bullet}$ radical scavenging activities significantly rose after 15 min of maceration and were constant during 90 min, but at 120 min maceration period a significant drop only in the ABTS antioxidant activity can be noticed, which is in correlation to the lower measured TF yield (Table 1). The yield of polyphenols and flavonoids, as the main plant antioxidants in the solvent, greatly increased with the extension of the extraction duration from 15 to 90 min, as demonstrated in the study. Nevertheless, despite the longer extraction time of up to 120 min, the yield of TP stayed constant or even decreased. According to the literature, a final equilibrium between the solute concentrations (in this case antioxidants) in the solid matrix and the solvent may be attained after a specific time, could explain these phenomena well [39]. On the other hand, the extraction time did not have a statistically significant effect on the ferric reducing antioxidant power of *S. montana* extracts (Table 1). This result can be explained by the fact that apart from polyphenols, other plant compounds present in the extracts, such as unquantified phenolics and/or synergism that exists between these compounds, and other types of compounds that are characterized by a much larger molecular weight, exhibit ferric reducing antioxidant potential [40]. Namely, the mentioned substances have different solubility in various ethanol-water mixtures, thus their release can take place very quickly in the extraction medium, already at the initial phase of the extraction. Therefore, prolonged extraction time did not influence the ferric reducing antioxidant

potential. However, in the case of cupric ion reducing antioxidant capacity, extended extraction time had a significantly negative impact. In specific, antioxidant capacity was the highest after 15 min and continuously decreased up to 90 min of maceration. Some flavonoids do not contain the necessary chelating functional groups for aluminum binding used in the determination of flavonoid contents. On the other hand, the mentioned flavonoids can be responsible for the cupric ion-reducing antioxidant potential of the extracts. Therefore, this can explain a high value of the antioxidant capacity of the extract in the CUPRAC assay and a lower value of the flavonoid content and *vice versa* [41]. Park *et al.* [42] reported that the limited correlation between the CUPRAC assay results and the flavonoid content was attributable to the nature of the measuring technique; a high flavonoid content as measured by aluminum chloride colorimetry does not necessarily represent a strong antioxidant capacity. When measuring flavonoids, the $AlCl_3$ colorimetric assay [43] does not measure flavonoids that do not contain the necessary chelating functional groups for Al^{3+} binding. As a general rule, flavones and flavonols react with Al^{3+}, but flavanones and flavanonols do not complex to the same degree (*e.g.* chrysin, apigenin, luteolin, *etc*.) [43]. Additionally, some flavonoids and phenolic acids are quite sensitive to oxygen, light, or organic solvent, and susceptible to degradation under prolonged exposure times [44].

Further, the extracts prepared using 1 g : 30 cm^3 and 1 g : 50 cm^3 ratios exhibited the highest ABTS radical scavenging activity, followed by the extract obtained at the 1 g : 40 cm^3 ratio, while the extract prepared by using the 1 g : 30 cm^3 ratio has shown the highest DPPH neutralization potential (*i.e*. the lowest IC_{50}), followed by the extracts obtained at 1 g : 40 cm^3 and 1 g : 50 cm^3 ratios (Table 1). The highest ferric and cupric ion reducing antioxidant potential was measured in the extract obtained using the 1 g : 50 cm^3 ratio. The lowest antioxidant activity in all four assays was detected in the extract obtained at the 1 g : 10 cm^3 ratio, which is in correlation to the lowest polyphenol and flavonoid extracted amounts. The effects of the solid-to-solvent ratio on antioxidant capacity have only been the subject in several research studies [18,19]. But, nevertheless, it can be concluded that there is an increase in the antioxidant activity due to the decrease in the solid-to-solvent ratio until the optimal level is reached. Keeping in mind that polyphenols and flavonoids are the chemical compounds responsible for the antioxidant capacity of the extracts, and both TFC and TPC values being higher with the lower of the used solid-to-solvent ratio, it is logical for the 1 g : 10 cm^3 ratio to show the least favourable antioxidant characteristics [45].

3. 3. The extraction yield

The efficiency of the procedure used to extract specific active components from the plant material employed, such as polyphenols, tannins, flavonoids, proteins, and so forth, is indicated by the extraction yield. The extraction time did not have a statistically significant effect on the extraction yield at the solid-to-liquid ratio of 1 g : 20 cm^3 , which varied in a range from 53.6±2.8 to 57.3±3.0 % for the extracts obtained at different extraction times (Table 2).

Table 2. *Extraction yield (EY), conductivity (G), density (ρ), surface tension (γ), and viscosity (η) of Satureja montana L. extracts obtained using different extraction times and solid-to-solvent ratios; 50 % ethanol and maceration*

Extraction time, min (solid-to-solvent ratio of 1:20)	*EY* / %	*G* / mS cm^{-1}	*ρ* / kg m^{-3}	*γ* / mN m^{-1}	*η* / mPa·s
15	56.4±2.5^{a}	0.59±0.03^{ab*}	875±3^{b}	27.8±0.2^{a}	2.85±0.02^{a}
30	53.6±2.8^{a}	0.61±0.01^{a}	878±2^{b}	27.6±0.8^{a}	2.87±0.01^{a}
45	57.3±3.0^{a}	0.57±0.01^{b}	877±2^{b}	27.4±0.3^{a}	2.90±0.04^{a}
60	56.8±1.9^{a}	0.55±0.01^{b}	898±3^{a}	27.7±0.2^{a}	2.89±0.02^{a}
90	56.1±2.8^{a}	0.56±0.01^{b}	892±4^{a}	27.8±0.1^{a}	2.86±0.02^{a}
120	54.5±2.3^{a}	0.60±0.01^{a}	882±3^{b}	27.7±0.2^{a}	2.85±0.02^{a}
Solid-to-solvent ratio, g cm^{-3} ** (extraction time 30 min)					
1:10	30.6±1.5^{e}	0.91±0.03^{a}	898±1^{c}	28.1±0.1^{b}	2.77±0.01^{c}
1:20	56.8±1.9^{c}	0.55±0.01^{b}	898±2^{c}	27.7±0.2^{c}	2.89±0.02^{a}
1:30	49.9±2.5^{d}	0.48±0.01^{c}	893±4^{c}	28.3±0.2^{b}	2.62±0.01^{d}
1:40	71.6±3.0^{b}	0.40±0.01^{d}	941±2^{a}	29.0±0.1^{a}	2.84±0.01^{b}
1:50	86.0±2.9^{a}	0.29±0.01^{e}	817±2^{b}	27.2±0.4^{c}	2.42±0.01^{e}

*Values with different letters (a-e) in variable group showed statistically significant differences (p<0.05; n=3; analysis of variance, Duncan's *post-hoc* test); **the solid-to-solvent ratio represents the mass of plant material per volume of the extraction solvent

It can be seen in the literature that the extraction yield primarily depends on the extraction time, grind size, used solvent, and temperature [46]. The literature states that the extraction yield is expected to be higher with a prolonged extraction time, since the solvent can penetrate the plant more extensively [47,48], but there are also examples in accordance with our results, that show that the increase in the duration of maceration does not always lead to a higher yield, which can be related to the plant type [49].

On the other hand, the solid-to-solvent ratio significantly affected the extraction yield at the extraction time of 30 min (Table 2). Namely, the highest extraction yield was in the extract prepared using 1 g : 50 cm^3 ratio (86.0±2.9 %), while the lowest was in the extract with a 1 g : 10 cm^3 ratio (30.6±1.5 %). The presented results of the extraction yield did not correlate with the TP yield which can be explained by the fact that the amount of the extracted ballast substances, such are lipids, sugars, and proteins also influenced the value of the extraction yield [50]. The literature states that the extraction yield is expected to increase with a lower solid-to-solvent ratio [51]. This could be explained by the fact that there is an excessive amount of plant material (at a 1 g : 10 cm^3 ratio) [23]. Additionally, a higher amount of the solvent (at a lower solid-to-solvent ratio) prevents the saturation of the extraction medium, and therefore allows prolonged release of the active and non-active compounds.

3. 4. Conductivity, density, surface tension, and viscosity of the extracts

According to Suliman *et al.* [52], conductivity represents an indicator of total dissolved compounds, as well as a predictor of the antioxidant potential of a sample. The conductivity of *S. montana* extracts significantly differs only between some samples prepared at various extraction times, but without a noticeable trend due to quite low conductivity values (0.55 to 0.61 mS cm^{-1}), with some minor differences (Table 2). On the other hand, conductivity continuously decreased with the decrease in the solid-to-solvent ratio (from 0.91 to 0.29 mS cm^{-1}). According to the literature data [53], the number of ions per unit volume and their drift velocity affect the electrical conductivity of a liquid. Drift velocity of an ion depends on the strength of the electric field, the ion mass, temperature of the solution, as well as on other variables. Thus, the electrical conductivity of various liquids may have a wide range of values. One study [54] reported that plant extracts with lower conductivities showed lower antioxidant capacities. Nevertheless, this was not the case with *S. montana* ethanol extracts in the present study. The reason is probably related to different compounds in the extracts that can affect the conductivity but do not possess antioxidant potential.

Since the molecules in liquids are loosely packed, several parameters can affect the density of liquids, the most important being temperature along with the composition. As can be seen in Table 2, density of *S. montana* extracts varied from 875 to 941 kg m^{-3}, whereas the surface tension varied from 27.4 to 29.0 mN m^{-1}. However, the highest density (among the extracts obtained at different extraction times) was determined after 60 and 90 min of maceration (898±3 and 892±4 kg m^{-3}, respectively), while the extracts obtained at other extraction times had statistically significantly lower density. The extract prepared at a 1 g : 40 cm^3 ratio had the highest density (941±2 kg m^{-3}), while the extract obtained at a 1 g :50 cm^3 ratio showed the lowest density (817±2 kg m^{-3}). According to the literature [55], density correlated to the extraction yield, which was the case with some of the *S. montana* ethanol extracts obtained at different extraction times, where the density is correlated to the TPC yield as well. But in the case of *S. montana* extracts prepared at different solid-to-solvent ratios, it was the opposite (Table 2). However, this finding can be explained by the fact that the amount of the extraction solvent also influences the density of the extracts, thus lower solid-to-solvent ratio causes lower density regardless of the extraction yield and polyphenol content.

Ability of a liquid surface to operate like a stretched elastic membrane is known as surface tension. The fundamental factors affecting this physical characteristic are the forces of attraction between the particles at the interface of the liquid and gas, solid, or another liquid [56]. Surface tension did not differ significantly between the extracts obtained at different extraction times (Table 2). On the other hand, the extract obtained at the 1 g : 40 cm^3 ratio exhibited statistically significantly higher surface tension (29.0±0.1 mN m^{-1}) in comparison to the extracts obtained at other ratios, where the lowest values of surface tension were measured in extracts obtained at 1 g : 20 cm^3 and 1 g : 50 cm^3 ratios (27.7±0.2 and 27.2±0.4 mN m^{-1}, respectively). Higher surface tension is related to the relatively high interaction between water molecules by hydrogen bonds that can cause a decrease in polyphenol diffusion [57]. However, this is in

agreement only with the results of flavonoid content obtained at 1 g : 20 cm^3 and 1 g : 30 cm^3 ratios (Table 1), where *S. montana* extracts that exhibited lower surface tensions (Table 2) contained higher flavonoid amounts.

Viscosity is the measure of a liquid's resistance to flow. Viscosity often varies with the temperature generally decreasing as the temperature is increased. The viscosity of *S. montana* extracts obtained at different extraction times did not differ statistically, and values varied from 2.85 to 2.90 mPa·s. However, as was expected, the viscosity of the extracts prepared using different solid-to-solvent ratios differed significantly. Namely, the extract obtained using the 1 g : 20 cm^3 ratio has shown the highest viscosity (2.89±0.02 mPa·s), while the extract prepared at the 1 g : 50 cm^3 ratio had the lowest viscosity (2.42±0.01 mPa·s). However, it was not the case with *S. montana* ethanol extracts, where probably hydrolysis of various compounds in ethanol extracts (with higher solid to solvent ratio) resulted in a lower viscosity [58]. Namely, according to the literature data [59,60], polyphenol compounds are susceptible to degradation (hydrolytic and oxidative reactions), particularly in the surrounding water (also presented in our 50 % ethanol extracts).

3. 5. Potential applications of *Satureja montana* extracts

The present study provides information on the physicochemical properties and antioxidant potential of *S. montana* extracts. Due to the long-term use of *S. montana* as an antioxidant, anti-inflammatory, and antimicrobial agent, the obtained extracts can be implemented in dermal pharmaceutical and cosmetic formulations. However, additional investigations in terms of the antimicrobial and anti-inflammatory activities of the extracts should be performed. Furthermore, due to the diuretic, antidiarrheal, antispasmodic, anticholinesterase, and cytotoxic effects of *S. montana*, the incorporation of its extracts in food, functional food, and *per os* pharmaceutical products can be examined. In that case, the encapsulation of the extracts is necessary with the aim to improve the stability and bioavailability of the polyphenols.

4. CONCLUSION

The aim of this work was to determine the optimal extraction time and solid-to-solvent ratio for obtaining extracts from the plant material of cultivated, rare chemotype of *S. montana* (ct. thymol), with the highest total polyphenol and flavonoid contents, antioxidant activities, as well as satisfactory physical characteristics. In general, the amount of polyphenolic compounds increased with the lower solid-to-solvent ratio, and it was also the highest for the extraction period of 60 min. On the other hand, antioxidant potential in FRAP and CUPRAC assays reached the highest value after 15 min of maceration, while the highest $ABTS^{\bullet+}$ and $DPPH^{\bullet}$ neutralization capacity was obtained after a 30 min period. Additionally, antioxidant activity determined in ABTS, FRAP, and CUPRAC assays had the highest values for a solid-to-solvent ratio of 1 g : 50 cm^3 , while IC_{50} in the DPPH assay was the lowest (the highest $DPPH^{\bullet}$ radical scavenging potential) for extracts obtained at a ratio of 1 g : 30 cm^3 . Physical characteristics of the extracts did not statistically differ when the extraction time was the observed variable. However, the density and surface tension were the highest in the extract obtained at the 1 g : 40 cm^3 ratio, and the highest extract conductivity was acquired in the extract obtained at the 1 g : 10 cm^3 ratio. The extraction yield increased with the decrease in the solid-to-solvent ratio, thus being the highest for the 1 g : 50 cm^3 ratio, and the highest viscosity was found in the extract obtained at the 1 g : 20 cm^3 ratio. In conclusion, the optimized conditions for maceration process from *S. montana* depend on the future application of the extract. Future perspectives with regard to particular plant material may include its incorporation into a certain type of carrier, in order to acquire a product that might be further used in the pharmaceutical, food, or cosmetic industries.

5. NOMENCLATURE

ABTS	2,2'-azino-bis(3-ethylbenzothiazoline-6-sulphonic acid)	CE	catechin equivalent
CUPRAC	cupric ion reducing antioxidant capacity	DPPH	2,2-diphenyl-1-picrylhydrazyl
FRAP	ferric reducing antioxidant power	GAE	gallic acid equivalent
PCS	photon correlation spectroscopy	TE	Trolox equivalent
TFC	total flavonoid content	TPC	total polyphenol content

Acknowledgement: *The authors acknowledge their gratitude to the Ministry of Education, Science and Technological Development of Serbia, contract numbers 451-03-68/2022-14/200003, 451-03-68/2022-14/200287, 451-03-68/2022-14/200135, and 451-03-68/2022-14/200019.*

REFERENCES

[1] Šilić Č. Monographie der Gattungen Satureja L., Calamimtha Miller, Micromeria Bentham, Acinos Miller und Clinopodium L. *Der flora Jugoslawiens*, Zemaljski muzej BiH, Sarajevo. 1979; 24-117.

[2] Radanović D, Matković A, Đurović-Pejčev R, Marković T, Filipović V, Mrđan S, Vasin J, Preliminary results of winter savory (*Satureja montana* L.) cultivated under permeable mulch film in dry farming conditions of South Banat. *Lek Sir.* 2018; 38: 51-57 http://dx.doi.org/10.5937/leksir1838051M.

[3] Amiri H. The in vitro antioxidative properties of the essential oils and methanol extracts of *Satureja macrosiphonia* Bornm. *Nat Prod Res*. 2011; 25: 232-243 https://doi.org/10.1080/14786410903374694.

[4] Saeidnia S, Gohari AR, Manayi A, Kourepaz-Mahmoodabadi, *M. Satureja: ethnomedicine, phytochemical diversity and pharmacological activities*. Springer International Publishing, New York, USA. 2016; 9-10 https://doi.org/10.1007/978-3-319-25026-7.

[5] Ciani M, Menghini L, Mariani F, Pagiotti R, Menghini A, Fatichenti F, Antimicrobial properties of essential oil of *Satureja montana* L. on pathogenic and spoilage yeasts. *Biotechnol Lett*. 2000; 22: 1007-1010 https://doi.org/10.1023/A:1005649506369.

[6] Ćavar S, Maksimović M, Šolić ME, Jerković-Mujkić A, Bešta R, Chemical composition and antioxidant and antimicrobial activity of two *Satureja* essential oils. *Food Chem*. 2008; 111: 648-653 https://doi.org/10.1016/j.foodchem.2008.04.033.

[7] Panizzi L, Flaminib G, Cionib PL, Morelli I, Composition and antimicrobial properties of essential oils of four Mediterranean Lamiaceae. *J Ethnopharmacol*. 1993; 39: 167-170 https://doi.org/10.1016/0378-8741(93)90032-Z.

[8] Silva FV, Martins A, Salta J, Neng NR, Nogueira JM, Mira D, Gaspar N, Justino J, Grosso C, Urieta JS , Palavra AM. Phytochemical profile and anticholinesterase and antimicrobial activities of supercritical versus conventional extracts of *Satureja montana*. *J Agric Food Chem*. 2009; 57: 11557-11563 https://doi.org/10.1021/jf901786p.

[9] Skočibušić M, Bežić N. Chemical composition and antimicrobial variability of *Satureja montana* L. essential oils produced during ontogenesis. *J Essent Oil Res*. 2004; 16: 387-391 https://doi.org/10.1080/10412905.2004.9698751.

[10] Stanić G, Samaržija I. Diuretic Activity of *Satureja montana* subsp. Montana extracts and oil in rats. *Phytother Res*. 1993; 7: 363-366 https://doi.org/10.1002/ptr.2650070508.

[11] Skočibušić M, Bežić N. Chemical composition and antidiarrhoeal activities of winter savory (*Satureja montana* L.) essential oil. *Pharm Biol*. 2003; 41: 622-626 https://doi.org/https://doi.org/10.1002/ptr.2650070508.

[12] Elgndi MA, Filip S, Pavlić B, Vladić J, Stanojković T, Žižak Ž, Zeković Z. Antioxidative and cytotoxic activity of essential oils and extracts of *Satureja montana* L., *Coriandrum sativum* L. and *Ocimum basilicum* L. obtained by supercritical fluid extraction. *J Supercrit Fluids.* 2017; 128: 128-137 https://doi.org/10.1016/j.supflu.2017.05.025

[13] Radonić A, Miloš M. Chemical composition and *in vitro* evaluation of antioxidant effect of free volatile compounds from *Satureja montana* L. *Free Radic Res*. 2003; 37: 673-679. https://doi.org/10.1080/1071576031000105643.

[14] Miladi H, Slama RB, Mili D, Zouari S, Bakhrouf A Ammar E. Chemical composition and cytotoxic and antioxidant activities of *Satureja montana* L. essential oil and its antibacterial potential against Salmonella spp. strains. *J Chem*. 2013; 275698 https://doi.org/10.1155/2013/275698.

[15] Dewick P.M. Medicinal Natural Products; John Wiley & Sons, Chichester, England, 2002; 121.

[16] Ćetković GS, Mandić AI, Čanadanović-Brunet JM, Djilas SM, Tumbas VT. HPLC screening of phenolic compounds in winter savory (*Satureja montana* L.) extracts. *J Liq Chromatogr Relat Technol*. 2007; 30: 293-306 https://doi.org/10.1080/10826070601063559.

[17] Čančarević A, Bugarski B, Šavikin K, Zdunić G. Biological activity and ethnopharmaceutical use of *Thymus vulgaris* and *Thymus serpyllum*. *Lek Sir.* 2013; 33: 3-17 https://scindeks.ceon.rs/article.aspx?query=ISSID%26and%2611584&page=0&sort=8&stype=0&backurl=%2fissue.aspx%3fissue%3d11584 (in Serbian)

[18] Ćujić N, Šavikin K, Janković T, Pljevljakušić D, Zdunić G, Ibrić S. Optimization of polyphenols extraction from dried chokeberry using maceration as traditional technique. *Food Chem*. 2016; 194: 135-142 https://doi.org/10.1016/j.seppur.2017.01.055.

[19] Jovanović A, Đorđević V, Zdunić G, Šavikin K, Pljevljakušić D, Bugarski B. Ultrasound-assisted extraction of polyphenols from *Thymus serpyllum* and its antioxidant activity. *Hem Ind.* 2016; 70: 391-39 https://doi.org/10.2298/HEMIND150629044.

[20] Petrović P, Ivanović K, Octrue C, Tumara M, Jovanović A, Vunduk J, Nikšić M, Pjanović R, Bugarski B, Klaus A. Immobilization of Chaga extract in alginate beads for modified release: simplicity meets efficiency. *Hem Ind*. 2019; 73: 325-335 https://doi.org/10.2298/HEMIND190819028P.

[21] Gomes F, Dias MI, Lima Â, Barros L, Rodrigues ME, Ferreira IC, Henriques M. *Satureja montana* L. and *Origanum majorana* L. decoctions: Antimicrobial activity, mode of action and phenolic characterization. *Antibiotics*. 2020; 9(6): 294 https://doi.org/10.3390/antibiotics9060294.

[22] Azmin M, Manan A, Alwi W, Chua S, Mustaffa A, Yunus A. Herbal processing and extraction technologies. *Sep Purif Rev*. 2016; 45: 305-320 https://doi.org/10.1080/15422119.2016.1145395.
[23] Jovanović A, Đorđević V, Zdunić G, Pljevljakušić D, Šavikin K, Gođevac D, Bugarski B. Optimization of the extraction process of polyphenols from *Thymus serpyllum* L., herb using maceration, heat- and ultrasound-assisted extraction. *Sep Purif Technol*. 2017; 179: 369-380 https://doi.org/10.1016/j.seppur.2017.01.055.
[24] Singleton VL, Orthofer R, Lamuela-Raventós RM. Analysis of total phenols and other oxidation substrates and antioxidants by means of Folin-Ciocalteu reagent. *Methods enzymol*. 1999; 299: 152-178 https://doi.org/10.1016/S0076-6879(99)99017-1.
[25] Jovanović A, Djordjević V, Petrović P, Pljevljakušić D, Zdunić G, Šavikin K, Bugarski B. The influence of different extraction conditions on polyphenol content, antioxidant and antimicrobial activities of wild thyme. *J Appl Res Med Aromat Plants*. 2021; 25: 100328 https://doi.org/10.1016/j.jarmap.2021.100328.
[26] Savi PDRS, dos Santos L, Goncalves AM, Biesek S, de Lima CP. Analysis of total flavonoids present in some of the most consumed conventional and organic fruits and vegetables in southern Brazil/Analise de flavonoides totais presentes em algumas frutas e hortalicas convencionais e organicas mais consumidas na regiao Sul do Brasil. *Demetra*. 2017; 12: 275-288 https://doi.org/10.12957/demetra.2017.22391
[27] Prior RL, Wu X, Schaich K. Standardized methods for the determination of antioxidant capacity and phenolics in foods and dietary supplements. *J Agric Food Chem*. 2005; 53: 4290-4302 https://doi.org/10.1016/j.ijbiomac.2013.09.025.
[28] Mensor LL, Menezes FS, Leitão GG, Reis AS, Santos TCD, Coube CS, Leitão SG. Screening of Brazilian plant extracts for antioxidant activity by the use of DPPH free radical method. *Phytother res*. 2001; 15: 127-130 https://doi.org/10.1002/ptr.687
[29] Kammoun M, Haddar M, Kossentini Kallel T, Dammakc M, Sayari F. Biological properties and biodegradation studies of chitosan biofilms plasticized with PEG and glycerol. *Int J Biol Macromol*. 2013; 62: 433-438 https://doi.org/10.1016/j.ijbiomac.2013.09.025.
[30] Milošević MD, Marinković AD, Petrović P, Klaus A, Nikolić MG, Prlainović NŽ, Cvijetić IN. Synthesis, characterization and SAR studies of bis (imino) pyridines as antioxidants, acetylcholinesterase inhibitors and antimicrobial agents. *Bioorg Chem*. 2020; 102: 104073 https://doi.org/10.1016/j.bioorg.2020.104073.
[31] Liao J, Qu B, Liu D, Zheng N. New method to enhance the extraction yield of rutin from *Sophora japonica* using a novel ultrasonic extraction system by determining optimum ultrasonic frequency. *Ultrason Sonochem*. 2015; 27: 110-116 https://doi.org/10.1016/j.ultsonch.2015.05.005.
[32] Nayak B, Dahmoune F, Moussi K, Remini H, Dairi S, Aoun O, Khodir M. Comparison of microwave, ultrasound and accelerated-assisted solvent extraction for recovery of polyphenols from *Citrus sinensis* peels. *Food Chem*. 2015; 187: 507-516 https://doi.org/10.1016/j.foodchem.2015.04.08140.
[33] Vergara-Salinas J, Pérez-Jiménez J, Torres JL, Agosin E, Pérez -Correa J. Effects of temperature and time on polyphenolic content and antioxidant activity in the pressurized hot water extraction of deodorized thyme (*Thymus vulgaris*). *J Agric Food Chem*. 2012; 60: 10920-10929 https://doi.org/10.1021/jf3027759.
[34] Alu'datt MH, Alli I, Ereifej K, Alhamad M, Al-Tawaha AR and Rababah T. Optimisation, characterisation and quantification of phenolic compounds in olive cake. *Food Chem*. 2010; 123: 117-122 https://doi.org/10.1016/j.foodchem.2010.04.011.
[35] Ghafoor K, Choi YH. Optimization of ultrasound assisted extraction of phenolic compounds and antioxidants from grape peel through response surface methodology. *J Korean Soc Appl Bi*. 2005; 52: 295-300 https://doi.org/10.3839/jksabc.2009.052.
[36] Khedher O, Rigane G, Salem RB, Moussaoui Y. Optimization of polyphenols recovery from *Schinus molle* L. peel using response surface methodology (RSM). *Chem Africa*. 2020; 3: 813-820 https://doi.org/10.1007/s42250-020-00170-3
[37] Mustafa M, Turner C. Pressurized liquid extraction as a green approach in food and herbal plants extraction. *Anal Chim Acta*. 2011; 703: 8-18 https://doi.org/10.1016/j.aca.2011.07.018.
[38] Galvan D'Alessandro L, Kriaa K, Nikov I, Dimitrov K. Ultrasound assisted extraction of polyphenols from black chokeberry. *Sep Purif Technol*. 2012; 93: 42-47 https://doi.org/10.1016/j.seppur.2012.03.024.
[39] Silva EM, Rogez H and Larondelle Y. Optimization of extraction of phenolics from Inga edulis leaves using response surface methodology. *Sep Purif Technol*. 2007; 55: 381-387 https://doi.org/10.1016/j.seppur.2007.01.008.
[40] Imeh U, Khokhar S. Distribution of conjugated and free phenols in fruits: antioxidant activity and cultivar variations. *J Agric Food Chem*. 2002; 50: 6301-6306 https://doi.org/10.1021/jf020342j.
[41] Chang CC, Yang MH, Wen HM, Chern JC. Estimation of total flavonoid content in propolis by two complementary colorimetric methods. *J Food and Drug Anal*. 2002; 10: 178-182 https://doi.org/10.38212/2224-6614.2748
[42] Park YS, Jung ST, Kang SG, Delgado-Licon E, Katrich E, Tashma Z, Trakhtenberg S, Gorinstein S. Effect of ethylene treatment on kiwifruit bioactivity. *Plant Foods Hum Nutr*. 2006; 61: 151-156 https://doi.org/10.1007/s11130-006-0025-5.
[43] Apak R, Güçlü K, Demirata B, Özyürek M, Çelik SE, Bektaşoğlu B, Berker KI, Özyurt D. Comparative evaluation of various total antioxidant capacity assays applied to phenolic compounds with the CUPRAC assay. *Molecules*. 2007; 12: 1496-1547 https://doi.org/10.3390/12071496.
[44] Shi J, Nawaz H, Pohorly J, Mittal G, Kakuda Y, Jiang Y. Extraction of polyphenolics from plant material for functional foods—Engineering and technology. *Food Rev Int*. 2005; 21: 139-166 https://doi.org/10.1081/FRI-200040606.

[45] Tan PW, Tan CP, Ho CW. Antioxidant properties: Effects of solid-to-solvent ratio on antioxidant compounds and capacities of Pegaga (*Centella asiatica*). *Int Food Res J*. 2011; 18: 557-562 http://www.ifrj.upm.edu.my/18%20(02)%202011/(13)%20IFRJ-2010-268.pdf.

[46] Farooq S, Mir SA, Shah MA, Manickavasagan A. Plant Extracts: Applications in the Food Industry. 1st ed., Cambridge, MA: Academic press; 2022: 23-37 https://doi.org/10.1016/B978-0-12-822475-5.00005-3.

[47] Cunha IDS, Sawaya ACHF, Caetano FM, Shimizu MT, Marcucci MC, Drezza FT, Povia, GS, Carvalho, PO. Factors that influence the yield and composition of Brazilian propolis. *J Brazilian Chem Soc*. 2004; 15: 964-970 https://doi.org/10.1590/S0103-50532004000600026.

[48] Trusheva B, Trunkova D, Bankova V. Different extraction methods of biologically active components from propolis: a preliminary study. *Chem Cent J*. 2007; 1: 13-17 https://doi.org/10.1186/1752-153X-1-13

[49] Ecem-Bayram N, Gercek Y. Appropriate maceration duration for the extraction of propolis. *Fresenius Environ Bull*. 2019; 28: 188-192 https://avesis.istanbul.edu.tr/publication/showdocument/5b77ffc0-8cc5-4e62-a313-34d269b3c17e

[50] Jovanović A, Vajić J, Mijin D, Zdunić G, Šavikin K, Branković S, Kitić D, Bugarski B. Polyphenol extraction in microwave reactor using by-product of *Thymus serpyllum* L. and biological potential of the extract. *J Appl Res Med Arom Plants*. 2022; 31: 100417 https://doi.org/10.1016/j.jarmap.2022.100417.

[51] Milenović DM, Veljković VB, Todorović BT, Stanković MS. Extraction of resinoids from St. John's wort (*Hypericum perforatum* L): I. Efficiency and optimization of extraction. *Hem Ind*. 2002; 56: 54-59 https://doi.org/10.2298/HEMIND0202054M.

[52] Saad R, Asmani F, Saad M, Hussain M, Khan J, Kaleemullah M, Othman NB, Tofigh A, Yusuf E. A new approach for predicting antioxidant property of herbal extracts. *Int J Pharmacogn Phytochem Res*. 2015; 7: 166-174 http://impactfactor.org/PDF/IJPPR/7/IJPPR,Vol7,Issue1,Article25.pdf

[53] Rhoades JD, Raats PAC, Prather RJ, Effects of liquid-phase electrical conductivity, water content, and surface conductivity on bulk soil electrical conductivity. *Soil Sci Soc America J.* 1976; 40: 651-655. https://doi.org/10.2136/sssaj1976.03615995004000050017x.

[54] Jurinjak Tušek A, Benković M, Valinger D, Jurina T, Belščak-Cvitanović A, Gajdoš Kljusurić J. Optimizing bioactive compounds extraction from different medicinal plants and prediction through nonlinear and linear models. *Ind Crops Prod.* 2018; 126: 449-458 https://doi.org/10.1016/j.indcrop.2018.10.040.

[55] Mladenović J, Đurić M, Šekularac G, Brković D, Stepanović J, Mašković P, Bošković Rakočević Lj. Determination of the content of bioactive components in different extracts of *Portulaca oleracea* L. *Acta Agric Serb.* 2013; 23: 223-231 https://doi.org/10.5937/AASer1846223M.

[56] Ono S, Kondo S. Structure of Liquids/Struktur der Flüssigkeiten. 1st ed., Heidelberg, DE: Springer, Berlin, 1960, 134-280 https://doi.org/10.1007/978-3-642-45947-4_2.

[57] Peng X, Duan MH, Yao XH, Zhang YH, Zhao CJ, Zu YG, Fu YJ. Green extraction of five target phenolic acids from *Lonicerae japonicae* Flos with deep eutectic solvent. *Sep Purif Technol*. 2016; 157: 249-257. https://doi.org/10.1016/j.seppur.2015.10.065.

[58] Boros D, Marquardt RR, Slominski BA, Guenter W. Extract viscosity as an indirect assay for water-soluble pentosan content in rye. *Cereal Chem.* 1993; 70: 575-580 https://www.cerealsgrains.org/publications/cc/backissues/1993/Documents/70_575.pdf

[59] Vergara-Salinas J, Pérez-Jiménez J, Torres JL, Agosin E, Pérez-Correa J. Effects of Temperature and Time on Polyphenolic Content and Antioxidant Activity in the Pressurized Hot Water Extraction of Deodorized Thyme (*Thymus vulgaris*). *J Agric Food Chem.* 2012; 60: 10920-10929. https://doi.org/10.1021/jf3027759.

[60] Vuleta G, Milić J, Savić S. Farmaceutska tehnologija. Faculty of Pharmacy, University of Belgrade: Belgrade, Serbia, 2012 ISBN: 978-86-6273-003-0 (in Serbian)

Optimizacija procesa ekstrakcije iz biljke *Satureja montana* l.: fizičkohemijska karakterizacija ekstrakata

Natalija Čutović[1], Petar Batinić[1], Tatjana Marković[1], Dragoja Radanović[1], Aleksandar Marinković[2], Branko Bugarski[2] i Aleksandra A. Jovanović[3]

[1]Institut za proučavanje lekovitog bilja "Dr Josif Pančić", Tadeuša Košćuška 1, Beograd, Srbija, Belgrade, Serbia
[2]Univerzitet u Beogradu, Tehnološko-metalurški fakultet, Karnegijeva 4, Beograd, Srbija
[3]Univerzitet u Beogradu, Institut za primenu nuklearne energije INEP, Banatska 31b, Zemun, Beograd, Srbija

(Naučni rad)

Izvod

Prikazana studija je imala za cilj da optimizuje ekstrakciju polifenola iz biljke *Satureja montana* L. sa oglednog polja Instituta za proučavanje lekovitog bilja „Dr Josif Pančić", Srbija, variranjem najvažnijih parametara maceracije, odnosa biljnog materijala i rastvarača, i ekstrakcionog vremena. Dobijeni ekstrakti su okarakterisani u pogledu ukupnog sadržaja polifenola (*engl.* total total polyphenol content, TPC), ukupnog sadržaja flavonoida (*engl.* total flavonoid content, TFC), antioksidativnog potencijala, prinosa ekstrakcije, provodljivosti, gustine, površinskog napona i viskoznosti. Vrednosti ukupnog sadržaja polifenola (*engl.* Total Polyphenol Content - TPC) i ukupnog sadržaja flavonoida (*engl.*Total Flavonoid Content - TFC) su bile u opsezima 7,2-92,2 mg ekvivalenta galne kiseline (*engl.* gallic acid equivalent GAE) / g i 3,7-10,9 mg ekvivalenta katehina (*engl.* catechin equivalent CE)/g, redom. Najveće antioksidativne aktivnosti dobijene su u ekstraktima pripremljenim u odnosu biljnog materijala i rastvarača 1 g : 50 cm^{-3}. Najveći prinos ekstrakcije takođe je dobijen u tom ekstraktu (86,0%), dok vreme ekstrakcije nije imalo značajan uticaj. Najveća provodljivost izmerena je u ekstraktu pripremljenom u odnosu biljnog materijala i rastvarača 1 g :10 cm^{-3}. Najveća gustina i površinski napon su bili u ekstraktu pripremljenom u odnosu 1 g : 40 cm^{-3} (941 kg m^{-3} i 29,0 mN m^{-1}, redom). Najveća viskoznost je izmerena u ekstraktu pripremljenom u odnosu 1 g : 20 cm^{-3} (2,89 mPa·s). Naša studija pokazuje mogućnosti za proizvodnju polifenolima bogatog ekstrakta biljke *S. montana* koji se može koristiti u farmaceutskim, prehrambenim ili kozmetičkim proizvodima..

Ključne reči: antioksidativna aktivnost; flavonoidi; izolacija; polifenoli; planinski čubar

Antimicrobial activity of different wound dressing products treated with silver

Katarina R. Mihajlovski[1], Željka Stajčić[2] and Vesna M. Lazić[3]

[1]*Faculty of Technology and Metallurgy, University of Belgrade, Belgrade, Serbia*
[2]*Koloid company, Prve pruge 7, Belgrade, Serbia*
[3]*Centre of Excellence for Photoconversion, Vinča Institute of Nuclear Sciences - National Institute of the Republic of Serbia, University of Belgrade, Belgrade, Serbia*

Abstract

The main goal of this work was to optimize the method of processing wound dressing products (like gauzes, sanitary pads, cotton wool, compresses, and bandages) with a commercial silver colloidal solution (Koloid doo, Belgrade, Serbia) and then to examine the antimicrobial properties of the obtained items in order to potentially reach the market with new improved wound dressing products. The influence of different silver concentrations used for treatment on antimicrobial activity was investigated only against *Escherichia coli*. The antimicrobial activity of different types of materials treated with silver solutions of 30 ppm was investigated against Gram-negative bacteria *Escherichia coli* and *Pseudomonas aeruginosa*, Gram-positive bacteria *Staphylococcus aureus, Bacillus subtilis,* and *Enterococcus faecalis,* as well as the fungus *Candida albicans*. The microbial reduction of the tested materials loaded with a silver solution of 30 ppm (15-20 µg of Ag on 1 g of fabric) against the Gram-negative bacteria *E. coli* and *P. aeruginosa* was almost maximal after 2 h of contact (*i.e.* 95 and 99 %, respectively). In the case of Gram-positive bacteria *S. aureus, B. subtilis*, and *E. faecalis*, a longer time is needed to completely eradicate bacteria (over 99 %). Antifungal activity testing against the fungus *C. albicans* gave moderate antifungal activity results.

Keywords: process optimization; textile materials; cotton; microorganisms; silver colloidal solution.

Available on-line at the Journal web address: http://www.ache.org.rs/HI/

TECHNICAL PAPER

UDC: 616-089.4+546.57:632.953

Hem. Ind. **77(4)** 265-273 (2023)

1. INTRODUCTION

Spreading infections by pathogenic microorganisms, especially in hospitals, is an actual and global problem. Also, due to the uncontrolled use of antibiotics, microorganisms have become more and more resistant to various antimicrobial agents known up to now. It is of great importance to find an antimicrobial agent that is non-toxic, easily available, and cheap. Also, preventing the spread of infection, especially in medical facilities, is crucial and is achieved precisely by using medical devices that already have antimicrobial properties. Medical textiles that are in constant use, provided that they exhibit antimicrobial properties, can greatly improve the situation in terms of preventing and reducing infections.

As the production of medical, healthcare, hygiene, and protective textile materials is steadily growing, interest in effective, non-toxic, long-lasting, and cost-effective antimicrobial finishing of these products is quickly rising [1,2]. In this respect, reduction in microbial survival on textile materials is crucial since germs can degrade both the fabric and the wearer's comfort. In other words, the microbial presence may have a variety of detrimental impacts, including the production of offensive odor, stains, material decolorization, and a reduction in the mechanical strength of the fabric [3,4]. Production of textiles for sports, leisure, medical non-implantables (such as bandages, plasters, gauze dressings, lint, wadding, and adsorbent pads) and healthcare/hygiene products (such as surgical gowns and hosiery, sheets, pillowcases, uniforms, and blankets) is particularly based on the use of cotton fibers [1]. However, cotton is

Corresponding authors: Vesna M. Lazić, Centre of Excellence for Photoconversion, Vinča Institute of Nuclear Sciences - National Institute of the Republic of Serbia, University of Belgrade, Mike Petrovića Alasa 12-14, Belgrade
E-mail: vesna.lazic@vin.bg.ac.rs
Paper received: 19 January 2023; Paper accepted: 24 August 2023; Paper published: 6 September 2023.
https://doi.org/10.2298/HEMIND230113021M

particularly vulnerable to microbial infection because of its extraordinary capacity to absorb moisture. Thus, cotton may serve as a nutrient, acting as a good medium for bacterial and fungal development under specific humidity and temperature circumstances [3,4].

The growing issue of multi-antibiotic-resistant microorganisms has revoked interest in silver and its compounds, which have previously been known to be effective biocides for more than 650 different microbes [5,6]. Silver can be applied to textile fabrics to provide a desired level of antibacterial activity without significantly altering the fabric color [7-11]. Also, a small concentration of silver is needed to achieve satisfactory antimicrobial effects, while being below the toxicity level of 1 mg dm^{-3} [12].

This work aimed to examine the method of processing different medical wound dressing products (gauze, sanitary pads, cotton wool, compress, and bandages) with a commercially available colloidal silver solution (company Koloid). After optimizing the process, the silver content was determined followed by examination of the antimicrobial properties of all obtained materials against Gram-negative bacteria *Escherichia coli* and *Pseudomonas aeruginosa,* Gram-positive bacteria *Staphylococcus aureus, Bacillus subtilis,* and *Enterococcus faecalis,* and the fungus *Candida albicans*.

2. EXPERIMENTAL

The cotton materials used as medical supplies in this work are gauze, sanitary pads, cotton wool, compresses, and bandages made by NIVA company (Zabalj, Serbia). Silver colloid solutions at different concentrations were made by the company Koloid doo (Belgrade, Serbia).

2. 1. Impregnation of dressing products with silver

Two processing methods were tested together with four different concentrations of the antimicrobial agent. For processing, we used a colloidal silver solution with concentrations of 2, 5, 10 and 30 ppm.

The cotton materials were processed by two methods:

1) "deep coating" - immersing 1 g of the material in the colloid solution for 30 min, then air-drying at room temperature, and
2) “micro-dispersion” – spraying the material with the colloidal silver solution in a precisely determined amount and ratio (2 cm^3 per 1 g of fabric).

2. 2. Determination of silver content

The silver content in cotton materials treated with Ag colloid solution at the concentration of 30 ppm was determined using inductively coupled plasma optic emission spectroscopy (ICP-OES Thermo Scientific iCAP 7400, producer, country). The amount of 1 g of material was immersed in 1 M nitric acid to disperse silver from the material. The concentration of silver in the solution was measured after dilution.

2. 3. Antimicrobial performance

Antimicrobial testing of cotton materials impregnated with Ag was performed by the contact method against pathogenic microorganisms, Gram-negative bacteria *Escherichia coli* ATCC 25922 and *Pseudomonas aeruginosa* ATCC 27833, Gram-positive bacteria *Staphylococcus aureus* ATCC 25923, *Bacillus subtilis* ATCC 6633, and *Enterococcus faecalis* ATCC 29812, and the fungus *Candida albicans* ATCC 10259.

The method used for antimicrobial testing is the standard method for textile materials. A 1 g cotton material sample was immersed in a 50 cm^3 saline solution containing around 10^5 CFU cm^{-3} microorganisms in a sterile 300 cm^3 Erlenmeyer flask. After the contact of 2 h and 24 h under mixing in a rotary shaker (150 rpm), 100 mm^3 of aliquot is taken for further dilution and seeded on a tryptone soy agar medium in Petri dishes, which is then thermostated at 37 °C for 24 h (48 h for *C. albicans*). Grown colonies are counted and microbial reduction (*R* / %) is calculated according to the following formula:

$$R = \frac{C_0 - C}{C_0} 100 \quad (1)$$

where C_0 is the initial number of colonies in 1 cm^3 (CFU cm^{-3}) in t = 0, while C is the number of colonies in 1 cm^3 after the contact of the sample with the bacterial suspension.

3. RESULTS AND DISCUSSION

The main purpose of the experiments carried out in this work was to optimize the process of treating several wound dressing products with a commercial silver colloidal solution (Koloid company, Serbia) to achieve the best product that can be commercialized. First, it was necessary to determine an adequate method of processing the samples, which does not significantly change the external appearance of the product and leads to improved performance. Second, the antimicrobial properties of the obtained products were determined in order to evaluate improvement in the desired performance.

In order to establish the efficiency of the processing and to choose the best method, antimicrobial activity against a reference culture the Gram (–) bacterium *E. coli* was performed (Table 1).

Table 1. *Antimicrobial activity against E. coli of samples treated with Ag colloid solutions by the "deep coating" method, after 24 h, C_0 = 290,000 CFU cm^{-3}*

Sample	Concentration of Ag in the colloid solution, ppm			
	2		5	
	C / CFU cm^{-3}	R / %	C / CFU cm^{-3}	R /%
Gauze	40,000	86.21	1,200	99.59
Sanitary pads	4,000	98.62	1,400	99.52
Cotton wool	18,000	93.79	800	99.72
Compress	2,200	99.24	300	99.90
Bandage	9,400	96.76	4,700	98.38

Treatment of the samples by the "deep coating" method gave good results using colloid solutions with low concentrations of the antimicrobial agent. In specific, 99 % of bacteria were inhibited with all tested samples treated with 5 ppm colloid. Only the bacterial reduction by the bandage was slightly lower amounting to ~98 %. This result may be due to the bandage hydrophobicity compared to other samples, so the contact between silver and bacteria is difficult due to non-wetting. Also, the hydrophobicity of the bandage could be the reason for the lower impregnation of silver. The initial number of bacteria of 10^5 was reduced to 10^2 to 10^3 after just 2 h of contact between bacteria and the sample in saline solution. Samples treated with a colloid concentration of 2 ppm induced a lower reduction of bacteria but were still considered as a good antimicrobial activity with more than 85 % reduction for all tested samples.

However, after the "deep coating" method, some of the samples lost their original shape (sanitary pads, cotton wool, and compresses). Also, this method would be slow and inadequate for the quantities of materials planned for industrial production. Because of these two reasons, another processing method was tested, that is spraying the sample with colloid solutions. The pilot process was created and owned by the company Koloid doo (Belgrade, Serbia). In the present work, the process was optimized so that 1 g of the material was sprayed with 2 cm^3 of the Ag colloidal solution.

It can be seen from Table 2 that the antimicrobial activity of all tested samples treated with a colloid concentration of 10 ppm is unsatisfactory, while samples treated with a colloid concentration of 30 ppm show excellent antimicrobial properties against *E. coli* after 2 h of contact. All further tests of antimicrobial activity against selected strains will be done with samples treated with the Ag colloid of 30 ppm.

Table 2. *Antimicrobial activity of samples processed by the micro-dispersion method against E. coli after 24 h, C_0 = 250,000 CFU cm^{-3} for 10 ppm, C_0 = 300,000 CFU cm^{-3} for 30 ppm*

Sample	Concentration of Ag in the colloidal solution, ppm			
	10		30	
	C / CFU cm^{-3}	R / %	C / CFU cm^{-3}	R / %
Gauze	110,000	56.00	40,000	92.00
Sanitary pads	160,000	36.00	6,200	98.76
Cotton wool	40,000	84.00	1,200	99.76
Compress	10,000	96.00	1,200	99.76
Bandage	60,000	76.00	700	99.86

Figure 1 presents photographs of the samples before and after the treatment showing insignificant changes in the sample shape or color.

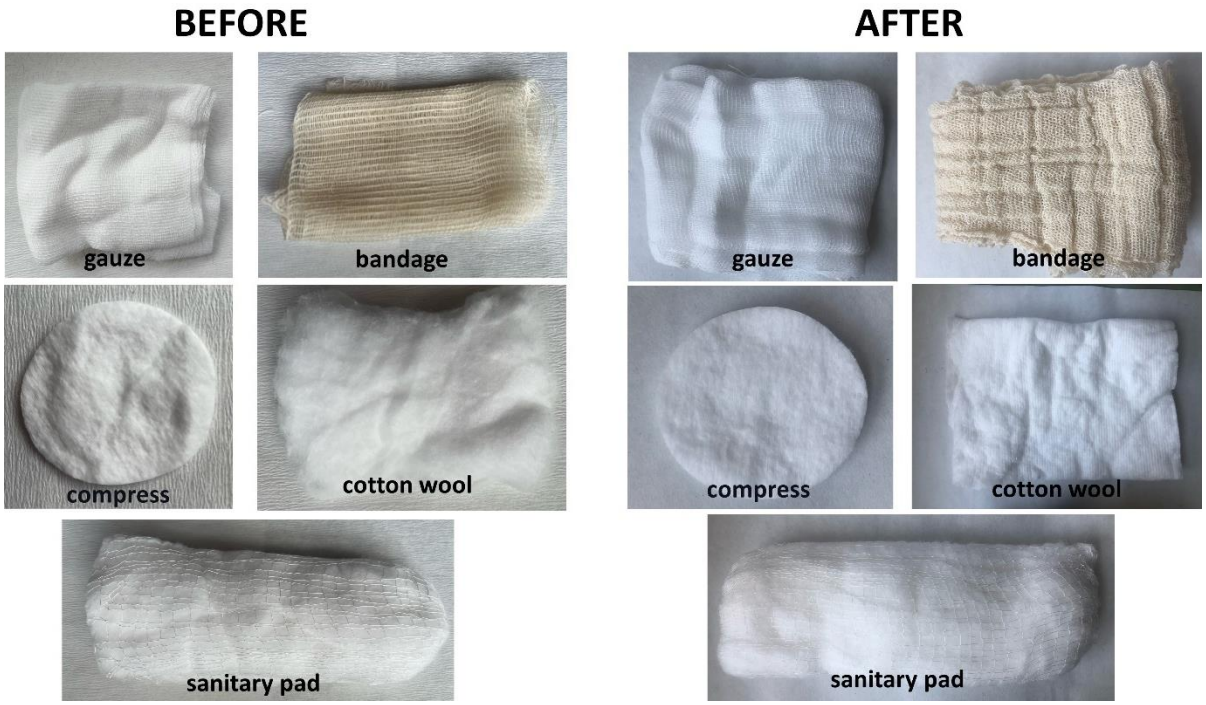

Figure 1. *Photographs of samples before and after the treatment by the micro- dispersion method with a colloidal solution with the Ag concentration of 30 ppm*

Therefore, the amount of silver that remained on 1 g of the material after treatment with the 30 ppm colloid solution was determined (Fig. 2).

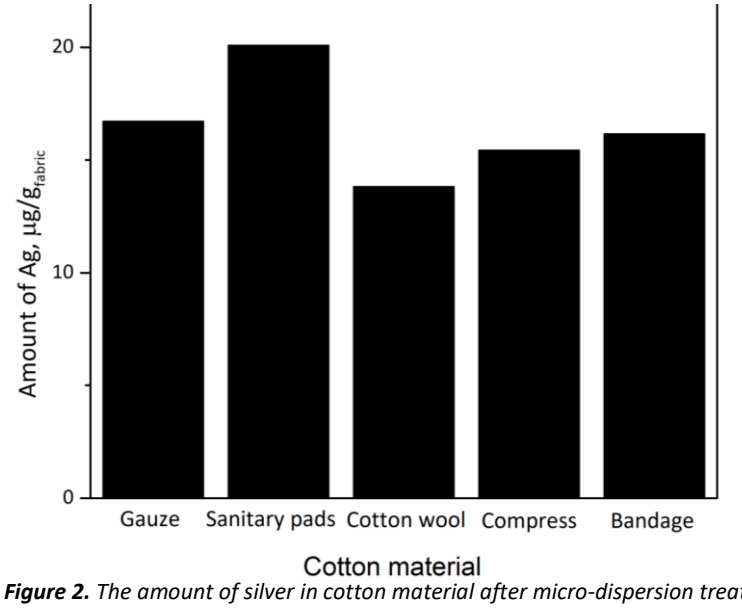

Figure 2. *The amount of silver in cotton material after micro-dispersion treatment with a 30 ppm colloidal solution*

Figure 2 shows that the amount of silver in the materials is roughly three-fold lower than that anticipated based on the processing method (2 cm^3 of the 30 ppm colloidal solution per 1 g of the material). The calculated amount should be ~60 g per 1 g of the material, but only 13-20 μg g^{-1} was measured. Given that a certain amount of Ag is lost throughout the drying and squeezing steps of processing, the outcome is to be expected.

The amount of silver found on fabrics is far below the environmental regulatory limit: 1 g of fabric immersed in 50 cm^3 of saline solution results in a silver concentration of 0.3 to 0.4 mg dm^{-3}, while the environmental toxic limit is 1 mg dm^{-3} [13]. It is important that the amount of Ag found in the material provides good antimicrobial properties to selected microorganisms, and on the other hand, that it is not toxic to the environment after use and is within the limits according to the European standards of ecological toxicity [13].

All selected microorganisms are the most common causes of infections in humans and belong to the group of strains that are often resistant to many antibiotics. Gram (–) bacteria *E. coli* is a common cause of urinary and gynaecological infections, while *P. aeruginosa* is a common hospital infection and a bacterium that lives in ventilation openings and thus easily contaminates hospitals. Representatives of Gram (+) bacteria are *S. aureus*, which is very common in skin infections and resistant to most antibiotics, then *B. subtilis,* as an example of a sporogenous microorganism, and *E. faecalis* which are also very often resistant to antibiotics and occur in the intestines and gastrointestinal tract and there cause very severe infections. Finally, one fungus, *C. albicans*, was also examined, with the most used reference pathogenic microorganism, which often appears after the use of antibiotics, multiplies quickly, and causes problems mostly in the intimate region.

Antimicrobial activity against pathogenic Gram–negative bacteria *Escherichia coli* and *Pseudomonas aeruginosa* are presented at Tables 3 and 4, respectively.

Table 3. *Antimicrobial activity of tested samples treated by the microdispersion method with the 30 ppm colloidal solution after 2 (C_0 = 500,000 CFU cm^{-3}) and 24 h (C_0 = 400,000 CFU cm^{-3}) of contact with Escherichia coli*

Sample	Time of contact with *Escherichia coli*, h			
	2		24	
	C / CFU cm^{-3}	*R* / %	*C* / CFU cm^{-3}	*R* / %
Gauze	40,000	92.00	< 10	99.99
Sanitary pads	6,200	98.76	< 10	99.99
Cotton wool	1,200	99.76	1,300	99.68
Compress	1,200	99.76	< 10	99.99
Bandage	700	99.86	1,100	99.73

Table 4. *Antimicrobial activity of tested samples treated by the micro-dispersion method with colloid concentration 30 ppm after 2 (C_0 = 900,000 CFU cm^{-3}) and 24 h (C_0 = 400,000 CFU cm^{-3}) of contact with Pseudomonas aeruginosa*

Sample	Time of contact with *Pseudomonas aeruginosa*, h			
	2		24	
	C / CFU cm^{-3}	*R* / %	*C* / CFU cm^{-3}	*R* / %
Gauze	3,100	99.66	< 10	99.99
Sanitary pads	120	99.99	< 10	99.99
Cotton wool	500	99.94	22	99.99
Compress	320	99.96	< 10	99.99
Bandage	400	99.96	< 10	99.99

After 24 hours of contact between the tested Gram (-) bacteria and the samples, a complete reduction of bacteria occurred (Tables 3 and 4). There are practically no visible surviving bacteria after contact with gauze, pads, and compresses for both investigated bacteria, so the reduction is 99.99 %. About 1,000 surviving colonies remain on cotton wool and bandages also. The bandages most likely due to low wettability have a slower release of silver. The cotton wool due to high absorption and swelling makes mixing difficult and decreases the release of silver. After 2 h of contact, the reduction is slightly lower for both tested bacteria but satisfactory. The reduction of *P. aeruginosa* is over 99 % even after 2 h of contact, while the reduction of *E. coli* is over 90 %. We can conclude that the contact time affects the complete extinction of bacteria if the initial number of bacteria is over 10^5 CFU cm^{-3}, which is the case with strong infections with these bacteria. If the materials are used preventively or in places where the infection is just beginning, the antimicrobial protection provided by the samples processed in this way is sufficient to prevent the further spread of the infection. The antimicrobial results obtained for this fabric against *E. coli* agree with our previous results [5,6,14-16].

The tests of antimicrobial activity were performed against the Gram (+) bacteria *Staphylococcus aureus, Bacillus subtilis*, and *Enterococcus faecalis*. Tables 5, 6, and 7 show the results of antimicrobial activity against these bacteria.

Table 5. *Antimicrobial activity of tested samples treated by the micro-dispersion method with colloid concentration 30 ppm after 2 (C_0 = 400,000 CFU cm^{-3}) and 24 h (C_0 = 200,000 CFU cm^{-3}) of contact with Staphylococcus aureus*

Sample	Time of contact with *Staphylococcus aureus*, h			
	2 h		24 h	
	C / CFU cm^{-3}	*R* / %	*C* / CFU cm^{-3}	*R* / %
Gauze	85,000	78.75	3000	98.50
Sanitary pads	50,000	87.50	< 10	99.99
Cotton wool	90,000	77.50	1	99.99
Compress	30,000	92.50	7	99.99
Bandage	300,000	25.00	6200	96.90

Table 6. *Antimicrobial activity of tested samples treated by the micro-dispersion method with colloid concentration 30 ppm after 2 (C_0 = 200,000 CFU cm^{-3}) and 24 h (C_0 = 200,000 CFU cm^{-3}) of contact with Bacillus subtilis*

Sample	Time of contact with *Bacillus subtilis*, h			
	2		24	
	C / CFU cm^{-3}	*R* / %	*C* / CFU cm^{-3}	*R* / %
Gauze	800	96.00	30	99.85
Sanitary pads	500	97.50	53	99.74
Cotton wool	300	98.50	40	99.80
Compress	200	99.00	165	99.18
Bandage	400	98.00	17	99.92

Table 7. *Antimicrobial activity of tested samples treated by the micro-dispersion method with colloid concentration 30 ppm after 2 (C_0 = 600,000 CFU cm^{-3}) and 24 h (C_0 = 1,500,000 CFU cm^{-3}) of contact with Enterococcus faecalis*

Sample	Time of contact with *Enterococcus faecalis*, h			
	2 h		24 h	
	C / CFU cm^{-3}	*R* / %	*C* / CFU cm^{-3}	*R* / %
Gauze	70,000	88.33	60,000	96.00
Sanitary pads	230,000	61.67	61	99.99
Cotton wool	70,000	88.33	2,600	99.83
Compress	120,000	80.00	1,100	99.93
Bandage	870,000	NA	5,900	99.61

The reduction of Gram (+) bacteria *Staphylococcus aureus, Bacillus subtilis*, and *Enterococcus faecalis* is at a satisfactory level even after 2 h, while after 24 h of the contact, the reduction is almost total (Tables 5, 6, and 7). The number of bacteria was reduced from 10^6 to 10^4 after 2 hours of contact between fabrics and *S. aureus*. The microbial reduction is over 75 % for all samples except for the bandage. On the other hand, after 24 h of contact, cotton wool, sanitary pad, and compress treated with colloid at a concentration of 30 ppm almost completely extinguish *S. aureus* bacteria, and after 24 h of contact, less than 10 bacteria survive per 1 cm^3 of suspension. With the gauze and bandage samples, 10^3 bacteria remain, but it is also excellent antimicrobial activity with over 96 % reduction of the initial bacterial count.

The reduction of *Bacillus subtilis* after 2 h of contact was over 96 % for all tested samples, while after 24 h of contact, the reduction was almost complete, over 99 %. The number of microorganisms decreased from 10^4 to 10^2 CFU cm^{-3}. All treated fabrics have effective antimicrobial activity after a short time of contact against the bacteria *B. subtilis*. The reduction of *E. faecalis* bacteria is slightly worse than *S. aureus*. After 2 h of contact, gauze, cotton wool, and compress showed antimicrobial activity with over 80 % reduction of bacteria. However, after 24 h of contact, all samples except for gauze reached a complete reduction of bacteria with over 99 %.

We can conclude that all samples treated with 30 ppm colloid showed excellent antimicrobial activity against all tested Gram-positive bacteria *Staphylococcus aureus, Bacillus subtilis*, and *Enterococcus faecalis*.

Finally, the antimicrobial activity against the pathogenic fungus *C. albicans* was tested, and the results are shown in Table 8.

According to their structure, fungi are different from bacteria. They are complex eukaryotic microorganisms with cells resembling animal cells. Tests have shown much weaker antimicrobial properties against this microorganism than against all other tested bacteria.

Table 8. *Antimicrobial activity of tested samples treated by the micro-dispersion method with colloid concentration 30 ppm after 2 (C_0 = 300,000 CFU cm^{-3}) and 24 h (C_0 = 260,000 CFU cm^{-3}) of contact with Candida albicans*

Sample	Time of contact with *Candida albicans*, h			
	2		24	
	C / CFU cm^{-3}	*R* / %	*C* / CFU cm^{-3}	*R* / %
Gauze	100,000	66.67	60,000	76.92
Sanitary pads	250,000	16.67	90,000	65.38
Cotton wool	190,000	36.67	90,000	65.38
Compress	160,000	46.67	9,100	96.50
Bandage	130,000	56.67	10,000	96.15

After 2 h of contact, the reduction is insignificant, while after 24 h of contact, the microbial reduction for compress and bandage is over 96 %, while for the other samples, it is between 65 and 77 %. We can say that there is low antimicrobial activity in the samples, and according to the results, there is no further reproduction of the fungus. Lower antimicrobial activity against *C. albicans* was observed for Ag attached to textile fibers [14] and inorganic supports such as hydroxyapatite [13] and magnetite [12], compared with the antibacterial performance of silver nanoparticles against *E. coli* [17,18]. However, this is also an indication that the samples treated with the 30 ppm colloidal solution would not be toxic to eukaryotic cells, so we can assume that they would not be toxic to human cells either. Consequently, these experiments will be done in the future.

4. CONCLUSION

The processing methodology for the treatment of wound dressing materials was optimized regarding the antimicrobial properties of the obtained materials against *E. coli* as a reference culture. Based on considerations of the appearance of the material, the structure after processing, as well as the antimicrobial activity, the "deep coating" method was rejected, precisely because of the damage to the material structure. The second method was spraying a precisely determined volume (2 cm^3 g^{-1} of the material) at a silver concentration of 30 ppm in the colloid solution. All tested samples treated with this solution showed satisfactory and, in some cases, excellent antimicrobial properties against all tested strains of microorganisms. The antimicrobial efficiency of the tested materials against the Gram-negative bacteria *Escherichia coli* and *Pseudomonas aeruginos*a was almost maximal after 2 h of contact (reduction of 95 and 99 %, respectively). After 24 h of the contact between the bacteria and the material, there was negligible growth of microorganisms, and we can consider that the efficiency is maximal.

In the case of Gram-positive bacteria *Staphylococcus aureus, Bacillus subtilis, and Enterococcus faecalis,* a longer time of contact is needed for the complete reduction of bacteria (over 99 %), except for *B. subtilis*. After 2 h of contact between samples and *S. aureus*, a satisfactory bacterial reduction was achieved, but after 24 h the bacterial reduction is maximal. This result is important taking into account the fact that *S. aureus* is considered one of the most common causes of skin infections. For *E. faecalis*, a longer contact time is needed to achieve maximum reduction. Antifungal activity testing against the fungus *C. albicans* gave moderate antifungal activity results.

The obtained results for all tested wound dressing products against tested microorganisms confirmed good antimicrobial activity, and we expect these products to reach the market soon.

Acknowledgement: *This study was supported by the Ministry of Science, Technological Development, and Innovations of the Republic of Serbia (grant numbers: 451-03-1/2023-14/200017), and the Innovation Fund of the Republic of Serbia (Innovation voucher No. 1141).*

REFERENCES

[1] Czajka R. Development of medical textiles. *Fiber Text East Eur.* 2005; 13: 13-15 http://www.fibtex.lodz.pl/49_06_13.pdf.

[2] Wong YWH, Yuen CWM, Leung MYS, Ku SKA, Lam LI. Selected applications ofnanotechnology in textiles. *Autex Res. J.* 2006; 6: 1-8 https://www.autexrj.com/cms/zalaczone_pliki/1-06-1.pdf.

[3] Gao Y, Cranston R. Recent advances in antimicrobial treatments of textiles. *Text Res J.* 2008; 78:60–72 https://doi.org/10.1177/0040517507082.

[4] Gorenšek M, Recelj P. Nanosilver functionalized cotton fabric. *Text Res J.* 2007; 77: 138-141. https://doi.org/10.1177/00405175070763.

[5] Ilić V**,** Šaponjić Z, Vodnik V, Potkonjak B, Jovančić P, Nedeljković J, Radetić M. The influence of Silver Content on Antimicrobial Activity and Color of Cotton Fabrics Functionalized with Ag Nanoparticles. *Carbohyd Polym.* 2009; 78: 564-569 https://doi.org/10.1016/j.carbpol.2009.05.015.

[6] Davidović S, Miljković M, Lazić V, Jović D, Jokić B, Dimitrijević S, Radetić M. Impregnation of cotton fabric with silver nanoparticles synthesized by dextran isolated from bacterial species *Leuconostoc mesenteroides* T3. *Carbohyd Polym.* 2015; 131: 331-336 https://doi.org/10.1016/j.carbpol.2015.06.024.

[7] El-Rafie MH, Ahmed HB, Zahran MK. Characterization of nanosilvercoated cotton fabrics and evaluation of its antibacterial efficacy. *Carbohyd Polym.* 2014; 107: 174-181. https://doi.org/10.1016/j.carbpol.2014.02.024.

[8] Gorjanc M, Kovač F, Gorenšek M. The influence of vat dyeing on the adsorption of synthesized colloidal silver onto cotton fabrics. *Text Res J.* 2012; 82(1): 62-69 https://doi.org/10.1177/0040517511420754.

[9] Knetsch MLW, Koole LH. New strategies in the development of antimicrobial coatings: The example of increasing usage of silver and silver nanoparticles. *Polymers*. 2011; 3: 340–366 https://doi.org/10.3390/polym3010340.

[10] Lee HJ, Jeong SH. Bacteriostatic and skin innoxiousness of nano size silver colloids on textile fabrics. *Text Res J.* 2005; 75:551-556 https://doi.org/10.1177/0040517505053952.

[11] Pohle D, Damm C, Neuhof J, Rosh A, Munstedt H. Antimicrobial prop-erties of orthopaedic textiles after in-situ deposition of silver nanoparticles. *Polym Polym Compos.* 2007; 15: 357-363 https://doi.org/10.1177/096739110701500502.

[12] Lazić V, Mihajlovski K, Mraković A, Illés E, Stoiljković M, Ahrenkiel SP, Nedeljković J. Antimicrobial activity of silver nanoparticles supported by magnetite. *Chemistry Select.* 2019; 4: 4018-4024 https://doi.org/10.1002/slct.201900628.

[13] Lazić V, Smičiklas I, Marković J, Lončarević D, Dostanić J, Ahrenkiel SP, Nedeljković JM. Antibacterial ability of supported silver nanoparticles by functionalized hydroxyapatite with 5-aminosalicylic acid. *Vacuum.* 2018; 148**:** 62-68 https://doi.org/10.1016/j.vacuum.2017.10.039.

[14] Radetić M, Ilić V,Vodnik V, Dimitrijević S, Jovančić P, Šaponjić Z, Nedeljković J, Antibacterial effect of silver nanoparticles deposited on corona-treated polyester and polyamide fabrics. *Polym Advan Technol.* 2008; 19: 1816-1821 https://doi.org/10.1002/pat.1205.

[15] Ilić V, Šaponjić Z, Vodnik V, Mihailović D, Jovančić P, Nedeljković J, Radetić M. A study of the antibacterial efficiency and coloration of dyed polyamide and polyester fabrics modified with colloidal Ag nanoparticles. *J Serb Chem Soc.* 2009; 74: 349-357 https://doi.org/10.2298/JSC0903349I.

[16] Lazić V**,** Šaponjić Z, Vodnik V, Dimitrijević S, Jovančić P, Nedeljković J, Radetić M. The study of antibacterial activity and stability od dyed cotton fabrics modified with different forms of silver. *J Serb Chem Soc.* 2012; 77(2): 225-234 https://doi.org/10.2298/JSC110505167L.

[17] Ilić V**,** Šaponjić Z, Vodnik V, Molina R, Dimitrijević S, Jovančić P, Nedeljković J, Radetić M. Antifungal efficiency of corona pretreated polyester and polyamide fabrics loaded with Ag nanoparticles. *J Mater Sci.* 2009; 44: 3983-3990 https://doi.org/10.1007/s10853-009-3547-z.

[18] Duran N, Marcato PD, De Souza GIH, Alves OL, Esposito E. Antibacterial effect of silver nanoparticles produced by fungal process on textile fabric and their effluent treatment. *J Biomed Nanotech.* 2007; 3: 203-208 https://doi.org/10.1166/jbn.2007.022.

Antimikrobna aktivnost medicinskih materijala obrađenih srebrom

Katarina R. Mihajlovski[1], Željka Stajčić[2] i Vesna M. Lazić[3]

[1]Tehnološko-metalurški fakultet, Univerzitet u Beogradu, Beograd, Srbija
[2]Koloid d.o.o., Prve pruge 7, Beograd, Srbija
[3]Centar za konverziju svetlosne energije, Institut za nuklearne nauke „Vinča", Univerzitet u Beogradu, Beograd, Srbija

(Stručni rad)

Izvod

Cilj ovog rada je ispitivanje antimikrobne efikasnosti pamučnih materijala kao što su gaza, higijenski ulošci, vata, komprese i zavoji obrađeni komercijalnim koloidnim rastvorom srebra (kompanija Koloid doo). Ispitan je uticaj koncentracije koloidnog rastvora srebra kojim je obrađena tkanina na antimikrobnu aktivnost prema Gram-negativnim bakterijama *Escherichia coli* i *Pseudomonas aeruginosa,* Gram-pozitivnim bakterijama *Staphylococcus aureus, Bacillus subtilis* i *Enterococcus faecalis* i gljivici *Candida albicans*. Redukcija bakterija postignuta testiranim materijalima obrađenim rastvorom srebra koncentracije 30 ppm (15 do 20 µg Ag na 1 g materijala) prema Gram-negativnim bakterijama *E. coli* i *P. aeruginosa* je skoro maksimalna nakon dva sata kontakta, 95 i 99 %, redom. U slučaju Gram-pozitivnih bakterija *S. aureus, B. subtilis* i *E. faecalis*, potrebno je duže vreme za potpunu redukciju broja bakterija, osim za *B. subtilis*, gde je dovoljno dva sata kontakta za maksimalno smanjenje početnog broja bakterija. Antifungalna aktivnost prema gljivici *C. albicans* je umerena.

Ključne reči: optimizacija procesa; tekstilni materijali; pamuk; mikroorganizmi; koloidni ratvor srebra

Influence of suspension heating rate on properties of zeolite 13X

Mladen B. Janković[1], Mitar D. Perušić[2], Vladimir M. Damjanović[1], Radislav Lj. Filipović[1,2], Zoran B. Obrenović[1,2], Goran S. Tadić[2] and Duško D. Kostić[2]

[1]*Alumina Ltd, Karakaj bb, 75400 Zvornik, Republic of Srpska, Bosnia and Herzegovina*

[2]*University of East Sarajevo, Faculty of Technology, Karakaj 34A, 75400 Zvornik, Republic of Srpska, Bosnia and Herzegovina*

Abstract

It is known that the temperature of crystallization during the synthesis of zeolite is one of the most important process parameters. However, during the research work on the synthesis of zeolite 13X and the introduction of this material into regular industrial production, it was noticed that the heating rate of the starting reaction suspension can have an equally important influence. This influence can be so pronounced that a difference of just a few minutes in reaching the crystallization temperature can make a significant difference in product quality, affect the presence of other phases in the crystal, or even determine the direction of zeolite crystallization. Therefore, the aim of this work was to show the influence of the heating rate on the quality of the obtained 13X zeolite powders. The obtained samples were analysed in terms of crystallinity (by X-ray diffraction), chemical composition, granulometry and specific surface area (by Brunauer-Emmett-Teller analysis), and regarding water and CO_2 adsorption capacities. Additionally, scanning electron microscopy analysis of the samples showed the morphological characteristics of different 13X zeolite powders. The analysis results of the obtained powders confirmed the influence of the heating rate and helped to define the optimal synthesis parameters *i.e.* the initial temperature and heating time, that resulted in stable product quality.

Keywords: Heating rate, Linde type A zeolites, suspension, synthesis

Available on-line at the Journal web address: http://www.ache.org.rs/HI/

ORIGINAL SCIENTIFIC PAPER

UDC: 661.183.6: 621.78.014

Hem. Ind. **77(4)** 275-282 (2023)

1. INTRODUCTION

Zeolite 13X is one of the most commercially popular synthetic zeolites thanks to the characteristics of its crystal structure. This type of zeolite stands out primarily for its adsorption characteristics, so it has found application in a large number of adsorption processes. Some of the most important of these processes are oxygen production [1], processing of natural and liquid petroleum gas [2], industrial production and purification of hydrogen (H_2) [3], refining of biofuels [4], industrial production and purification of alcohol [5], refining of petroleum compounds [2], *etc*.

Based on the great possibilities for the application of zeolite 13X and the potential growth in demand due to the development of new adsorption processes, especially those related to the reduction of greenhouse gas emissions (GHG) [6], it was of particular interest to find optimal parameters for the synthesis of this type of zeolite for wider commercial use.

During hydrothermal synthesis of zeolite powders, including zeolite 13X, several factors affect the quality of the synthesized product. The crystallization temperature, the duration of crystallization, the molar ratio of Si/Al in the system and the alkalinity of the synthesis system are among the most important process parameters, whose influence on synthesis is most often investigated [7-9].

However, in order to obtain a pure phase of zeolite 13X with satisfactory quality, in specific industrial conditions a number of other influences occur that are less mentioned in literature most likely because this type of zeolite is a commercial product.

The initial reaction suspension for the synthesis of zeolites 13X, as well as the hydrothermal conditions of synthesis, can easily lead to the formation of other forms of zeolites, which would by their presence violate the purity of the phase

Corresponding authors: Mitar D. Perušić, Department of Chemical Engineering, University of East Sarajevo, Faculty of Technology, Zvornik, Bosnia and Herzegovina

E-mail: mitar.perusic@tfzv.ues.rs.ba

Paper received: 18 Aplil 2023; Paper accepted: 22 October 2023; Paper published: 3 November 2023.

https://doi.org/10.2298/HEMIND230418023J

of zeolite 13X and thus other quality characteristics of the product. During heating, conditions are suitable for the formation of other crystalline zeolite forms, especially those corresponding to a lower crystallization temperature, such as Linde type A (LTA) zeolites or Sodalite [10]. Therefore, the focus of this paper is research on the influence of the heating rate of the reaction suspension (reaching the crystallization temperature in the targeted time) on the quality of zeolite 13X the synthesized powders.

To determine the quality and characterization of synthesized powders, the degree of crystallinity of the obtained powders, the mean diameter of the particle, the specific surface area, and the adsorption capacity for water and CO_2 were determined. In addition, samples of the obtained powders were analyzed regarding the morphology and structure by scanning electron microscopy, to correlate these properties with the other quality parameters.

2. EXPERIMENTAL

2. 1. Synthesis

Experimental syntheses of zeolite 13X were carried out in a reactor (V = 1 m^3) with a vertical stirrer (P = 3 kW, 10-120 rpm) of the Pilot zeolite production plant, company Alumina Ltd. Zvornik, (Bosnia and Herzegovina) as part of a wider research work on determining optimal technological parameters to produce this zeolite type.

The starting raw materials for zeolite synthesis were: NaOH solution (50 %) procured for industrial production in the factory (BorsodChem, Hungary); $NaAlO_2$ solution obtained by dissolving aluminium hydrate ($Al(OH)_3$, approximately 65 % Al_2O_3) in NaOH solution; waterglass produced in the factory by dissolving quartz sand (SiO_2) in NaOH solution, which is otherwise used for zeolite production purposes and demineralized water, which is also used in the factory in a number of processes.

Heating of the reaction suspension as well as maintaining the crystallization temperature is carried out by heating using water vapor. The reactor was a closed vessel with indirect heating through the jacket equipped with the previously described type of stirrer. The temperature in the reactor was set and maintained automatically through a system (Schneider Electric, France) that regulates the flow of steam indirectly with the possibility of setting the heating rate of ~0.8 °C min^{-1}, Temperature measurement was performed using a measuring probe inserted directly into the reaction space.

A total of nine (9) experimental syntheses are performed at different heating times between 60 and 120 min. Relevant experimental process conditions are shown in Table 1.

Table 1. *Experimental process conditions of obtained zeolite samples S1-S9 at a crystallization temperature of 85 °C*

Sample unit	Molar ratio $M(SiO_2)/M(Al_2O_3)$	Initial suspension temperature, °C	τ_{heat} / min	Concentration of (Na_2O) in filtrate, g dm^{-3}
S1	2.49	35	120	44.32
S2	2.39	34	120	43.28
S3	2.41	35	120	44.94
S4	2.42	36	90	45.33
S5	2.29	36	90	43.87
S6	2.38	35	90	42.76
S7	2.32	35	60	44.99
S8	2.42	34	60	42.28
S9	2.35	35	60	44.81

Apart from the difference in the heating time of the reaction suspension, all syntheses were performed under industrial conditions, with almost equal controlled process parameters at 85 °C based on previous industrial experiments for optimal crystallization temperature for the FAU (Faujasite) form of zeolite 13X.

During the experimental synthesis, demineralized water, and waterglass (sodium-silicate) as well as a part of NaOH solution are first added to the reactor, while the second part of the solution during this time is used to dissolve aluminium hydrates*, i.e.* to obtain sodium aluminate solution. After dissolving the hydrate, the resulting sodium aluminate solution is dosed into the reactor and mixed with other raw materials, considering the constant speed of

mixing, the dosage rate of the aluminate solution and the temperature. The resulting reaction suspension is then homogenized for a certain period before it begins to be heated from the homogenization temperature to the crystallization temperature. The difference between these temperatures was ~50 °C and the time of reaching this temperature difference is a parameter whose influence was further examined in the work.

2..2. Characterization

The degree of crystallinity of zeolites (%) obtained in the syntheses was determined in the Central Laboratory of Alumina Ltd. Zvornik, by X-ray diffraction (XRD) analysis using the reference sample method (Bruker Discover) XRD was performed on the X-ray diffractometer Bruker D8 ENDEAVOR (Bruker Corporation, USA) with an X-ray tube with a cobalt anode, using CoKα wavelength radiation λ = 0.178897 nm, in the range of diffraction angles 2θ from 25.0 to 29.0° with an angle step of 0.02° and an exposure of 0.50 s per step.

Particle size distribution and $D_{s50\%}$ diameter determination were performed on the CILAS 1090 liquid device (CPS, USA) ranging from 0.02 to 500 μm, with 30 s of sonication, according to the internal method for determining particle size distribution, MA. GX 032a.

The specific surface area was analysed according to the Brunauer–Emmett–Teller (BET) method in gaseous nitrogen (N_2) current on the Device GEMINI VII (Micromeritics Instrument Corporation, USA) with the preparation of a sample of 13X zeolite by thermal activation in ceramic pots in the furnace for a period of 4 h (520 °C) and 1 h (400 °C) by degassing in the nitrogen stream in the Flow-Prep block of the same device. Determination of the adsorption capacity of CO_2 was also performed by using the same device. The sample is prepared by degassing in a stream of nitrogen for 4 h at 520 °C and 1 h at 400°C. Determination of water adsorption capacity was performed in the Cambic KK-105-CH air chamber (CiK Solutions GmbH, Germany) under conditions of 20 °C, relative humidity *rH* = 50±2, 24 h. The method also prescribes pre-preparation of the sample by thermal activation in the furnace at *t* = 350-550 °C.

Imaging of zeolite crystals to characterize the morphology of the powders was performed by using a scanning electron microscope MIRA3 TESCAN device (TESCAN Group a.s., Czech Republic), with magnifications up to 10,000 times, operating at 20 kV. Before the examination, all samples were sputter-coated with gold using a sputter coater to avoid the electrostatic charge.

3. RESULTS AND DISCUSSION

The data obtained from the analyses of synthesized zeolite powders $D_{s50\%}$ and specific area are shown in Table 2 as well as relative crystallinity (%) in the diagrams shown in Figure 1 and H_2O and CO_2 adsorption in Figure 2. As can be seen, the heating time of the initial reaction suspension shows a significant impact on the analysed properties of the powders. The heating time affects both the degree of crystallinity of zeolite powders in terms of the desired Faujasite form of zeolite 13X (FAU), as well as the presence of other crystalline zeolite structures.

In addition to the FAU form, the presence of LTA form zeolite (4A), is also quantified and evident, and these values are listed among the results of the analysis (Figure 1).

A very high presence of LTA crystal structure crystals is evident in powder samples synthesized after 120 min of heating the suspension, up to almost 40 % of the relative crystallinity. By shortening the heating time*, i.e.* increasing the rate of heating, the presence of LTA form is reduced, so this phase is practically not recorded in powder samples synthesized after 60 min of heating (Figure 1).

On the other hand, reducing the heating time to 60 min before the period of crystallization itself, resulted in a high degree of relative crystallinity of FAU zeolites 13X crystal structure, so that all three samples (S7-S9) synthesized under these suspension heating conditions have satisfactory relative crystallinity of over 95 %, or even over 100 % (relatively), measured against the standard FAU sample or 0 % to the standard LTA sample of zeolite S8-S9, Figure 1.

However, powders synthesized after 90 min of heating of the reaction suspension did not have a satisfactory degree of relative FAU crystallinity form.

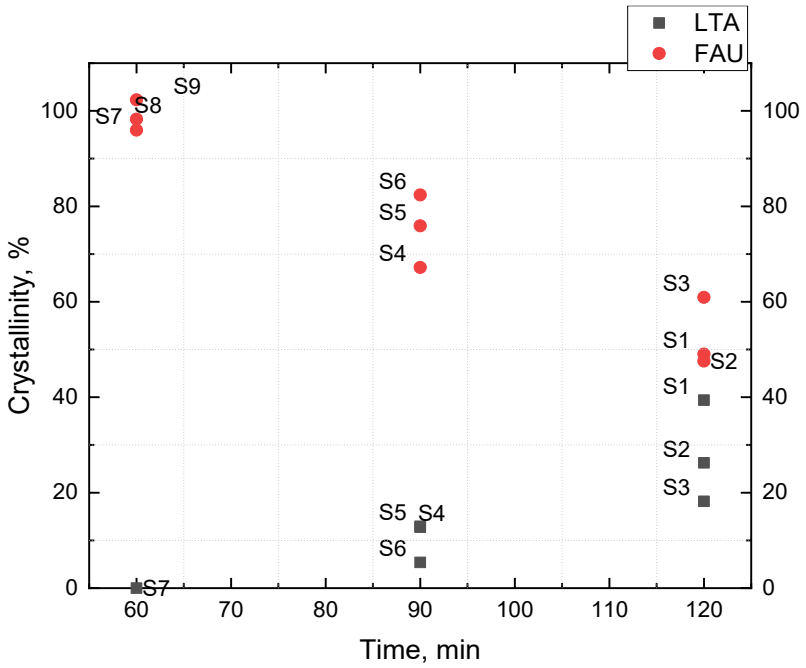

Figure 1. *Correlation of the degree of crystallinity of synthesized powders in relation to the heating time*

Table 2. *Specific surface area and particle size distribution values of 13X zeolite powders*

Sample	S1	S2	S3	S4	S5	S6	S7	S8	S9	SD[c]
$D_{s50\%}$ / µm[a]	3.92	4.31	3.68	4.28	3.98	4.15	3.39	3.08	2.99	0.66
Specific area, $m^2\ g^{-1}$ [b]	384.19	383.43	401.32	412.58	449.39	474.85	542.51	550.66	560.29	124.52

[a]he $D_{s50\%}$ is the medium value of the particle size distribution.
[b]Specific area is a specific particle surface area determined by the BET method.
[c]Standard deviation

The observed mean diameter of the prticles (Table 2), does not show a constant correlation with the degree of relative crystallinity of the zeolite 13X phase (compared with Figure 1), but it is noticeable that three samples that have high and satisfactory crystallinity (S7-S9) have the smallest mean particle diameter. However, it is possible to correlate the measured values of the mean diameters to the degree of crystallinity of all the phases present in one sample, or with the presence of agglomerates that are noticeable in the SEM images of individual samples (Figure 4). The specific surface area of the analysed powders increases with the increase in the purity of the crystal phase of 13X zeolite, which indicates that this parameter corresponds to a more regular and uniform crystal structure and lower values of the mean particle size.

The values of water and carbon dioxide adsorption capacities (mass %) are presented graphically, as functions of the degree of relative crystallinity (Figure 2). As with crystallinity itself, it is noticeable that satisfactory values of adsorption capacities were obtained only in samples with high degrees of crystallinity of the 13X zeolite phase (S7-S9), without the presence of other crystallinity forms. That is, the satisfactory values of these two key parameters for the commercial application of 13X zeolite were achieved only with the highest heating rate of the reaction suspension, *i.e.* at a heating time of 60 min.

The results of relative crystallinity and the presence of phases are graphically shown by diffractograms in Figure 3. The presence of the LTA crystal line is clearly visible in samples of S1-S6 synthesized after 120 and 90 min (Figure 3a and b), while the pure phase of 13X zeolite can be observed in Figure 3c. In addition, the diffractograms in Figures 3a and 3b also show the presence of other crystalline forms that do not correspond to FAU or LTA crystal structures. These peaks are not fully qualitatively or quantitatively determined but, according to the positions of the peaks, could correspond to the sodalite form (SOD) or zeolite NaP (GIS crystallographic form) [11].

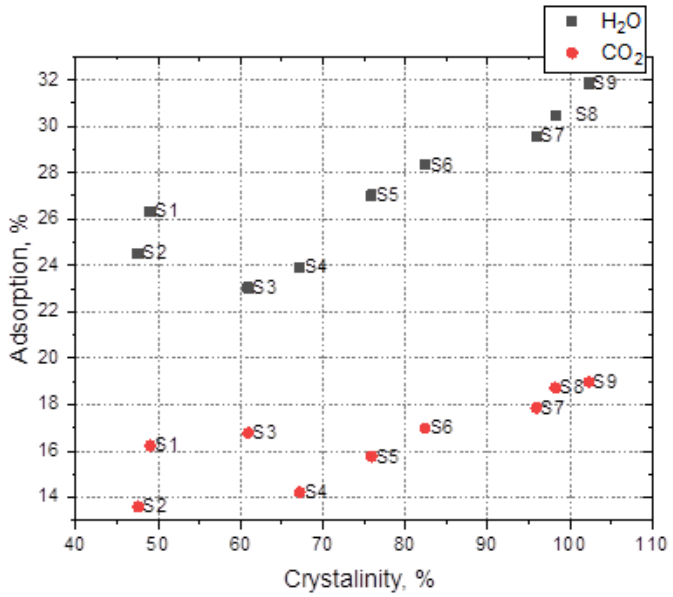

Figure 2. *Correlation of the adsorption capacity (mass %) of synthesized in relation to crystallinity (%) of 13X crystallographic form*

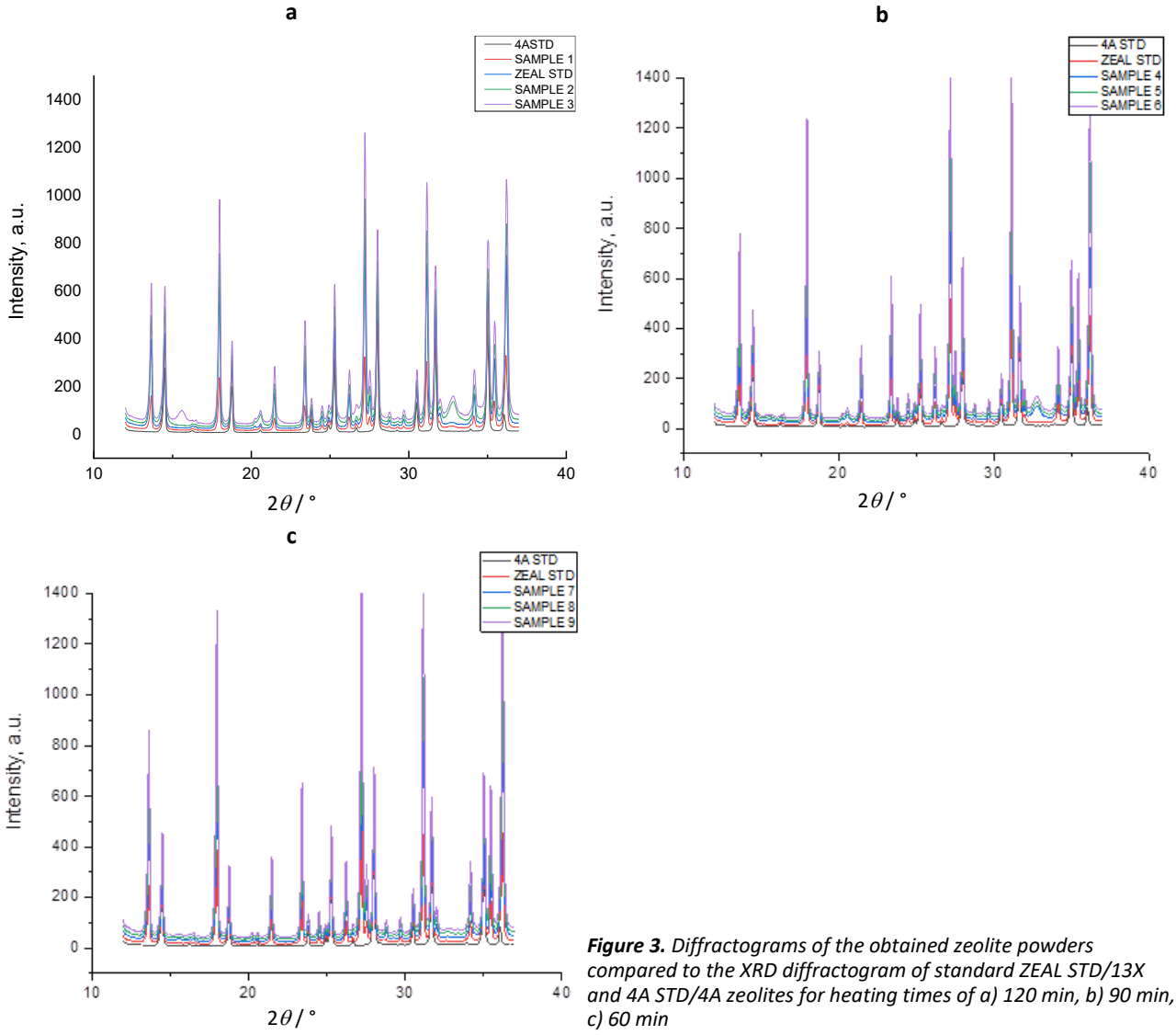

Figure 3. *Diffractograms of the obtained zeolite powders compared to the XRD diffractogram of standard ZEAL STD/13X and 4A STD/4A zeolites for heating times of a) 120 min, b) 90 min, c) 60 min*

In the SEM images (Figure 4), the presence of different shapes of particles and morphology can be noticed, expressed by crystallites of non-uniform size and morphology, which is especially pronounced in the samples (S1-S4), that according to the results of XRD analysis, had the greatest presence of unwanted phases.

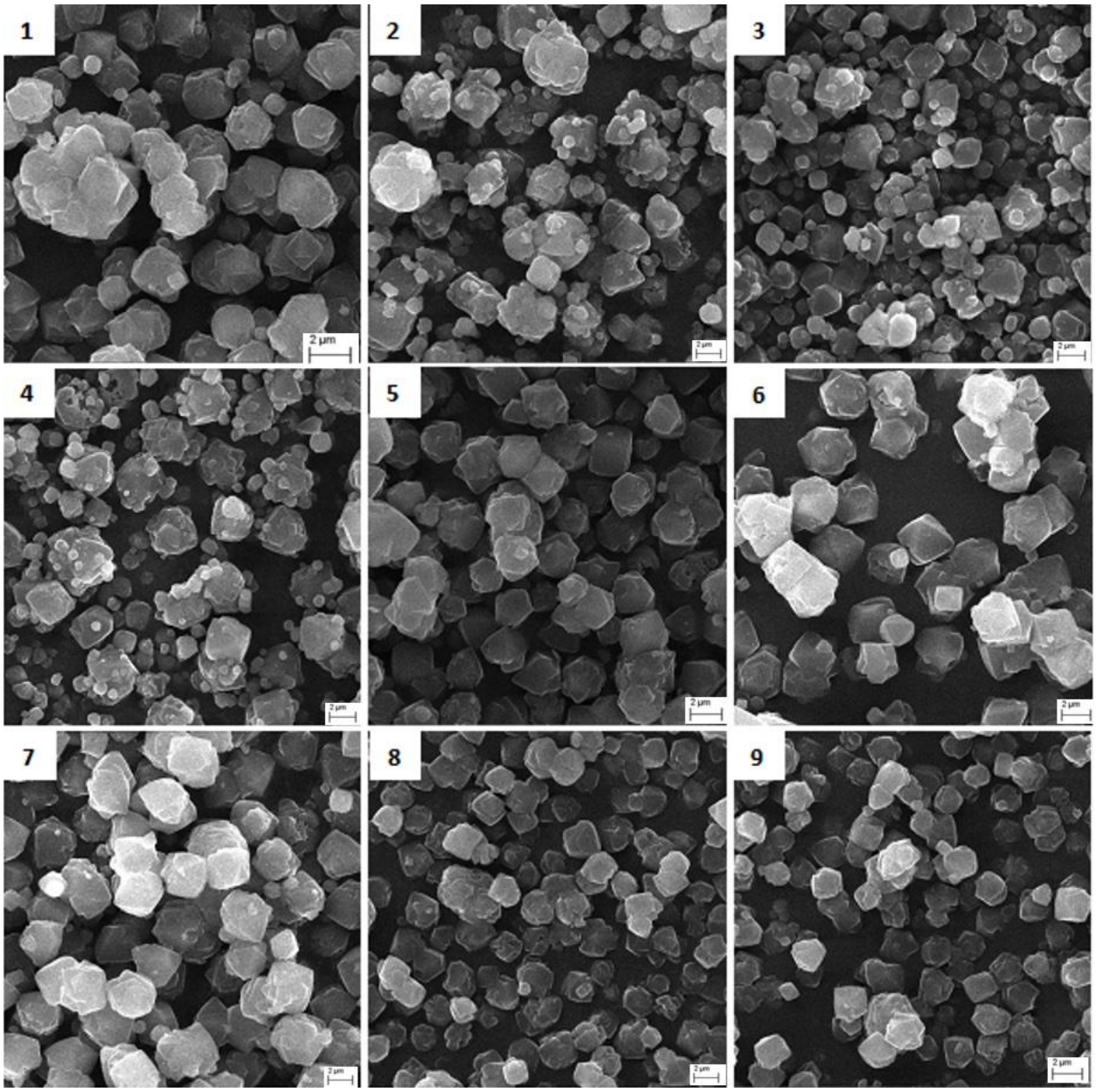

Figure 4. *SEM of the synthesized zeolite powders of samples S1 to S9, scale bar = 2 μm*

The presence of agglomerates is also evident in these samples. In samples S5 and S6, uniformity in the size and morphology of crystallites is greater, but the significant presence of agglomerates is still noticeable. SEM images of samples S7-S9 show uniform crystallite size and morphology, and the absence of agglomerates.

Experimental results follow data from the literature that lower or higher temperatures support the formation of other crystalline forms.

4. CONCLUSION

Based on the obtained results, it can be concluded that faster heating of the reaction suspension, results in a cleaner phase of zeolite 13X, a higher degree of crystallinity and a larger specific surface area of the material. Consequently, with a higher degree of crystallinity, the adsorption capacity of the obtained powders is higher, both in terms of water (H_2O) and CO_2 adsorption, as the two most important parameters that determine the quality of the product obtained and the possibility for its final application.

The results, especially those of XRD and SEM analyses, confirm the assumption that during the heating time, the crystallization system passes through different ranges that enables the formation of other zeolite phases, primarily LTA crystallographic form (zeolite type NaA) but also other forms of zeolite (SOD or NaP), and their presence is greater if the heating is slower, due to the longer retention of crystallization systems in unfavourable temperature ranges. This indicates that crystallization nucleation of different zeolite phases can occur already during the heating period, and later in the process of crystallization can continue to grow, although the final conditions have been achieved to correspond to crystallization of the targeted zeolite form.

Finally, heating of the suspension for 60 min resulted in a very satisfactory quality of the zeolite 13X product in the given process conditions and can be taken as the optimal value of this parameter in the tested crystallization system.

The presented study demonstrates the importance of considering the reaction preparatory conditions in zeolite 13X synthesis such as the heating rate of the reaction mixture, which is particularly important for specific industrial applications.

Acknowledgements: *The authors thank our colleagues of the University of Belgrade, Faculty of Technology and Metallurgy, Serbia for their professional contribution in performing the SEM analysis*.

REFERENCES

[1] Sameer SK, Eswaran P. Development and integration of oxygen generator for home air conditioner. *IOP Conf Ser Mater Sci Eng* 2020; 912: 042054 https://doi.org/10.1088/1757-899X/912/4/042054

[2] Esfandian H, Garshasbi V. Investigation of methane adsorption on molecular sieve zeolite (from natural materials). *Gas Process J* 2020; 8(2): 35-50. https://doi.org/10.22108/gpj.2020.121907.1080

[3] Brea P, Delgado JA, Águeda VI, Gutiérrez P, Uguina MA. Multicomponent adsorption of H2, CH4, CO and CO_2 in zeolites NaX, CaX and MgX. Evaluation of performance in PSA cycles for hydrogen purification. *Micropor Mesopor Mat* 2019; 286: 187-198. https://doi.org/10.1016/J.MICROMESO.2019.05.021

[4] Alshahidy BA, Abbas AS. Comparative study on the catalytic performance of a 13X zeolite and its dealuminated derivative for biodiesel production. *Bull Chem React Eng Catal* 2021; 16(4): 763-772. https://doi.org/10.9767/bcrec.16.4.11436.763-772

[5] Senol S, Kaya B, Salt I, Tirnakci B, Salt Y. Pervaporation separation of ethylacetate-ethanol suspensions using zeolite 13X-filled poly(dimethylsiloxane) membrane. *Chem Eng Commun* 2022; 209 (8): 1048-1057. https://doi.org/10.1080/00986445.2021.1940155

[6] Anbia M, Nejati FM, Jahangiri M, Eskandari A, Garshasbi V. Optimization of Synthesis Procedure for NaX Zeolite by Taguchi Experimental Design and its Application in CO2 Adsorption *J Sci IRI.* 2015; 26(3): 213–222 . https://jsciences.ut.ac.ir/article_55309.html

[7] Ma Y, Yan C, Alshameri A, Qiu X, Zhou C, Li D. Synthesis and characterization of 13X zeolite from low-grade natural kaolin. *Adv Powder Technol* 2014; 25(2): 495-499. https://doi.org/10.1016/J.APT.2013.08.002

[8] Zhang X, Tang D, Zhang M, Yang R. Synthesis of NaX zeolite: Influence of crystallization time, temperature and batch molar ratio SiO2/Al2O3 on the particulate properties of zeolite crystals. *Powder Technol* 2013; 235: 322-328. https://doi.org/10.1016/J.POWTEC.2012.10.046

[9] Ngoc DT, Pham TH, Hong Nguyen KD. Synthesis, characterization and application of nanozeolite NaX from Vietnamese kaolin. *Adv Nat Sci Nanosci Nanotechnol* 2013; 4(4): 045018. https://doi.org/10.1088/2043-6262/4/4/045018

[10] Prokof'ev VY, Gordina NE. Preparation of granulated LTA and SOD zeolites from mechanically activated suspensions of metakaolin and sodium hydroxide. *Appl Clay Sci* 2014; 101: 44-51. https://doi.org/10.1016/J.CLAY.2014.07.008

[11] Sharma P, Song JS, Han MH, Cho CH. GIS-NaP1 zeolite microspheres as potential water adsorption material: Influence of initial silica concentration on adsorptive and physical/topological properties. *Sci Rep* 2016; 6: 22734. https://doi.org/10.1038/srep22734

Uticaj brzine zagrejavanja suspenzije na osobine zeolita 13X

Mladen B. Janković[1], Mitar D. Perušić[2], Vladimir M. Damjanović[1], Radislav Lj. Filipović[1,2], Zoran B. Obrenović[1,2], Goran S. Tadić[2] i Duško D. Kostić[2]

[1]*Alumina d.o.o., Karakaj bb, 75400 Zvornik, Republika Srpska, BiH*

[2]*Univerzitet u Istočnom Sarajevu, Tehnološki fakultet Zvornik, Karakaj 34A, 75400 Zvornik, Republika Srpska, BiH*

(Naučni rad)

Izvod

Poznato je da temperatura kristalizacije tokom sinteze zeolita predstavlja jedan od najznačajnijih procesnih parametara. Međutim, tokom istraživačkog rada na sintezi zeolita 13X i uvođenju ovog materijala u redovnu industrijsku proizvodnju, primećeno je da i brzina zagrejavanja polazne reakcione smeše može da ima jednako bitan uticaj. Ovaj uticaj može biti do te mere izražen, da razlika od samo nekoliko minuta u postizanju temperature kristalizacije može da napravi značajnu razliku u kvalitetu proizvoda ili utiče na prisustvo drugih faza u kristalu, odnosno čak da odredi i pravac kristalizacije zeolita. Stoga, cilj ovog rada bio je da se prikaže uticaj brzine zagrejavanja na kvalitet dobijenih prahova zeolita 13X. Dobijeni uzorci analizirani su u pogledu kristaličnosti, hemijskog sastava, granulometrije i specifične površine, te su određivani kapaciteti adsorpcije vode i CO_2. Dodatno, snimci uzoraka pomoću skenirajuće elektronske mikroskopije prikazali su i morfološke karakteristike različitih prahova zeolita 13X. Rezultati analiza dobijenih prahova potvrdili su uticaj brzine zagrejavanja i pomogli da se definišu optimalni parametri sinteze koji su rezultovali stabilnim kvalitetom proizvoda zeolita 13X..

Ključne reči: Brzina zagrejavanja, LTA, sinteza, suspenzija, 13X

Numerical simulation of titanium alloy hip replacement implants behaviour under static and dynamic loads

Tamara Smoljanić[1], Aleksa Milovanović[1], Simon Sedmak[1], Ljubica Milović[2] and Aleksandar Sedmak[3]

[1]Innovation Center of the Faculty of Mechanical Engineering, Belgrade, Serbia
**University of Belgrade, Faculty of Technology and Metallurgy, Belgrade, Serbia*
[3]University of Belgrade, Faculty of Mechanical Engineering, Belgrade, Serbia

Abstract

This paper presents development of numerical models for simulation of the behaviour of titanium alloy hip implants under static and dynamic loads, which is a part of extensive research involving the structural integrity of such implants under various loading conditions, as well as under exposure to aggressive environments. Numerical models were created in ABAQUS and ANSYS software packages, in order to determine the stress/strain distribution, the number of cycles to failure and stress intensity factors, for two different hip implant geometries. The ABAQUS models were used for static and ANSYS models for dynamic loads. The next stage in this analysis involved comparing these two cases, to determine the one with the better behaviour, depending on the exploitation conditions, which can greatly vary between different groups of patients. The targeted patient weight for all numerical simulations was 90 kg, while failure assessment diagrams were made for both implant geometries, assuming a crack length of 1 mm.

Keywords: hip implants; Ti-6Al-4V; Finite element method; Fatigue crack; Failure assessment diagram.

Available on-line at the Journal web address: http://www.ache.org.rs/HI/

ORIGINAL SCIENTIFIC PAPER

UDC: 519.876.5: 616 089. 843:616.728.2:669.295

Hem. Ind. **77(4)** 283-292 (2023)

1. INTRODUCTION

Design of hip implants is of great importance, due to the complex loading and exploitation conditions. The most important factors to consider include the selection of material and the geometry of the implant. Materials should be both resistant to various adverse effects (corrosion and fatigue being the most common problems), while sufficiently safe for use. Previous experience, especially in recent decades, has shown that titanium-based alloys represent a good choice for such implants, due to their suitable mechanical properties, resistance to corrosion, and biocompatibility [1-4]. Geometry plays a significant role as it can directly lead to stress concentrations in certain locations (usually in cases where there are sharp angles or noticeable changes in the cross-section). One of the questions in this research was related to the thickness of the neck part of the implant – would the increase in the thickness be an actual improvement? While having a larger load-bearing cross-section certainly helps in increasing the work life of the implant, it also limits mobility.

For the purpose of the present research, the finite element method was used, both in its classic and extended forms [5-11], in order to determine behaviour of the models with different neck geometries under both static and dynamic loads. These loads were defined in accordance with the most extreme cases which could occur in real conditions, such as stumbling [11]. The extended finite element method was used for fatigue crack growth simulations, since it represents an effective and reliable means of simulating fatigue and was developed for that specific purpose.

Corresponding authors: Tamara Smoljanić, Innovation Center of the Faculty of Mechanical Engineering, Belgrade, Serbia
E-mail: tmijatovic@mas.bg.ac.rs
Paper received: 18 November 2022; Paper accepted: 15 October 2023; Paper published: 1 December 2023.
https://doi.org/10.2298/HEMIND2211180026S

2. MATERIALS AND METHODS

2. 1. Experimental basis

Experimental investigation of the hip implants included tensile tests, fatigue tests and determining of chemical composition of material. The hip implant (an example of which, along with its components, can be seen in Figure 1 was made of titanium-aluminium-vanadium alloy (Ti-6Al-4V), known as Titanium Grade 5 alloy, which was initially used in the aerospace industry, but has also found wide application in biomedicine. It exhibits a favourable combination of mechanical properties, biocompatibility, corrosion, and wear resistance, and in this case, the mechanical properties were the most important since they were used as the input data for the numerical calculations. Namely, yield stress and tensile strength are needed for the modelling, and they were experimentally determined [7] as follows:

- Yield stress – 881 MPa
- Tensile strength – 971 MPa

Additionally, the elasticity module of 120 GPa was adopted, along with a Poisson's ratio of 0.3. To performing the fatigue crack growth analyses in ANSYS, it is necessary to define the Paris law coefficients [12], in accordance with the well known formula (Eq. (1)):

$$\frac{\mathrm{d}a}{\mathrm{d}N} = C\Delta K^{m} \tag{1}$$

Where a is the crack length, N is the number of cycles, ΔK is the stress intensity threshold, and C and m represent the coefficients - C was determined to be 6.72×10^{-13} and m was 2.2. Finally, the fracture toughness of this material was needed in order to draw the failure assessment diagram during the later stage of these simulations. Fracture toughness, in this case, was K_{Ic} = 2100 MPa mm$^{0.5}$ [7].

Figure 1. An example of a real hip implant with its components

The material fatigue crack growth resistance was determined by applying the ASTM E647 standard procedure [12], which prescribes measurement of the fatigue crack growth rate da/dN, where a is the crack length and N is the number of cycles of applied load. Experimental testing of Ti-6Al-4V alloy was described previously [12]. Characteristic diagrams of the fatigue crack growth rate, that the da/dN -change in the range of the fatigue threshold values, ΔK, for the TI-6Al-4V alloy tested at room temperature are shown in [12].

The most commonly used alloy for orthopaedic applications is Ti-6Al-4V, due to its high ratio of strength and weight, good corrosion resistance, and positive biocompatibility. The chemical composition of the alloy used in this paper is given in Table 1., as the average value of a more detailed test [12].

Table 1. Chemical composition of the alloy

Element	Al	V	C	Fe	N	O	H	Ti
Content, %	6.67	4.08	0.012	0.24	0.018	0.08	0.001	remain

The tensile properties were determined by using micro-specimens, as defined by the standard ISO 6892-1:2016 [12]. More detailed results of testing of tensile properties are given in [12].

Fracture toughness is measured by using compact tension (CT) specimens, and a detailed overview of the results can be found in literature [12]. These results indicated relatively brittle behaviour, in accordance with a thickness that has met the plane-strain condition.

As it was shown previously, this particular titanium alloy has a strength value above the titanium average and good resistance to fatigue, allowing it to withstand a considerable number of loading cycles [12], as will be shown by the results of the numerical simulations presented.

2. 2. Previous numerical simulations using static loads

This section of the paper presents the initial numerical calculations, which were performed with static loading, for the purpose of determining the critical locations in the hip implant, where cracks would be expected to occur. Its goal was to accurately locate the area in the model, which is subjected to highest tensile stresses, and was expected in the implant neck area.

The finite element method, used in order to simulate the behaviour of titanium alloy hip im-plants under different loading conditions, was done in ABAQUS v6.14 (Dassault Systèmes Simulia Corp., Providence, RI, USA) for the former and ANSYS R19.2 (ANSYS, Inc., Canonsburg, PA, USA) for the latter case. This decision was made after some practical experience had shown that the ANSYS software is somewhat easier and faster to use for fatigue-related calculations.

Two versions of the hip implants were considered in these simulations – one with a neck diameter of 9 mm and the other with 14.6 mm. The load was defined based on a weight of 90 kg [7], in the form of a concentrated force. For this calculation the worst-case scenario was assumed, which involved stumbling, thus greatly increasing the intensity of the load. Boundary conditions were defined as fixed along the surface of the stem.

Some of the results of static simulations, performed in the previous analyses in order to determine the locations where highest tensile stresses would occur, can be seen in Figure 2 [8].

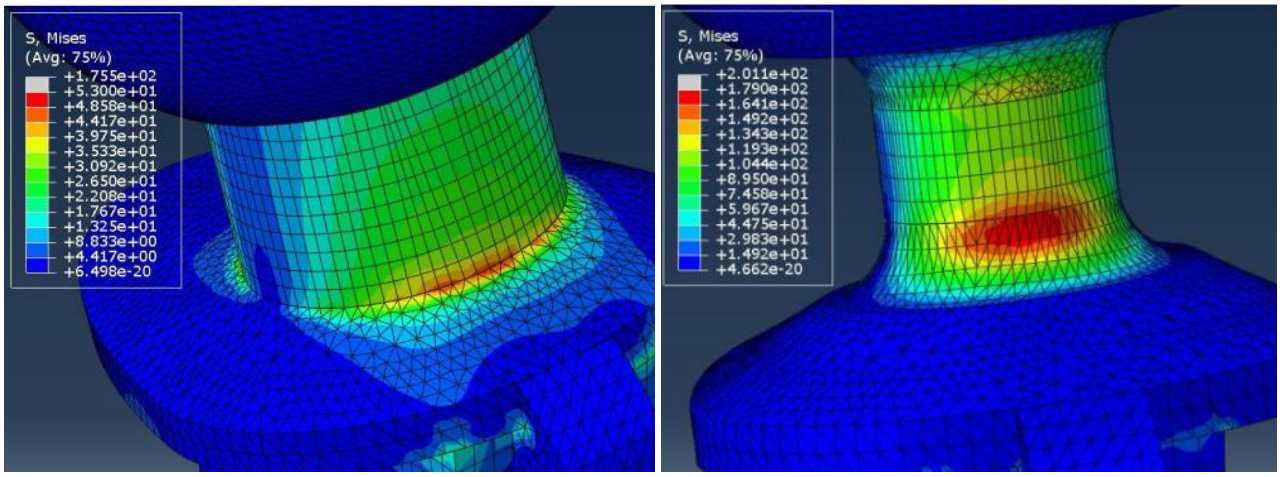

Figure 2. Left- Stress distribution for the model with a 14.6 mm neck; Right- Stress distribution for the model with a 9 mm neck [8]. Permissions under Attribution 4.0 International (CC BY-NC-ND 4.0 DEED)

These results have shown that the decrease in neck thickness affects considerably the stress magnitudes, causing maximum tensile stresses to increase more than three times – in the case of the 14.6 mm neck, their value was around 52 MPa, whereas, for the 9 mm neck, they were 179 MPa. As expected, stress concentrations were most prominent in the transition area between the neck and the collar (Figure 3). This finding was important since it provided the exact location where a fatigue crack would be most likely to initiate. This assumption was used as the base for the extended finite element method (XFEM) simulations which included the fatigue crack growth.

As for the fatigue crack growth simulations, the model that was used can be seen in Figure 3 for both investigated implant geometries. Boundary conditions were defined in the same way as for the static models (stem-bone contact was fixed), and the load was also applied as a concentrated force, with a magnitude that corresponded to a 90 kg person during normal walk (the loading here is cyclic, since simulation of repeated stumbling would not be reasonable).

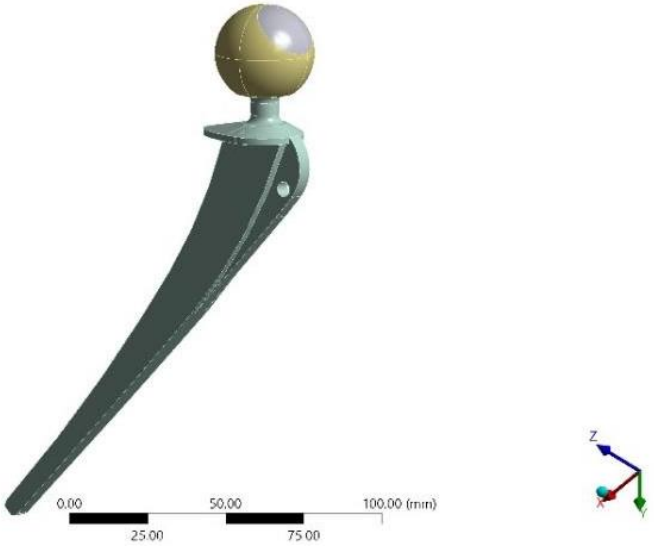

Figure 3. Geometry of the finite element model used for fatigue crack growth simulations in ANSYS [7]. Permissions under Attribution 4.0 International (CC BY 4.0)

The initial crack length was adopted as 1 mm since this is considered to be the minimum crack length that can be detected by using non-destructive test methods. The crack was placed at the stem-collar connection area, where the highest tensile stresses were determined during the static loading simulation stage. It should be noted that there was a noticeable difference in finite element meshes for the static and dynamic models – for static ones, a combination of linear hexahedral (HEX) and tetrahedral (TET) elements were used, whereas dynamic load models were made entirely out of TET elements, due to the specifications of the ANSYS software, i.e., the fatigue crack growth can only be simulated in a TET mesh.

3. RESULTS OF NEW FATIGUE BEHAVIOUR SIMULATIONS

Results of fatigue crack growth simulations are shown in the following section of the paper, starting with the stress distribution around the fatigue crack during its growth, shown in Figures 4 and 5.

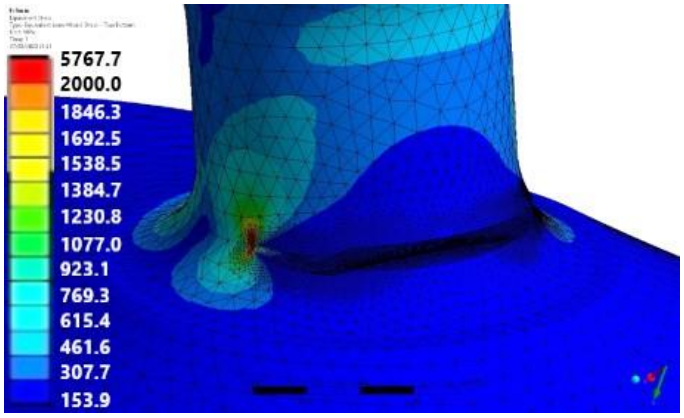

Figure 4. Fatigue crack growth in the 9 mm neck model [7]. Permissions under Attribution 4.0 International (CC BY 4.0)

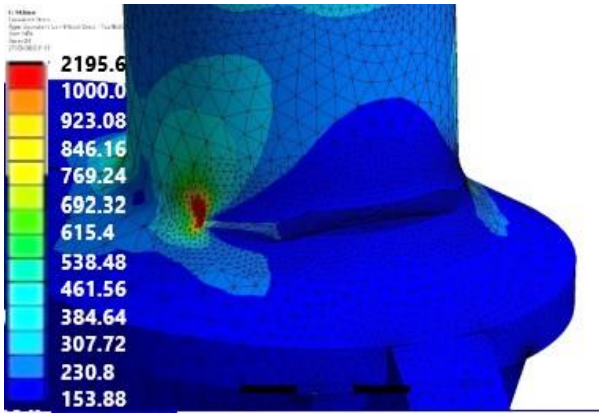

Figure 5. Fatigue crack growth in the 14.6 mm neck model [7]. Permissions under Attribution 4.0 International (CC BY 4.0)

As expected, the highest stresses were concentrated around the crack tip, and their values in the case of the 9 mm neck were almost three times larger compared to the 14.6 mm case (5760 and 2195 MPa, respectively). High values of stress were the result of using the linear-elastic fracture mechanics' approach. Since elastic-plastic fracture mechanics cannot be still reliably combined with XFEM fatigue simulations, linear-elastic fracture mechanics (LEFM) was adopted. The relation between the obtained numbers of cycles for both cases was also similar – around three times greater for the 14.6 mm neck

(5.2 million *vs.* 1.6 million). The aforementioned results indicated that the model with a wider neck has a considerably longer fatigue life. Its design allowed the fatigue crack to propagate to a much greater length compared to the 9 mm model. Of course, there is still a disadvantage to the 14.6 mm model, mainly in terms of mobility. Thus, additional analyses were performed to further determine the effects of geometry on hip implant integrity in more detail.

For this purpose, stress intensity factors were calculated for both models. Results were taken for crack lengths of approximately 1 mm (initial crack length) and are shown in Figure 6.

Following this step, it was concluded that the results would be more representative if an additional model was included, whose neck thickness would be between the other two values. This neck thickness was adopted as the mean value of 9 and 14.6 mm, *i.e.* 11.8 mm. Stress intensity factor results for this model are shown in Figure 7. This was done in order to determine the transition between different dimensions in a more detailed manner, and because creating an additional model was simple with the existing base, since the only change was the neck thickness.

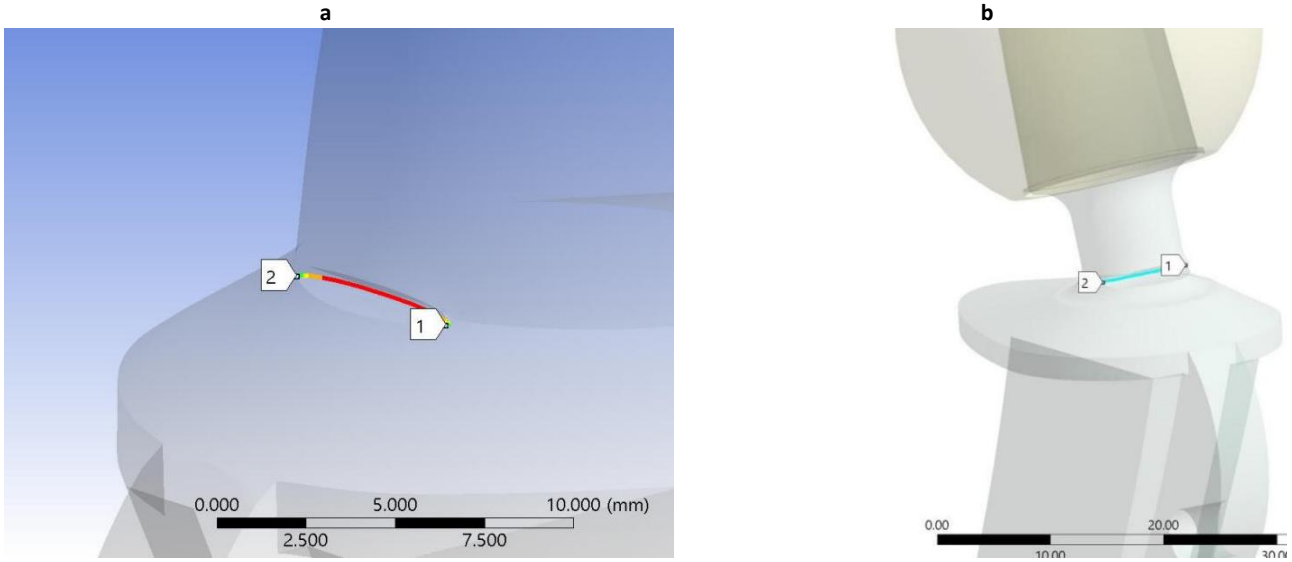

Figure 6. Stress intensity factors for the 14.6 mm neck model (a) and 9 mm neck model (b)

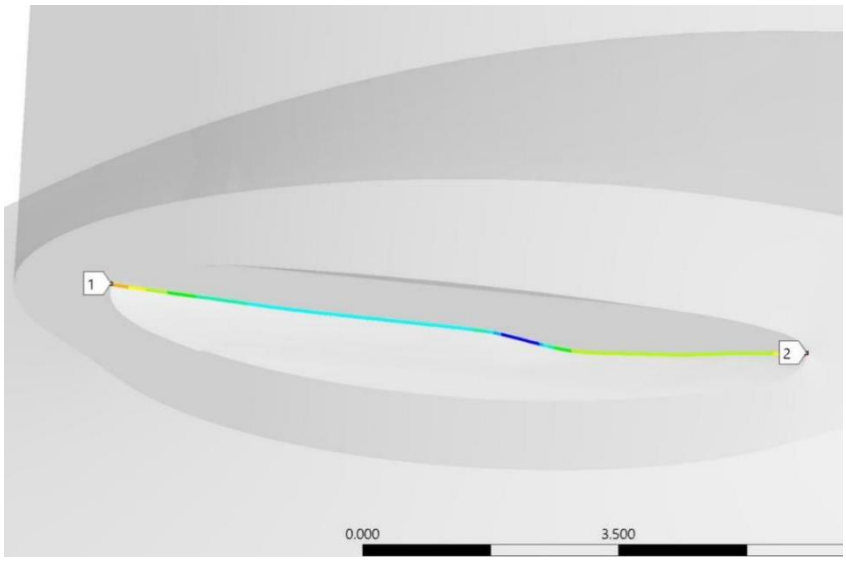

Figure 7. Stress intensity factors (SIFs) for 11.8 mm neck model

The reason for determining stress intensity factors (SIFs) was to create Failure assessment diagrams for both models and observe the potential differences between them. Analysis of the Failure assessment diagrams for these models will be shown in the following section of the paper.

4. FAILURE ASSESSMENT DIAGRAMS FOR HIP IMPLANTS

Failure assessment diagrams (FAD) represent a relatively simple and very reliable methodology for assessing the integrity of structures [13-19]. They are based on stresses and stress intensity factors for a given structure and indicate the probability of failure, as well as its nature (brittle fracture or plastic collapse). The basic concept is to establish the so-called limit curve in the coordinate system of two non-dimensional quantities, $S_r=\sigma/\sigma_c$ and $K_r=K_I/K_{Ic}$, as follows. S_r is the ratio of stresses in the observed material (σ) and its yield stress (σ_c), and K_r is the ratio of stress intensity factors around the crack (K_I) and the material's fracture toughness (K_{Ic}) (critical value of SIF). The starting point is to apply the Dugdale model valid for plane stress state and ideal plasticity, *i.e.* to equalize the stress intensity factors for a crack length (a)+plastic zone size (ρ) and for a closure forces, taken as yield stress in a plastic zone, Figure 8.

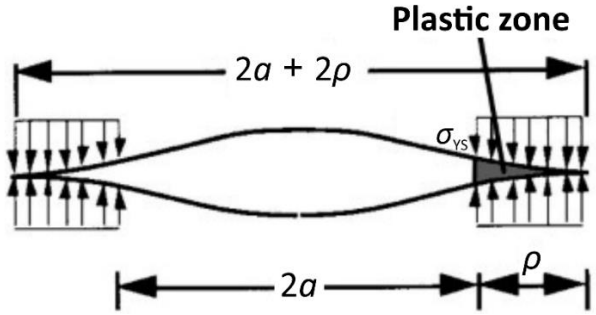

Figure 8 Dugdale model, where σ_{YS} represents yield stress

In this way, the following relation between the stress, crack length a and the plastic zone size ρ, is obtained (Eq. (2)):

$$\sigma\sqrt{\pi(a+\rho)}=\frac{2\sigma_{YS}}{\sqrt{\pi}}\sqrt{a+\rho}\arccos\left(\frac{a}{a+\rho}\right)\Rightarrow\left(\frac{a}{a+\rho}\right)=\cos\left(\frac{\pi\sigma}{2\sigma_{YS}}\right) \tag{2}$$

By using an expression for displacement v (3), one can get now the crack tip opening displacement (*Crack Tip Opening Displacement - CTOD*), denoted by δ:

$$\delta=\frac{8}{\pi}\frac{\sigma_{YS}a}{E}\ln\left|\sec\left(\frac{\pi\sigma}{2\sigma_{YS}}\right)\right| \tag{3}$$

Based on this expression and relation for the effective stress intensity factor, we have (Eq. (4)):

$$K_{eff}=\sqrt{\sigma_{YS}\delta} \tag{4}$$

valid for plane stress and ideal plasticity, one gets (Eq. (5)):

$$K_{eff}=\sigma_{YS}\sqrt{\pi a}\left[\frac{8}{\pi^2}\ln\sec\frac{\pi}{2}\frac{\sigma}{\sigma_{YS}}\right]^{1/2} \tag{5}$$

The next step in this procedure is to replace yield stress σ_{YS} with a more realistic quantity, the collapse (critical) stress, σ_C, which depends not only on the material, but also on geometry. For a structure under tension, plastic collapse occurs when the 'net' stress in cross section containing a crack reaches the critical value, σ_C. Finally, one can get the limit curve where the effective stress intensity factor is given in non-dimensional form (Equation (6)), K_{eff}/K_I:

$$\frac{K_{eff}}{K_I}=\frac{\sigma_c}{\sigma}\left[\frac{8}{\pi^2}\ln\sec\frac{\pi}{2}\frac{\sigma}{\sigma_c}\right]^{1/2} \tag{6}$$

where $K_I=\sigma\sqrt{\pi a}$. If K_{eff} is replaced by K_{Ic} and the following non-dimensional forms, $S_r=\sigma/\sigma_c$ and $K_r=K_I/K_{Ic}$, are used, one gets the final form (Eq- (7)) of the limit curve:

$$K_r=S_r\left[\frac{8}{\pi^2}\ln\sec\left(\frac{\pi}{2}S_r\right)\right]^{-1/2} \tag{7}$$

The limit curve separates the safe and potentially unsafe regions in the FAD, as shown in Figure 9, where points for all three hip implants are presented, calculated as explained in the following text.

To determine the points for the FAD for all hip implants, it was necessary to determine relevant stresses and stress intensity factors and then calculate their ratios – between the actual stresses and the yield stress and between the SIFs and fracture toughness, K_{Ic}. Values of the yield stress and K_{Ic} were determined as explained in the earlier part of the paper and were used as referent values in the calculation.

As for the stress in the model, the adopted values were taken from the model, based on the corresponding SIF results, in other words, stresses at the crack length of 1 mm, since that was the length for which stress intensity factors were determined. In the case of the 9 mm neck model, with the corresponding SIF value of 1441 MPa$\sqrt{}$mm, stress was 726 MPa, whereas for the 14.6 mm neck model the SIF and stress values were 348 MPa mm$^{0.5}$ and 175 MPa, respectively. Finally, for the third, "middle" model, the SIF value was 891 MPa mm$^{0.5}$, and the corresponding stress was 449 MPa.

By using the previously known values of yield stress for Ti-6Al-4V (881 MPa) and its fracture toughness (2100 MPa mm$^{0.5}$), the following coordinates were obtained for all three models in the FAD:

- For the 14.6 mm neck model – S_r = 0.2, K_r = 0.16
- For the 11.8 mm neck model – S_r = 0.51, K_r = 0.42
- For the 9 mm neck model – S_r = 0.82, K_r = 0.69

These points are shown in the FAD (Fig. 9). As can be seen, all three points fall in the safe region of the diagram (below the curve). As expected, the 9 mm model result is the least favourable and is quite near to the safe/failure regions limit curve. Considering that the final fatigue crack length obtained by the simulations given in [12] for the 9 mm model was much shorter than the one in 14.6 mm model (3.45 *vs.* 150 mm), the position of the point corresponding to the 9 mm model makes sense, taking into account the assumed initial crack length of 1 mm used for the SIF calculations.

Of course, the 14.6 mm neck version has the best values of S_r and K_r, making it the safest of the three models, with its corresponding point being close to the FAD origin. The model with an 11.8 mm neck was halfway between the two, also being much safer than the 9 mm one.

Since the point corresponding to the 9 mm neck was the most critical, *i.e.* closest to the limit curve, it was of particular interest to estimate the approximate crack length at which the point would coincide with the curve. Based on the interpolation of this point, it was determined that the limit curve stress intensity factor ratio (y-axis) would be around 1680 MPa mm$^{0.5}$. Based on this, it was determined that the corresponding crack length would be around 4 mm.

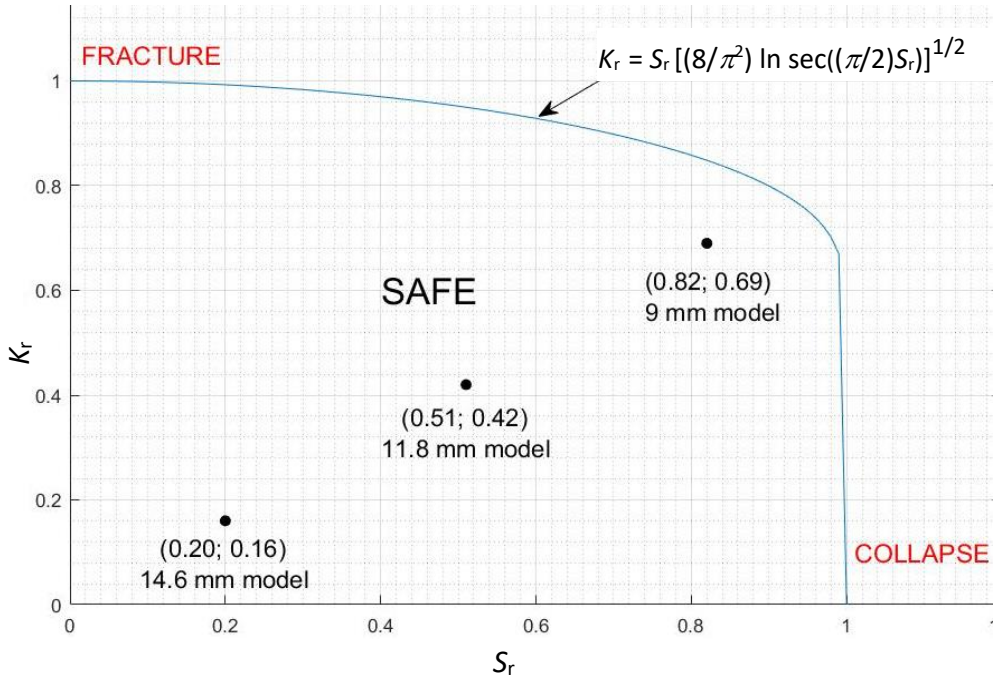

Figure 9. Failure assessment diagram for three different hip joint models

5. DISCUSSION

Results obtained for all three models also provided additional insights into the structural integrity of hip implants in the presence of a 1 mm fatigue crack, particularly in terms of how they are expected to fail – the thinnest neck being the closest to the limit curve. Based on the obtained fatigue crack lengths at failure in the previous simulations, and the somewhat high SIFs in this case, it was assumed that the 9 mm neck hip implant would have a predominantly brittle fracture. However, according to the FAD, it has exceeded its expectations and was closer to plastic collapse. Based on the diagram, the other two cases would eventually show similar behaviour, at higher stress/SIF levels. Anyhow, one should keep in mind that the FAD presented here is level I, based on the simple plasticity model, whereas levels 2 and 3 would provide additional plasticity reserve and less conservative, but still reliable failure assessment [21].

It needs to be emphasized that results for different crack lengths and/or geometries will not always necessarily align like in Figure 9. In the present case, the SIF value was almost equal to the mean value of the other two, but that was most likely a coincidence, and it does not suggest that adopting dimensions that are the average of two values will always result in SIFs and stresses which will also represent mean values of the initial two dimensions.

Both static and dynamic analyses confirmed that the 14.6 mm model has the best performance in terms of structural integrity (resistance to fatigue crack growth in this case). In fact, it has considerably better performance, with a notable difference in the number of cycles, and a significantly lower probability of failure, as determined by numerical simulations and the FAD. This suggests that hip implants with such geometry would be most favourable in cases where there is no need for increased hip mobility since it would be constrained by the aforementioned thick neck. In such cases, the patients would be able to use a single hip implant for extended periods of time without the need for replacement. Also, if a fatigue crack was to initiate in the implant, there would be a significantly wider time interval during which this problem could be detected, compared to the 9 mm case, where the fatigue crack would propagate to its maximum length considerably faster. The hip implant with the 11.8 mm neck should be also kept in mind, as it would offer the best compromise between mobility and fatigue life, while staying sufficiently safe.

Thus, the goal of this research, involving the analysis of fatigue behaviour of hip implants made of Ti-6Al-4V, was achieved in several ways, *i.e.* numerical and analytical - providing an accurate base of results. It also demonstrated the efficiency and effectiveness of numerical simulations, even when using different software.

5. CONCLUSIONS

In this paper three hip replacement implant geometries were considered (one of which was only analysed numerically), differing in thickness of the neck area. The neck area of the implant is essential for load distribution during physical activities, *i.e.* walking, running, climbing stairs, *etc*. Both geometries have specific advantages, *i.e.* thicker geometry provides longer structural life of the component, and thinner one increases patient mobility.

In order to estimate such claims, static and dynamic analyses were conducted: static for estimating locations with the highest stress concentrations and based on the obtained results research dynamic tests were conducted with initiated defects (*i.e.* cracks) on such locations. This paper is a continuation of previous research activities, including FAD for both geometries and one intermediate case, to get a better insight into selected hip implant structural integrity. All of the obtained points in FAD fall within the safe region, with thicker geometries being safer (*i.e.* closer to the FAD origin).

Acknowledgement: *The authors would like to thank the support from the Ministry of Education, Science and Technological Development of the Republic of Serbia by Contract Nos. 451-03-68/2022-14/200105 and 451-03-68/2022-14/200135.*

REFERENCES

[1] Sarraf M, Ghomi ER, Alipour S, Ramakrishna S, Sukiman NL. A state-of-the-art review of the fabrication and characteristics of titanium and its alloys for biomedical applications. *Bio-des. Manuf.* 2022; 5: 371-395. https://doi.org/10.1007/s42242-021-00170-3.

[2] Kirmanidou Y, Sidira M, Drosou ME, Bennani V, Bakopoulou A, Tsouknidas A, Michailidis N, Michalakis K. New Ti-Alloys and Surface Modifications to Improve the Mechanical Properties and the Biological Response to Orthopedic and Dental Implants: A Review. *BioMed Res Inter.* 2016; 2908570. https://doi.org/10.1155/2016/2908570.

[3] Eisenbarth E, Velten D, Muller M, Thull R, Breme J. Biocompatibility of beta-stabilizing elements of titanium alloys. *Biomaterials* 2004; 25(26): 5705-5713. https://doi.org/ 10.1016/j.biomaterials.2004.01.021.

[4] Niinomi M, Nakai M, Hieda J. Development of new metallic alloys for biomedical applications. *Acta Biomater.* 2012; 8(11): 3888-3903. https://doi.org/ 10.1016/j.actbio.2012.06.037.

[5] Sedmak A, Čolić K, Burzić Z, Tadić S. Structural integrity assessment of hip implant made of cobalt-chromium multiphase alloy. *Struct Integr Life.* 2010; 10(2): 161-164. http://divk.inovacionicentar.rs/ivk/ivk10/161-IVK2-2010-AS-KC-ZB-ST.pdf.

[6] Milovanović A, Sedmak A, Čolić K, Tatić U, Đorđević B. Numerical analysis of stress distribution in total hip replacement implant. *Struct Integr Life.* 2017; 17(2): 139-144. http://divk.inovacionicentar.rs/ivk/ivk17/139-IVK2-2017-AM-AS-KC-UT-BDj.pdf.

[7] Milovanović A, Sedmak A, Grbović A, Mijatović T, Čolić K. Design Aspects of Hip Implant Made of Ti-6Al-4V Extra Low Interstitials Alloy. *Procedia Struct Integr.* 2020; 26: 299-305. https://doi.org/10.1016/j.prostr.2020.06.038.

[8] Mijatović T, Milovanović A, Sedmak A, Milović Lj, Čolić K. Integrity assessment of reverse engineered TI-6AL-4V ELI total hip replacement implant. *Struct Integr Life.* 2019; 19(3): 237-242. http://divk.inovacionicentar.rs/ivk/ivk19/237-IVK3-2019-TM-AM-AS-LjM-KC.pdf.

[9] Sedmak A, Čolić K. Fracture and fatigue behaviour of implants made of Ti alloys. *Procedia Struct Integr.* 2019; 23: 45-50. https://doi.org/10.1016/j.prostr.2020.01.061.

[10] Čolić K, Sedmak A, Legweel K, Milošević M, Mitrović N, Mišković Ž, Hloch S. Experimental and numerical research of mechanical behaviour of titanium alloy hip implant. *Teh Vjesn.* 2017; 24(3): 709-713. https://doi.org/10.17559/TV-20160219132016.

[11] Čolić K, Sedmak A, Grbović A, Tatić U, Sedmak SA, Đorđević B. Finite element modeling of hip implant static loading. *Procedia Eng.* 2016; 149: 257-262. https://doi.org/10.1016/j.proeng.2016.06.664.

[12] Sedmak A, Čolić K, Grbović A, Balać I, Burzić M. Numerical analysis of fatigue crack growth of hip implant. *Eng Fract Mech.* 2019; 216: 106492. https://doi.org/ 10.1016/j.engfracmech.2019.106492.

[13] Sedmak A, Kirin S, Martić I, Jeremić L, Vučetić I, Golubović Sedmak T, Sedmak SA. Structural Integrity and Life Assessment of Pressure Vessels - Risk Based Approach. In: *Experimental and Computational Investigations in Engineering, Proceedings of the International Conference of Experimental and Numerical Investigations and New Technologies*, *CNNTech2020*, Springer, 2020: 274–293. https://doi.org/10.1007/978-3-030-58362-0_16.

[14] Golubović T, Sedmak A, Spasojević Brkić V, Kirin S, Rakonjac I. (2018). Novel Risk Based Assessment of Pressure Vessels Integrity. *Teh Vjesn.* 2018; 25(3): 803-807. https://doi.org/ 10.17559/tv-20170829144636.

[15] Kirin S, Jeremić L, Sedmak A, Martić I, Sedmak SA, Vučetić I, Golubović T. Risk based analysis of RHPP penstock structural integrity. *Frat ed Integrita Strutt.*2020; 14(53): 345-352. https://doi.org/ 10.3221/IGF-ESIS.53.27.

[16] Golubović T, Sedmak A, Spasojević Brkić V, Kirin S, Veg, E. Welded joints as critical regions in pressure vessels – Case study of vinyl-chloride monomer storage tank. *Hem Ind.* 2018; 72(4): 177-182. https://doi.org/10.2298/HEMIND171009006G.

[17] Sedmak A, Zaidi R, Vujičić B, Šarkočević Ž, Kirin S, Stamenić Z, Đukić M, Bakić G. Corrosion effects on structural integrity and life of oil rig drill pipes. *Hem Ind.* 2022; 76(3):167-177. https://doi.org/10.2298/HEMIND220222014S.ž

[18] Zaidi R, Sedmak A, Kirin S, Grbović A, Wei L, Lazić Vulićević Lj, Šarkočević Ž. Risk assessment of oil drilling rig welded pipe based on structural integrity and life estimation. *Eng Fail Anal.* 2020; 112: 104508. https://doi.org/10.1016/j.engfailanal.2020.104508.

[19] Kirin S, Sedmak A, Zaidi R, Grbović A, Šarkočević Ž. Comparison of experimental, numerical and analytical risk assessment of oil drilling rig welded pipe based on fracture mechanics parameters. *Eng Fail Anal.* 2020; 114: 104600. https://doi.org/10.1016/j.engfailanal.2020.104600

[20] Chen, X.G, Wu, X.G, Yan, M.G. Dugdale model for strain hardening materials. *Eng. Fract. Mech.* 1992; 41(6):843-871. https://doi.org/10.1016/0013-7944(92)90236-8.

[21] Lee, J-S, Ju, J-B, Jang, J-I, Kim, W-S, Kwon, D. Weld crack assessments in API X65 pipeline: failure assessment diagrams with variations in representative mechanical properties. *Mater Sci Eng. A* 2004; 373:122-130. https://doi.org/10.1016/j.msea.2003.12.039.

Numerička simulacija implantata kuka od legure titanijuma pod statičkim i dinamičkim opterećenjima

Tamara Smoljanić[1], Aleksa Milovanović[1], Simon Sedmak[1], Ljubica Milović[2] and Aleksandar Sedmak[3]

[1]*Inovacioni Centar Mašinskog fakulteta, Beograd, Srbija*
[2]*Univerzitet u Beogradu, Tehnološko-Metalurški fakultet, Beograd, Srbija*
[3]*Univerzitet u Beogradu, Mašinski fakultet, Beograd, Srbija*

(Naučni rad)

Izvod

U ovom radu je prikazan razvoj numeričkih modela za simulaciju implantata za zamenu zgloba kuka pod statičkim i dinamičkim opterećenjima, kao deo širokog istraživanja koje uključuje procenu integriteta implantata kuka u različitim uslovima, kao što su zamor i korozija. Numerički modeli su napravljeni u ABAQUS i ANSYS softverskim paketima, u cilju procene distribucije napon/deformacija i broja ciklusa do loma, kao i vrednosti faktora intenziteta napona za dve različite geometrije implanta kuka. ABAQUS modeli su korišćeni za simulaciju pod statičkim, a ANSYS modeli za simulaciju pod dinamičkim opterećenjima. Sledeća etapa analize uključuje poređenje ova dva slučaja, kako bi se odredilo koja od ove dve geometrije pruža bolje ponašanje u eksploatacionim uslovima, a koje mogu značajno varirati zavisno od pacijenta. Simulacije su vršene za pacijenta mase 90 kg. Za ovu svrhu, dijagrami procene rizika su napravljeni za obe navedene geometrije, pod pretpostavkom da je dužina inicijalne prsline 1 mm.

Ključne reči: Implantat kuka; Ti-6Al-4V; metoda konačnih elemenata; zamorna prslina; dijagram procene rizika

Prediction of thermal and mechanical properties of acrylate-based composites using artificial neural network modeling

Vanja Z. Mališić[1], Milada L. Pezo[2], Aleksandra N. Jelić[3], Aleksandra S. Patarić[4] and Slaviša S. Putić[1]

[1]*University of Belgrade, Faculty of Technology and Metallurgy, Belgrade, Serbia*
[2]*University of Belgrade, Department of Thermal Engineering and Energy, "Vinča" Institute of Nuclear Sciences - National Institute of the Republic of Serbia, Belgrade, Serbia*
[3]*Academy of Applied Technical Studies Belgrade, Belgrade, Serbia*
[4]*University of Belgrade, Institute of Chemistry, Technology and Metallurgy, Department for Materials and Metallurgy, Belgrade, Serbia*

Abstract

Poly(methyl methacrylate) (PMMA) has a broad spectrum of uses, especially in medical applications. The role of fine-grained alumina particles of PMMA composites was investigated in this study. The composites were based on PMMA modified with dimethyl itaconate (DMI) as a matrix and alumina particles (Al_2O_3) and alumina doped with iron (Al_2O_3-Fe) modified with 3-aminopropyl-trimethoxysilane (AM) and flax oil fatty acid methyl esters (biodiesel) as reinforcements. Three particle sizes were measured (~0.4, ~0.6 and ~1.2 μm). The highest thermal conductivity values were measured for the composite 5 wt.% Al_2O_3-Fe-AM. With the addition of 3 wt.% Al_2O_3-AM to the PMMA/DMI matrix, mechanical properties were improved (tensile strength, strain, and modulus of elasticity). An artificial neural network model based on the Broyden-Fletcher-Goldfarb-Shanno iterative algorithm was investigated for prediction of thermal conductivity and mechanical properties of the composites showing satisfactory results. This is relevant for applications for optimization of dental materials to produce dentures, which were exposed to variations in temperature during the application.

Keywords: Composite materials; thermal conductivity; Al_2O_3 particles.

Available on-line at the Journal web address: http://www.ache.org.rs/HI/

ORIGINAL SCIENTIFIC PAPER

UDC: 678.744.32-025.26: 675.017.5:004.414.23

Hem. Ind. **77(4)** 293-302 (2023)

1. INTRODUCTION

Poly(methyl methacrylate) (PMMA) is a transparent thermoplastic polymer that has a wide range of applications, such as wide use of acrylic bone cements, based on PMMA in dentistry and orthopedic surgery [1-7].

A biomaterial intended for such purposes has to be biocompatible exhibiting certain properties, such as being non-toxic, non-injurious, and not causing immunological rejection. Biomaterials include various metals, ceramics, polymers and composites. Toxicity of a material is very important, especially in applications in which the material is in contact with the body. Biomaterials based on PMMA are often used because of their good biocompatibility, non-toxicity, good adhesion to human tissues, and easy handling.

Nevertheless, PMMA has several drawbacks such as poor thermal stability, low toughness, and toxicity of residual monomers. In the case of monomer leakage from the material, the surrounding tissue can be irritated. Also, such a leakage can create structural damages like cracks that could lead to mechanical fracture of the material [8]. The amount of residual monomers methyl methacrylate (MMA) can be significantly reduced by adding dimethyl itaconate to PMMA [9-10].

Physical and mechanical properties of polymer materials can be modified by incorporation of inorganic particulate fillers in the polymer matrix in order to control the shrinkage and mechanical properties of the material [11]. These fillers can be SiO_2, Al_2O_3, $Mg(OH)_2$ or $CaCO_3$ micro- or nanoparticles, which were shown to improve stiffness, strength, modulus and hardness of the resulting composite material [12-13]. Mechanical properties can be adjusted by using fillers with the controlled crystal structure [14-15]. Alumina or aluminum oxide (Al_2O_3) is often used in composites as reinforcement and

Corresponding authors: Aleksandra S. Patarić, University of Belgrade, Institute of Chemistry, Technology and Metallurgy, Department for Materials and Metallurgy, Belgrade, Serbia
E-mail: aleksandra.pataric@ihtm.bg.ac.rs
Paper received: 19 January 2023; Paper accepted: 2 Decembarr 2023; Paper published: xx December 2023.
https://doi.org/10.2298/HEMIND230119029M

as materials for high-temperature applications because of their extraordinary chemical properties (*e.g.* resistance to the action of chemical substances, insoluble in acids) Regarding composite materials, different structures and morphologies of aluminum oxide can be obtained by thermal treatment [16]. The aim of this work was to synthesize novel composite materials based on a matrix made of PMMA/itaconate copolymer and to investigate the possibility of predicting the thermal conductivity, tensile strength, strain and modulus of elasticity by using artificial neural network (ANN) modeling.

2. MATERIALS AND METHODS

Commercial PMMA (Biocril (Galenika AD, Serbia)), (chemical grade *p.a.*) and dimethyl-itaconate (DMI) (Sigma-Aldrich, USA) (*p.a.*) were used to produce samples. The procedure for obtaining PMMA starts with preparation of a two-component system: a liquid component consisting of methyl methacrylate (MMA) (*p.a.*) as a monomer and ethylene glycol dimethacrylate (EGDMA) (*p.a.*) as a modifier, and a powder component consisting of prepolymerized PMMA coated with benzoyl peroxide (*p.a.*) as the initiator. The powder component, has been characterized in literature as follows: molecular weight is $M_n = 1.27\times10^5$ g·mol^{-1}, $M_w = 3.82\times10^5$ g·mol^{-1}, and the polydispersity index PI = 3.01, with a 4.3 wt.% of monomer content and an average particle size of 55 μm [17].

Submicron ferrous oxide (*p.a.*) doped alumina particles (Al_2O_3-Fe) were used as reinforcement. In specific, aluminium hydroxide chloride in crystallized state (Locron L; $Al_2(OH)_5Cl\times2.5H_2O$, Clariant, Swiss) (*p.a.*) was used as alumina forerunner, while iron chloride ($FeCl_3\times6H_2O$) (Sigma Aldrich, USA), (*p.a.*) was used as a source of iron ions. The ferrous oxide doped alumina particles were prepared from these two components in demineralized water by a sol-gel technique, according to the previously described method [18]. In the end product the mass ratio of Al_2O_3 to Fe_2O_3 would be 90/10. The obtained gel was ground and calcined for two hours at 900 °C, The obtained particles were characterized by a particle size analyzer (Zetasizer Nano-ZS, Malvern, UK) yielding three fractions with average diameters: d (0.1) = 0.4 μm, d (0.5) = 0.6 μm, d (0.9) = 1.2 μm [19]. The crystal structure was determined previously by X-ray diffraction (XRD) analysis and it was as follows: η-Al_2O_3 (39.4 %), ƙ-Al_2O_3 (35.1 %) and α-Al_2O_3 (25.5 %) [14].

The particles were modified with 3-aminopropyl, trimethoxysilane (AM), (*p.a.*), (Sigma Aldrich, USA) and methyl esters of linseed oil fatty acids (biodiesel - BD, (*p.a.*) (Sigma Aldrich, USA) and denoted as Al_2O_3-AM, Al_2O_3-BD, Al_2O_3-Fe-AM, and Al_2O_3-Fe-BD. In order to enable the bonding of alumina particle to the matrix, first trimethoxysilane (AM) was attached to the surface of the particles by using the procedure described previously [20]. Commercial aluminum oxide (Al_2O_3) nanoparticles were used as fillers, doped with iron oxide, and then integrated in different content (1, 3 and 5 wt.%).

2. 1. Preparation of PMMA/DMI composites reinforced with alumina particles

DMI is added to the liquid monomer followed by addition of PMMA powder so to obtain the PMMA matrix with 5 wt.% DMI. To avoid agglomeration and to obtain a good dispersion, composite materials were prepared by adding alumina particles to the monomer followed by dispersion in an ultrasonic bath for 30 min. Next, the powder component (63 wt.%) was added into the liquid forming a paste poured into a mold made of aluminium alloy and stirred for 5 min. The mold was then closed and heated at 70 °C for 1 h. The polymerization was completed at 100 °C within 30 min. Using 1, 3 and 5 wt.% of different alumina particles (13 sample groups prepared with iron oxide and alumina nanoparticles with two surface modifications), were prepared as it was described in a previous work [17]. PMMA combined with DMI creates polymer matrix (PMMA/DMI), hereinafter referred to as DMI. The composition of all 13 tested samples is given in Table 1.

Table 1. Thermal conductivity of PMMA/DMI matrix and obtained composites [17]. Permissions under Attribution 4.0 International (CC BY 4.0)

Sample	λ / W m-1·K-1	Sample	λ / W m^{-1}·K^{-1}
PMMA/DMI	0.2	1 wt.% Al_2O_3-Fe-AM	0.7
1 wt. % Al_2O_3-AM	0.6	3 wt.% Al_2O_3-Fe-AM	0.7
3 wt. % Al_2O_3-AM	0.5	5 wt.% Al_2O_3-Fe-AM	0.8
5 wt. % Al_2O_3-AM	0.7	1 wt.% Al_2O_3-Fe-BD	0.7
1 wt. % Al_2O_3-BD	0.6	3 wt.% Al_2O_3-Fe-BD	0.7
3 wt. % Al_2O_3-BD	0.6	5 wt.% Al_2O_3-Fe-BD	0.7
5 wt. % Al_2O_3-BD	0.6		

2. 2. Experimental data for ANN modeling

In our earlier research, thermal conductivity and mechanical characterization (tensile strength, strain and modulus of elasticity) of all 13 samples were examined [17]. In order to determine the mechanical properties of the specimens, the testing machine (Instron Testing Machine, model 6025, China) was used. The samples were in the form of a block with dimensions 2×5 mm and 5 cm in length. The obtained results were used in the present work to investigate possibilities to predict thermal conductivity and mechanical properties of the composites by using artificial neural network modeling (ANN model).

2. 3. Artificial neural network modeling

The artificial neural network (ANN) model was developed in the form of a multi-layer perceptron model (MLP), which consisted of three layers (input, hidden, and output). It was used for prediction of thermal conductivity, tensile strength, strain, and modulus of elasticity based on the composite composition, addition of Fe and modifier. In the literature, the ANN model was proven as quite capable for approximating nonlinear functions [19-22]. Before the calculation, both input and output data were normalized (according to min - max normalization scheme) to improve the behavior of the ANN. During this iterative process, input data were repeatedly presented to the network [23-25]. The Broyden-Fletcher-Goldfarb-Shanno (BFGS) algorithm was used as an iterative method for solving unconstrained nonlinear optimization during the ANN modeling.

The experimental database for ANN was randomly divided into training, cross-validation, and testing data (with 60, 20 and 20 % of experimental data, respectively). The training data set was used for the learning cycle of ANN and for the evaluation of the optimal number of neurons in the hidden layer and the weight coefficient of each neuron in the network. A series of different topologies were used, in which the number of hidden neurons varied from 5 to 20, and the training process of the network was run 100,000 times with random initial values of weights and biases. The optimization process was performed based on validation error minimization (the used error function was sum of square - SOS). It was assumed that successful training was achieved when learning and cross-validation curves approached zero.

Coefficients associated with the hidden layer (weights and biases) were grouped in matrices W_1 and B_1. Similarly, coefficients associated with the output layer were grouped in matrices W_2 and B_2. It is possible to represent the neural network by using matrix notation Eq. (1), (Y is the matrix of the output variables, f_1 and f_2 are transfer functions in the hidden and output layers, respectively, and X is the matrix of input variables) [25]:

$$Y = f_1(W_2 f_2(W_1 X + B_1)\, B_2 \tag{1}$$

Weight coefficients (elements of matrices W_1 and W_2) were determined during the ANN learning cycle, which updated them using optimization procedures to minimize the error between the network and experimental outputs [23,26-27] according to the sum of squares (SOS) and BFGS algorithm, used to speed up and stabilize convergence [28]. The coefficients of determination were used as parameters to check the performance of the obtained ANN model. The ANN model calculation was performed using computer program StatSoft Statistica 12 (Tibsco software, USA) [29].

2. 4. Sensitivity analysis

In order to determine the relative influence (*RI*) of input variables (particle amount, addition of Fe and modifiers) on output variables (thermal conductivity, tensile strength, strain and modulus of elasticity), the Yoon's interpretation method was applied. The following equation was used, developed by Yoon, Swales, & Margavio [30]:

$$RI_{ij} = \frac{\sum_{k=0}^{n}\left(w_{ik}w_{kj}\right)}{\sum_{i=0}^{m}\left|\sum_{k=0}^{n}\left(w_{ik}w_{kj}\right)\right|}100 \tag{2}$$

where, RI_{ij} is the relative importance of the i^{th} input variable on the j^{th} output, w_{ik} is the weight between the i^{th} input and the k^{th} hidden neuron, and w_{kj} is the weight between the k^{th} hidden neuron and the j^{th} output.

2. 5. Accuracy of the model

The numerical verification of the developed model was tested using the coefficient of determination (r^2), reduced chi-square (χ^2), mean bias error (MBE), root mean square error (RMSE), and mean percentage error (MPE). These commonly used parameters can be calculated as follows [31]:

$$\chi^2 = \frac{\sum_{i=1}^{N}(x_{\text{exp,i}} - x_{\text{pre,i}})^2}{N-n}, \quad (3)$$

$$\text{RMSE} = \left[\frac{1}{N}\sum_{i=1}^{N}(x_{\text{pre},i} - x_{\text{exp},i})^2\right]^{1/2}, \quad (4)$$

$$\text{MBE} = \frac{1}{N}\sum_{i=1}^{N}(x_{\text{pre},i} - x_{\text{exp},i}), \quad (5)$$

$$\text{MPE} = \frac{100}{N}\sum_{i=1}^{N}\frac{\left|x_{\text{pre},i} - x_{\text{exp},i}\right|}{x_{\text{exp},i}} \quad (6)$$

where $x_{\text{exp},i}$ stands for the experimental values and $x_{\text{pre},i}$ are the predicted values calculated by the model, N and n are the number of observations and constants, respectively.

The analysis and mathematical modeling were performed using StatSoft Statistica 12 (Tibsco software, USA) [29]..

3. RESULTS AND DISCUSSION

Thermal stability is crucial for materials, with applications in dentistry and medicine. It is acknowledged that aluminum oxide particles exhibit superior thermal conductivity in comparison to PMMA matrix. This difference is attributed to the variance in their crystal structures, [32-34]. Consequently, integrating these particles into the matrix can alter its thermal conductivity, as demonstrated by the results presented in Table 1, [17].

Compared to PMMA/DMI, an evident increase in thermal conductivity was obtained by the addition of fillers (Table 1). The addition of 1 wt.% particles increased heat conductivity in all samples, while the lowest value was found for the composite with 1 wt.% Al_2O_3-BD. As alumina exhibits higher thermal conductivity (12-38.5 W $m^{-1}\cdot K^{-1}$) as compared to PMMA (0.167-0.25 W $m^{-1}\cdot K^{-1}$) [34], further addition of particles induced higher thermal conductivity values. Due to the difference in chemical structure, dense crystal structure with a content of alpha phase in alumina, contributes to better thermal conductivity. It should be noticed that the highest conductivity values were determined for composites with Al_2O_3-Fe particles. The presence of BD on alumina surfaces decreases the thermal conductivity when compared to modification with AM and impedes further increase in the thermal conductivity [17].

Mechanical tests of all 13 were performed previously to examine the influence of different amounts of alumina particles on the tensile properties [17]. The values of tensile strength at break (R_m), strain (ε) and modulus of elasticity (E) are shown in Table 2. All specimens with the incorporation of 3 wt.% particles reveal an important increase in some of tested mechanical properties (R_m, ε and E). This increase may be attributed to the efficient scattering of Al_2O_3-Fe particles [35]. A larger number of dipol/dipol intermolecular synergy was created by hydroxyl groups on surface and polar groups of PMMA/DMI matrix. The newly created material with addition of 3 wt.% Al_2O_3-Fe AM, compared to PMMA/DMI, had the modulus of elasticity increased by 37 %. As it was shown in our previous work, new materials strengthened with particles modified with AM had improved compatibility in the PMMA/DMI matrix compared to those modified with BD [17].

It is important to mention that these are our first investigations of polymer composite material and that differences in the obtained results are expected. The obtained results represent the basis for further research and contribution in this research area.

Table 2. Mechanical properties of the PMMA/DMI matrix and the obtained composites: tensile stress, strain and modulus of elasticity depending on the amount and type of particles [17]. Permissions under Attribution 4.0 International (CC BY 4.0)

Sample	R_m / MPa	ε / %	E / MPa
PMMA/DMI	39.8	7.9	802.4
1 wt.% Al_2O_3-AM	48.9	7.6	761.7
3 wt.% Al_2O_3-AM	49.4	11.4	839.1
5 wt.% Al_2O_3-AM	36.2	5.2	550.5
1 wt.% Al_2O_3-BD	38.0	9.7	567.9
3 wt.% Al_2O_3-BD	46.9	12.8	592.2
5 wt.% Al_2O_3-BD	25.9	8.6	471.9
1 wt.% Al_2O_3-Fe-AM	36.7	6.1	897.3
3 wt.% Al_2O_3-Fe-AM	47.1	5.6	1096.7
5 wt.% Al_2O_3-Fe-AM	35.2	4.4	827.3
1 wt.% Al_2O_3-Fe-BD	37.1	9.9	745.8
3 wt.% Al_2O_3-Fe-BD	42.1	9.5	774.8
5 wt.% Al_2O_3-Fe-BD	29.6	8.2	630.8

3. 1. Artificial neural network model

The artificial neural network (ANN) model was developed in the form of multi-layer perceptron model (MLP), with 5 inputs (input variables were particle amount and addition of ferrous oxide as continuous variables, and addition of modifier as a categorical variable, with logical values 0, AM and BD), 9 neurons in the hidden layer and 4 output variables (thermal conductivity, tensile strength, strain and modulus of elasticity). The acquired optimal neural network model showed a good generalization capability for the experimental data and could be used to accurately predict the output values based on the input variables. To obtain the highest values of r^2 (during the training cycle r^2 for output variables were: 0.998; 0.999; 0.999; and 0.999, respectively), shown in Table 3.

Table 3 Artificial neural network model summary (performance and errors), for training, testing, and validation cycles

Network name	ANN performance			Error			Training algorithm	Error function	Hidden activation	Output activation
	Train.	Test.	Valid.	Train.	Test.	Valid.				
MLP 5-9-4	0.999	0.998	0.998	0.001	0.003	0.002	BFGS[a] 226	SOS	Logistic sigmoidal	Identity

Train. –TTraining cycle; Test. – Testing cycle, Valid. – validation cycle during ANN developing.
Performance term represents the coefficients of determination, while error terms indicate a lack of data for the ANN model
BFGS - Broyden-Fletcher-Goldfarb-Shanno algorithm

The obtained ANN model for prediction of output variables was complex (94 weights-biases) because of the high nonlinearity of the observed system [36,37].

The accuracy of the ANN model could be visually assessed by presenting dispersion of points from the diagonal line in the graphics shown in Figure 1. For the ANN model, the predicted values were very close to the measured values in most cases, in terms of r^2 values. SOS values obtained with the ANN model were of the same order of magnitude as experimental errors for the outputs i.e. thermal conductivity, tensile strength, strain, and modulus of elasticity.

The elements of matrix W_1 and vector B_1 (presented in the bias column) are presented in Table 4, while in Table 5 are shown the elements of matrix W_2 and vector B_2 (bias) for the hidden layer, used for calculation in Eq. 2.

The goodness of fit between experimental measurements and model-calculated outputs, represented as ANN performance (sum of r^2 between measured and calculated output variables), during training, testing and validation steps, are shown in Table 6.

A high r^2 is indicative that the variation was accounted for and that the data fitted the proposed model satisfactorily [38].

The residual analysis of the developed model was presented in Table 7. The ANN model had an insignificant lack of fit tests, which means the model satisfactorily predicted the thermal and mechanical properties of the acrylate-based composites.

The ANN model predicted experimental variables reasonably well for a broad range of the process variables.

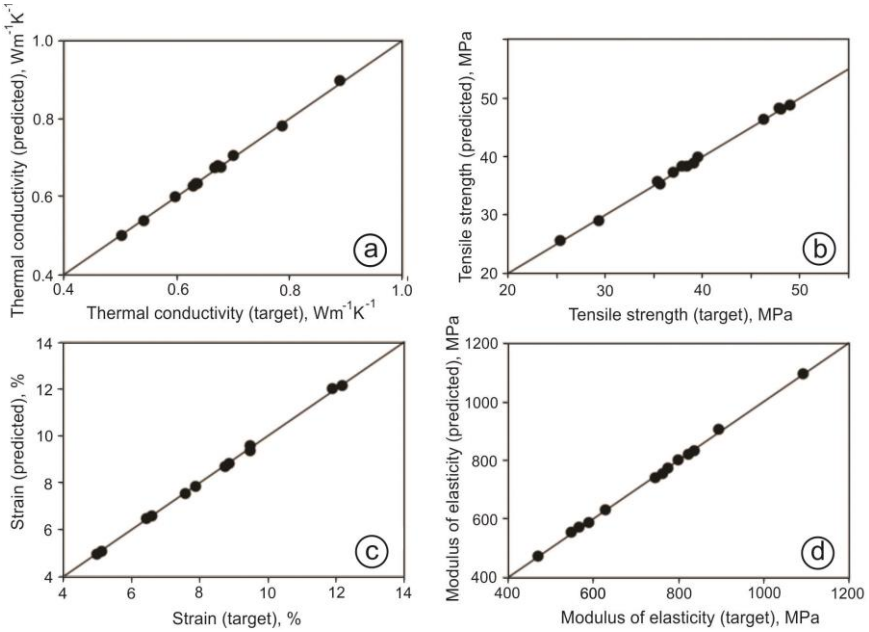

Figure 1. Comparison between experimental and calculated values of thermal conductivity (a), tensile strength (b), strain (c) and modulus of elasticity (d)

Table 4 Elements of matrix W_1 and vector B_1 (presented in the bias column)

Input variables	Neurons								
	1	2	3	4	5	6	7	8	9
Particle amount	-3.069	-6.347	-0.327	-7.049	-3.393	-0.294	-3.355	-1.601	-3.239
Addition of Fe	1.775	1.296	-0.113	-3.405	-1.850	2.122	5.535	4.369	-0.343
Addition of modifier (0)	-0.565	-1.429	0.891	-0.218	1.619	-0.513	-0.287	0.789	-0.430
Addition of modifier (AM)	0.333	0.496	-0.951	0.614	-0.717	1.129	-1.135	-1.874	-0.429
Addition of modifier (BD)	0.192	0.217	2.267	4.222	1.543	-0.287	-1.879	5.152	1.515
Bias	-0.004	-0.790	2.235	4.696	2.571	0.311	-3.291	3.886	0.809

Table 5 Elements of matrix W_2 and vector B_2 (presented in the bias column)

Outputvariables	Neurons									Bias
	1	2	3	4	5	6	7	8	9	
Thermal conductivity	1.812	-2.589	0.640	-1.416	2.018	-1.226	1.760	-1.022	-1.290	1.414
Tensile strength	-1.051	-4.847	-1.441	0.545	1.380	1.425	3.989	-1.102	0.904	0.740
Strain	1.200	-2.736	-0.094	2.033	-2.613	-0.871	-0.097	-1.713	1.109	2.325
Modulus of elasticity	0.866	-3.052	-1.944	-0.110	0.241	-0.729	1.728	0.921	0.531	1.300

Table 6. The "goodness of fit" tests for the developed ANN model

Output variable	χ^2	RMSE	MBE	MPE	r^2
Thermal conductivity	0.000	0.004	0.001	0.577	0.998
Tensile strength	0.043	0.172	0.038	0.362	0.999
Strain	0.004	0.054	-0.027	0.607	1.000
Modulus of elasticity	16.999	3.430	0.444	0.355	1.000

Table 7. The residual analysis of the ANN model

Output variable	Skew	Kurt	Mean	SD	Var
Thermal conductivity	-1.141	0.736	0.001	0.004	0.000
Tensile strength	0.492	-0.443	0.038	0.174	0.030
Strain	0.704	-0.695	-0.027	0.049	0.002
Modulus of elasticity	-0.513	-0.239	0.444	3.541	12.535

Skew - skewness, Kurt - kurtoisis, Mean - mean value of residuals, SD - standard deviation of residuals,
Var - variation of residual values

3. 2. Global sensitivity analysis- the Yoon's interpretation method

In this section the influence of input variables (particle amount, addition of Fe and modifier) on relative importance (*RI*) for thermal conductivity, tensile force, strain, and modulus of elasticity was studied. According to Figure 2, particle amount (wt.%) was the most influential parameter with approximately relative importance of 34 % for thermal conductivity calculation, while the influence of modifier BD was negative (-29 %). The particle amount (wt.%) was the most influential parameter with approximately relative importance of 28 % for tensile strength calculation, while the influence of modifier BD was negative (-31 %). Similarly, the particle amount (wt%) was the most influential parameter for strain calculation with approximately relative importance of 25 %, while the influence of addition of Fe was negative (-44 %). Finally, the particle amount (wt.%) and addition of Fe were the most influential parameters for modulus of elasticity calculation with approximately relative importance of 25 and 35 %, respectively, while the influence of modifier AM was negative (16 %).

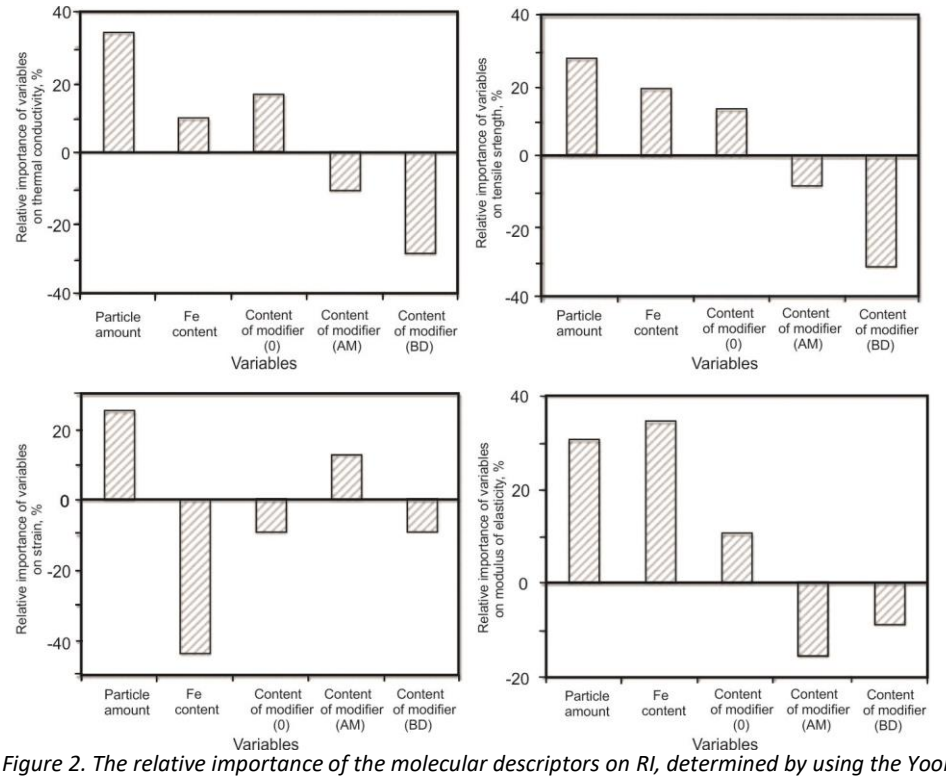

Figure 2. The relative importance of the molecular descriptors on RI, determined by using the Yoon interpretation method

Review of the available literature has shown that application of the ANN model in this field is lacking, and it can be considered that a database for this model is newly formed in the present work. Based on the results of the developed model, it was shown that the model is well suited and that filling the database with new experimental data will enable its wider validation and utilization. It was shown that the particle amount has the greatest influence on all tested properties, and that the addition of Fe has a high influence on the modulus of elasticity. Very high values of the coefficient of determination (r^2), obtained by the model, show the matching of the calculated values with the experimental results.

4. CONCLUSION

Based on the results of this study, thermal conductivity, tensile strength, strain, and modulus of elasticity of PMMA/DMI composites were improved by adding alumina-based reinforcement to the polymer matrix. Aluminum oxide-based particles were used as reinforcement modified with organosilane-3-aminopropyl-trimethoxylane (AM) and in the second stage with fatty acid methyl esters (biodiesel). Surface modification provided better bonding of particles

with the polymer matrix by covalent and hydrogen bonds and dipole-dipole interactions. Mechanical and thermal properties of the newly obtained composites were improved by adding these particles.

The artificial neural network model was shown to be adequate for prediction of thermal and mechanical properties (i.*e.* thermal conductivity, tensile force, strain, and modulus of elasticity) as output variables as functions of input variables (*i.e.* particle amount, addition of Fe and modifier) (the r^2 values during training cycle for these variables were: 0.998; 0.999; 0.999 and 0.999, respectively). It has been established that there are evident overlaps between the predictions of the applied mathematical models and the obtained experimental data, so we can conclude that the artificial neural network model has a good perspective in predicting thermal and mechanical properties in this field of composite materials.

Acknowledgements: *This work was supported by the Ministry of Science, Technological Development and Innovation of the Republic of Serbia (Contract No. 451-03-47/2023-01/20023)*

REFERENCES

[1] Kurtz SM, Villarraga ML, Zhao K, Edidin AA. Static and fatigue mechanical behavior of bone cement with elevated barium sulfate content for treatment of vertebral compression fractures. *Biomaterials*. 2005; 26: 3699-3712. https://doi.org/10.1016/j.biomaterials.2004.09.055

[2] Pascual B, Vtiquez B, Gurruchaga M, Goti I, Ginebra MP, Gil FJ, Planell JA, Levenfeld B, San Romans J. New Aspects of the Effect of Size and Size Distribution on the Setting Parameters and Mechanical Properties of Acrylic Bone Cements. *Biomaterials*. 1996; 17: 509-516. https://doi.org/10.1016/0142-9612(96)82725-6

[3] Serbetci K, Korkusuz F, Hasirci N. Thermal and Mechanical Properties of Hydroxyapatite Impregnated acrylic bone cements. *Polym Test*. 2004; 23: 145-155. https://doi.org/10.1016/S0142-9418(03)00073-4

[4] Provenzano MJ, Murphy KPJ, Riley LH. Bone Cements: review of their physiochemical and biochemical properties in percutaneous vertebroplasty. *AJNR Am J Neuroradiol.* 2004; 25: 1286-1290. http://www.ajnr.org/content/25/7/1286.short

[5] Haas SS, Brauer GM, Dickson GA. Characterization of Poly Methyl Methacrylate Bone Cement. *J Bone Joint Surg Am*. 1957; 57: 380-391. https://pubmed.ncbi.nlm.nih.gov/1123392/

[6] Postawa P, Szarek A, Koszkul J. DMTA method in determining strength parameters of acrylic cements. *Arch Mater Sci Eng*. 2007; 28: 309-312. http://www.amse.acmsse.h2.pl/vol28_5/28512.pdf

[7] Khaled SMZ, Charpentier PA, Rizkalla AS. Physical and mechanical properties of PMMA bone cement reinforced with nano-sized titania fibers. *J Biomater Appl.* 2011; 25: 515-537. https://doi.org/10.1177/0885328209356944

[8] Fernández-Garcia M, Fuente JL, Madruga EL, Thermal behavior of poly(dimethyl itaconate) and poly(di-n-butyl itaconate) copolymerized with methyl methacrylate. *Polym Eng Sci.* 2001; 41: 1616-1625. https://doi.org/10.1002/pen.10859

[9] EN ISO 20795-1:2013 Dentistry - Base polymers- Part 1: Denture base polymers (ISO 20795-1:2013).

[10] Spasojević P, Stamenković D, Pjanović R, Bošković Vragolović N, Dolić J, Grujić S, Veličković S. Diffusion and solubility of commercial poly(methyl methacrylate) denture base material modified with dimethyl itaconate and di-n-butyl itaconate during water absorption/desorption cycles. *Polym Int.* 2012; 61: 1272-1278. https://doi.org/10.1002/pi.4202

[11] Alzarrug FA, Dimitrijević MM, Jančić Heinemann RM, Radojević V, Stojanović DB, Uskoković PS, Aleksić R. The use of different alumina fillers for improvement of the mechanical properties of hybrid PMMA composites. *Mater Des.* 2015; 86: 575-581. https://doi.org/10.1016/j.matdes.2015.07.069

[12] Fu SY, Feng XQ, Lauke B, Mai YW. Effects of particle size, particle/matrix interface adhesion and particle loading on mechanical properties of particulate-polymer composites. *Compos B Eng.* 2008; 39: 933-961. https://doi.org/10.1016/j.compositesb.2008.01.002

[13] Johnsen BB, Fromyr TR, Thorvaldsen T, Olsen T. Preparation and characterization of epoxy/alumina polymer nanocomposites. *Compos Interfaces.* 2013; 20: 721-740. https://doi.org/10.1080/15685543.2013.815603

[14] Lazouzi GA, Vuksanović MM, Tomić NZ, Mitrić M, Petrović M, Radojević V, Heinemann RJ. Optimized preparation of alumina based fillers for tuning composite properties. *Ceram Int.* 2018; 44: 7442-7449. https://doi.org/10.1016/j.ceramint.2018.01.083

[15] Mathieu A, Matteï S, Deschamps A, Martin B, Grevey D. Temperature control in laser brazing of a steel/aluminium assembly using thermographic measurements. *NDT E Int.* 2006; 39: 272-276. https://doi.org/10.1016/j.ndteint.2005.08.005

[16] Ma J, Wu B. Effect of surfactants on preparation of nanoscale-Al_2O_3 powders by oil-inwater micro emulsion. *Adv Powder Technol*. 2013; 24: 354-358. https://doi.org/10.1016/j.apt.2012.08.008

[17] Mališić V, Tomić N, Vuksanović M, Balač B, Stević Z, Marinković A, Jančić-Heinemann R, Putić S. An Experimental study of mechanical properties and heat transfer of acrylic composites with structural and surface modified Al_2O_3 particles. *Sci Sinter*. 2020; 52: 457-467. https://doi.org/10.2298/SOS2004457M

[18] Rizzo P, Scalea FL. Acoustic emission monitoring of carbon-fiber-reinforced polymerbridge stay cables in large-scale testing. *Exp Mech.* 2001; 41: 282-290. https://doi.org/10.1007/BF02323146

[19] Johnson DP, Stanforth A, Lulla V, Luber G. Developing an applied extreme heat vulnerability index utilizing socioeconomic and environmental data. *Appl Geogr.* 2012; 35: 23-31. https://doi.org/10.1016/j.apgeog.2012.04.006
[20] Yun TS, Jeong YJ, Han TS, Youm KS. Evaluation of thermal conductivity for thermally insulated concretes. *Energy Build*. 2013; 61: 125-132. https://doi.org/10.1016/j.enbuild.2013.01.043
[21] Kleijnen JPC. *Design and Analysis of Simulation Experiments*. Springer, US, 2018; 111-121. https://doi.org/10.1007/978-3-319-76035-3_1
[22] Pavlić B, Pezo L, Marić B, Peić Tukuljac L, Zeković Z, Bodroža Solarov M, Teslić N. Supercritical fluid extraction of raspberry seed oil: Experiments and modelling. *J Supercrit Fluids.* 2020; 157: 104687. https://doi.org/10.1016/j.supflu.2019.104687
[23] Kollo T, Rosen D. *Advanced Multivariate Statistics with Matrices*. Springer, Dordrecht, 2005. 98-125. https://link.springer.com/book/10.1007/1-4020-3419-9
[24] Pezo L, Ćurčić BLj, Filipović VS, Nićetin MR, Koprivica GB, Mišljenović NM, Lević LjB. Artificial neural network model of pork meat cubes osmotic dehydratation. *Hem Ind*. 2013; 67: 465-475. https://doi.org/10.2298/HEMIND120529082P
[25] Ochoa-Martínez CI, Ayala-Aponte AA. Prediction of mass transfer kinetics during osmotic dehydration of apples using neural networks. *LWT - Food Sci Technol*. 2007; 40: 638-645. https://doi.org/10.1016/j.lwt.2006.03.013
[26] Berrueta LA, Alonso-Salces RM, Héberger K. Supervised pattern recognition in food analysis. *J Chromatogr*. 2007; 1158: 196-214. https://doi.org/10.1016/j.chroma.2007.05.024
[27] Doumpos M, Zopounidis C. Preference disaggregation and statistical learning for multicriteria decision support: A review. *Eur J Oper Res.* 2011; 209: 203-214. https://doi.org/10.1016/j.ejor.2010.05.029
[28] Taylo BJ. *Methods and Procedures for the Verification and Validation of Artificial Neural Networks*. Springer Science & Business Media, New York, 2006; 51-67. https://doi.org/10.1007/0-387-29485-6
[29] https://statistica.software.informer.com/12.7/
[30] Yoon Y, Swales G , Margavio TM. A Comparison of Discriminant Analysis versus Artificial Neural Networks. *J Oper Res Soc*. 1993; 44: 51-60. https://doi.org/10.2307/2584434
[31] Aćimović M, Pezo L, Tešević V, Čabarkapa I, Todosijević M. QSRR Model for predicting retention indices of Satureja kitaibelii Wierzb. ex Heuff. essential oil composition. *Ind Crops Prod.* 2020; 154: 112752. https://doi.org/10.1016/j.indcrop.2020.112752
[32] Dos Santos WN, De Sousa JA, Gregorio R. Thermal conductivity behaviour of polymers around glass transition and crystalline melting temperatures. *Polym Test.* 2013; 32: 987-994. https://doi.org/10.1016/j.polymertesting.2013.05.007
[33] Friederich B, Laachachi A, Ferriol M, Ruch D, Cochez M, Toniazzo V. Tentative links between thermal diffusivity and fire-retardant properties in poly(methyl methacrylate)-metal oxide nanocomposites. *Polym Degrad Stab*. 2010; 95: 1183-1193. https://doi.org/10.1016/j.polymdegradstab.2010.04.008
[34] Patel T, Suin S, Bhattacharya D, Khatua BB. Transparent and Thermally Conductive Polycarbonate (PC)/Alumina (Al_2O_3) Nanocomposites: Preparation and Characterizations. *Polym Plast Technol Eng.* 2013; 52: 1557-1565. https://doi.org/10.1080/03602559.2013.824464
[35] Lazouzi GA, Vuksanović MM, Tomić N, Petrović M, Spasojević P, Radojević V, Jančić R H. Dimethyl Itaconate Modified PMMA - Alumina Fillers Composites With Improved Mechanical Properties. *Polym Compos.* 2019; 40: 1691-1701. https://doi.org/10.1002/pc.24952
[36] Montgomery DC. *Design and Analysis of Experiments*.Wiley, 2012; ISBN 9781118146927
[37] Chattopadhyay PB, Rangarajan R. Application of ANN in sketching spatial nonlinearity of unconfined aquifer in agricultural basin. *Agric Water Manag.* 2014; 133: 81-91. https://doi.org/10.1016/j.agwat.2013.11.007
[38] Erbay Z, Icier F. Optimization of hot air drying of olive leaves using response surface methodology. *J Food Eng*. 2009; 91: 533-541 https://doi.org/10.1016/j.jfoodeng.2008.10.004

Predviđanje termičkih i mehaničkih svojstava kompozita na bazi akrilata korišćenjem modela veštačke neuronske mreže

Vanja Z. Mališić[1], Milada L. Pezo[2], Aleksandra N. Jelić[3], Aleksandra S. Patarić[4] i Slaviša S. Putić[1]

[1]Univerzitet u Beogradu, Tehnološko -metalurški fakultet, Beograd, Srbija
[2]Univerzitet u Beogradu, Institut za nuklearne nauke Vinča, Institut od nacionalnog značaja za Republiku Srbiju, Beograd, Srbija
[3]Akademija tehničkih strukovnih studija Beograd, Beograd, Srbija
[4]Univerzitet u Beogradu, Institut za hemiju, tehnologiju i metalurgiju, Institut od nacionalnog značaja za republiku Srbiju, Beograd, Srbija

(Naučni rad)

Izvod

Poli (metil metakrilata) (PMMA) ima široku upotrebu, posebno u stomatologiji i medicini. Kompoziti su napravljeni od PMMA modifikovanog dimetil itakonatom (DMI) kao matrice. Kao pojačanje korišćene su čestice glinice (Al_2O_3) i glinice dopirane oksidom gvožđa (Al_2O_3-Fe) modifikovanim sa 3-aminopropil-trimetoksilanom (AM) i metil estrima masnih kiselina lanenog ulja (biodizel – BD). Prema merenjima toplotne provodljivosti, najveće vrednosti toplotne provodljivosti imao je kompozit sa česticama glinice 5 wt.% Al_2O_3-Fe-AM. Dodatkom modifikovanih čestica glinice u PMMA/DMI matricu, poboljšane su mehaničke osobine (zatezna čvrstoća, deformacija i modul elastičnosti). Razvijen je model veštačke neuronske mreže zasnovan na iterativnom algoritmu predloženom u literaturi (Broiden-Fletcher-Goldfarb-Shanno), za predviđanje toplotne provodljivosti i mehaničkih svojstava kompozita na bazi akrilata u kombinaciji sa česticama na bazi glinice, u zavisnosti od masenog udela čestica, i dodatka oksida gvožđa i modifikatora. Pokazano je da ovi matematički modeli mogu predvideti mehanička i termička svojstva kompozitnih materijala. Ovo je posebno relevantno za predviđanje toplotne provodljivosti materijala koji se koriste u stomatologiji za izradu proteza i koji su izloženi temperaturnim promenama tokom primene.

Ključne reči: kompozitni materijali; toplotna provodljivost; Al_2O_3 čestice

SPISAK RECENZENATA

Spisak recenzenata radova čije je procesiranje završeno tokom 2023. godine

List of reviewers of papers whose processing has been completed during 2023

1. **Stergios Adamopoulos**, *Department of Forest Biomaterials and Technology, Swedish University of Agricultural Sciences, Sweden*
2. **Ana Alil***, Tehnološko-metalurški fakultet, Univerzitet u Beogradu, Srbija*
3. **Koviljka Asanović**, *Tehnološko-metalurški fakultet, Univerzitet u Beogradu, Srbija*
4. **Desalegn Atalie**, *Bahir Dar University, Bahir Dar, Amhara, Ethiopia*
5. **Hasan Avdušinović***, Metalurško-tehnološki fakultet, Univerzitet u Zenici, Bosna i Hercegovina*
6. **Cemre Avşar**, *Toros Agri and Trade Co. Inc, R&D Center, Mersin, Turkey*
7. **Jelena Bajat***, Tehnološko-metalurški fakultet, Univerzitet u Beogradu, Srbija*
8. **Ivana Banković Ilić***, Tehnološki fakultet u Leskovcu, Univerzitet u Nišu, Srbija*
9. **Dejan Bezbradica***, Tehnološko-metalurški fakultet, Univerzitet u Beogradu, Srbija*
10. **Matejka Bizjak**, *Oddelka za tekstilstvo, grafiko in oblikovanje, Naravoslovnotehniška fakulteta, Univerza v Ljubljani, Slovenija*
11. **Luqman Buchori,** *Department of Chemical Engineering, Faculty of Engineering, Diponegoro University, Indonesia*
12. **Nevenka Bošković-Vragolović,** *Tehnološko-metalurški fakultet, Univerzitet u Beogradu, Srbija*
13. **Gradimir Cvetanović,** *Tehnološki fakultet u Leskovcu, Univerzitet u Nišu, Srbija*
14. **Aleksandar Ćirić,** *Institut za nuklearne nauke Vinča, Univerzitet u Beogradu, Srbija*
15. **Ljiljana Damjanović,** *Fakultet za fizičku hemiju, Univerzitet u Beogradu, Srbija*
16. **Slađana Davidović**, *Tehnološko-metalurški fakultet, Univerzitet u Beogradu, Srbija*
17. **Aleksandar Dekanski,** *Institut za hemiju tehnologiju i metalurgiju, Univerzitet u Beogradu, Srbija*
18. **Ivana Drvenica**, *Institut za medicinska istraživanja, Univerzitet u Beogradu, Srbija*
19. **Đorđe Đatkov,** *Fakultet tehničkih nauka, Univerzitet u Novom Sadu, Srbija*
20. **Raúl Hernández-Altamirano**, *Centro Mexicano para la Producción más Limpia, Instituto Politécnico Nacional, Ciudad de México, Mexico*
21. **Margarida Fernandes**, *Universidade do Minho Centro de Física, Portugal*
22. **Is Fatimah,** *Department of Chemistry, Faculty of Mathematics and Natural Sciences, Universitas Islam Indonesia, Yogyakarta, Indonesia*
23. **Nenad Filipović,** *Institut tehnickih nauka Srpske akademije nauka i umetnosti, Beograd, Srbija*
24. **Branimir Grgur,** *Tehnološko-metalurški fakultet, Univerzitet u Beogradu, Srbija*
25. **Jale Gülen***, Chemical Engineering Department, Yildiz Technical University, Esenler-Istanbul, Turkey*
26. **Dragana Kopitar**, *Institut za hemiju, tehnologiju i metalurgiju, Univerzitet u Beogradu, Srbija*
27. **Milan Kostić,** *Tehnološki fakultet Leskovac, Univerzitet u Nišu, Srbija*
28. **Stjepan Kožuh,** *Metalurški fakultet, Sveučilište u Zagrebu, Sisak, Hrvatska*
29. **Milan Kragović**, *Institut za nuklearne nauke Vinča, Univerzitet u Beogradu, Srbija*
30. **Vesna Lazić,** *Centar izvrsnosti za fotokonverziju, INN Vinča, Univerzitet u Beogradu, Srbija*
31. **Nataša Lukić,** *Tehnološki fakultet, Univerzitet u Novom Sadu, Srbija*
32. **Divna Majstorović,** *Tehnološko-metalurški fakultet, Univerzitet u Beogradu, Srbija*
33. **Marina Maletić,** *Inovacioni centar Tehnološko-metalurškog fakulteta, Univerzitet u Beogradu, Srbija*
34. **Branislav Marković**,*Institut za tehnologiju nuklearnih i drugih mineralnih sirovina, Beograd*
35. **Bojan Međo,** *Tehnološko-metalurški fakultet, Univerzitet u Beogradu, Srbija*
36. **Tatjana Mihailović**, *Tehnološko-metalurški fakultet, Univerzitet u Beogradu, Srbija*
37. **Marija Milić,** *Tehnološko-metalurški fakultet, Univerzitet u Beogradu, Srbija*
38. **Dušan Mijin***, Tehnološko-metalurški fakultet, Univerzitet u Beogradu, Srbija*

39. **Darko Motik,** *Fakultet šumarstva i drvne tehnologije, Sveučilište u Zagrebu, Hrvatska*
40. **Biswajit Nath,** *Department of Chemistry, Bodoland University, Kokrajhar, 783370, Assam, India*
41. **Marija Nikolić***, Tehnološko-metalurški fakultet, Univerzitet u Beogradu, Srbija*
42. **Branislava Nikolovski,** *Tehnološki fakultet, Univerzitet u Novom Sadu, Srbija*
43. **Leon Oblak,** *Biotehniška fakulteta, Univerza v Ljubljani, Ljubljana, Slovenija*
44. **Bojana Obradović,** *Tehnološko-metalurški fakultet, Univerzitet u Beogradu, Srbija*
45. **Vesna Panić,** *Inovacioni centar Tehnološko-metalurškog fakulteta, Univerzitet u Beogradu, Srbija*
46. **Jelena Pavlović**, *Inovacioni centar Tehnološko-metalurškog fakulteta, Univerzitet u Beogradu, Srbija*
47. **Stefan Pavlović**, *Institut za hemiju, tehnologiju i metalurgiju, Univerzitet u Beogradu, Srbija*
48. **Vladimir Pavičević**, *Tehnološko-metalurški fakultet, Univerzitet u Beogradu, Srbija*
49. **Jelena Petrović***, Institut za tehnologiju nuklearnih i drugih mineralnih sirovina, Beograd, Srbja*
50. **Viktor Pocajt**, *Tehnološko-metalurški fakultet, Univerzitet u Beogradu, Srbija*
51. **Danijela Popović**, *Inovacioni centar Tehnološko-metalurškog fakulteta, Srbija*
52. **Mirjana Rajilicć-Stojanović**, *Tehnološko-metalurški fakultet, Univerzitet u Beogradu, Srbija*
53. **Zoran Ristić,** *Centar izvrsnosti za fotokonverziju, Institut za nuklearne nauke Vinča, Univerzitet u Beogradu, Srbija*
54. **Ivana Salopek Čubrić,** *Tekstilno–tehnološki fakultet, Sveučilište u Zagrebu, Hrvatska*
55. **Marko Stamenić,** *Tehnološko-metalurški fakultet, Univerzitet u Beogradu, Srbija*
56. **Olivera Stamenković**, *Tehnološki fakultet Univerziteta u Nišu, Leskovac, Srbija*
57. **Snežana Stanković,** *Tehnološko-metalurški fakultet, Univerzitet u Beogradu, Srbija*
58. **Mirko Stijepović,** *Tehnološko-metalurški fakultet, Univerzitet u Beogradu, Srbija*
59. **Srećko Stopić,** *IME Metallurgische Prozesstechnik und Metallrecycling, RWTH Aachen, Germany*
60. **Marija Štulović**, *Inovacioni centar Tehnološko-metalurškog fakulteta, Srbija*
61. **Mariana Ursache**,*"Gh. Asachi" Technical University of Iasi, Romania*
62. **Simona Vasile,** *University College Gent, Belgium*
63. **Miodrag Višković,** *Fakultet tehničkih nauka, Univerzitet u Novom Sadu, Srbija*
64. **Marija Vuksanović,** *Tehnološko-metalurški fakultet, Univerzitet u Beogradu, Srbija*
65. **Koleta Zafirova***, Faculty of Technology and Metalllurgy, Ss. Cyril and Meyhodius University, Skopje, North Mcedonia*
66. **Predrag M. Živković,** *Tehnološko-metalurški fakultet, Univerzitet u Beogradu, Srbija*
67. **Emila Živković***, Tehnološko-metalurški fakultet, Univerzitet u Beogradu, Srbija*
68. **Irena Žižović,** *Faculty of Chemistry, Wroclaw University of Science and Technology, Wroclaw, Poland*